QUANTITATIVE IMAGING OF CISPLATIN IN TUMOUR SAMPLES BY LASER ABLATION INDUCTIVELY COUPLED PLASMA MASS SPECTROMETRY

Stefan Marković

Doctoral Dissertation
Jožef Stefan International Postgraduate School
Ljubljana, Slovenia

Supervisor: Prof. Dr. Janez Ščančar, Jožef Stefan Institute, Jamova 39, 1000, Ljubljana, Slovenia
Co-Supervisor: Assist. Prof. Dr. Janja Vidmar, Jožef Stefan Institute, Jamova 39, 1000, Ljubljana, Slovenia

Evaluation Board:
Prof. Dr. Aleksander Zidanšek, Chair, Jožef Stefan Institute, Jamova cesta 39, 1000 Ljubljana
Prof. Dr. Maja Čemažar, Member, Institute of Oncology Ljubljana, Zaloška cesta 2, 1000 Ljubljana
Prof. Dr. Joerg Feldmann, Member, University of Graz, Universitätsplatz 1, 8010 Graz, Austria

MEDNARODNA PODIPLOMSKA ŠOLA JOŽEFA STEFANA
JOŽEF STEFAN INTERNATIONAL POSTGRADUATE SCHOOL

Stefan Marković

QUANTITATIVE IMAGING OF CISPLATIN IN TUMOUR SAMPLES BY LASER ABLATION INDUCTIVELY COUPLED PLASMA MASS SPECTROMETRY

Doctoral Dissertation

KVANTITATIVNO SLIKANJE CISPLATINA V ONKOLOŠKIH VZORCIH Z LASERSKO ABLACIJO Z MASNO SPEKTROMETRIJO Z INDUKTIVNO SKLOPLJENO PLAZMO

Doktorska disertacija

Supervisor: Prof. Dr. Janez Ščančar

Co-Supervisor: Assist. Prof. Dr. Janja Vidmar

Ljubljana, Slovenia, August 2022

To my family

Acknowledgements

I would like to thank my supervisor Prof. Dr. Janez Ščančar and co-supervisor Assist. Prof. Dr Janja Vidmar for their guidance and support during my studies. Together with Prof. Dr. Radmila Milačič, they offered me valuable advice, opportunities, patience, and without their help, this work would not have been possible.

I want to thank the members of the evaluation board, Prof. Dr. Aleksander Zidanšek, Prof. Dr. Maja Čemažar and Prof. Dr. Joerg Feldmann, for reviewing and evaluating the work in this thesis.

I would also like the Department of Environmental Sciences of the Jožef Stefan Institute for funding.

I would like express gratitude to Katja Uršic and Simona Kranjc Brezar for their meticulous preparation of samples that requires both excellent skills and a strong stomach. Together with Prof. Dr. Maja Čemažar and Prof. Dr. Gregor Sersa, they provided me with hard-to-obtain samples and expert advice that made this thesis possible.

I wish to thank all my co-workers for their help, valuable input and company. Katarina, Matic, Mišel, Belma, Tjaša, Majda, Tea, Pia, Lucija, Marta and all the others, thank you.

My friends and former colleagues Mihajlo, Jovan, Đorđe V., Goran, Marjan, Marko, Marija, Katarina and Đorđe P. all provided me with excellent company and valuable advice throughout my studies.

Last but not least, my family who supported me through the entirety of my education. Biljana, Goran, Aleksandar, Milan, Vojkan and Ranka thank you for everything.

Abstract

Medicine relies on imaging techniques such as ultrasound, magnetic resonance, computed tomography and histopathological image analysis because they provide valuable data needed for the diagnosis and treatment of diseases and injuries. Laser ablation inductively coupled plasma mass spectrometry (LA-ICP-MS) is often used in research and for the advanced diagnosis and clinical treatment of different diseases and injuries. LA-ICP-MS is an instrumental analytical technique that is used for the spatially resolved microanalysis of solid samples and is capable of quantitative mapping (imaging) of metals and metalloids in tissue samples of animal or plant origin in a selected area of interest.

In this dissertation, LA-ICP-MS was used for the bioimaging of Pt from Pt-based chemotherapeutics in tumour samples. High sensitivity and the ability to create quantitative images with the 3D sample reconstruction of this technique allowed us to determine the quantitative Pt distribution in HT29 tumour spheroids treated with cisplatin (CDDP) or Texas Red cisplatin (TR-CDDP). Under optimized instrumental parameters, a high spatial resolution and high sensitivity, with low limits of detection was achieved. Matrix-matched gelatine standards and/or isotope dilution analyses were used to quantify the amount of Pt. The results of the LA-ICP-MS analysis revealed that the Pt in the CDDP-treated tumour spheroids was localized primarily in the outer rim of the spheroids and to a lesser extent in the intermediary layer and the necrotic core. Due to the steric effects, significantly lower Pt concentrations were accumulated in the spheroids treated with TR-CDDP (2.2-times lower than in the CDDP-treated spheroids), while the Pt was mostly distributed in the areas of the outer rim. Imaging with confocal fluorescence microscopy, which is commonly used in oncology research, was compared with that by LA-ICP-MS. The results of the two complementary techniques demonstrated good agreement in terms of the spatial distribution of the TR-CDDP, while the intensity of the fluorescence matched well with the concentrations of Pt determined with LA-ICP-MS.

The developed method was further applied for studying drug distribution and uptake on tumours of B16F10 and 4T1 cancer cell lines. Different drug application methods and exposure times were tested at the same CDDP dosage and characterised using LA-ICP-MS. Intratumoral application oversaturates the tumour tissue, entering into the tumour environment and bloodstream. The results show that intratumorally injected samples release CDDP with time. However, the CDDP concentrations in tumour tissue were significantly higher than in intravenous injection. When injected intravenously, CDDP binds unspecifically to DNA and proteins throughout the whole organism. Consequently, a lower CDDP concentration is delivered to the targeted tumorous tissue. Therefore, to achieve the same drug concentration in the tumour, a smaller dosage is needed with intratumoral administration. This allows for a more targeted approach, with reduced side effects from the treatment.

The potential to extend the applicability of the developed LA-ICP-MS method for other solid biological samples was proved by an analysis of Cr localisation in the leaves of the dandelion plant (*Taraxacum officinale).*

Povzetek

V medicini različne tehnike slikanja zagotavljajo podatke, ki so nujni v diagnostiki in zdravljenju bolezni in poškodb. Redno se uporabljajo tehnike, kot so ultrazvok, magnetna resonanca in računalniška tomografija ter histopatološka analiza mikroskopskih slik kirurških biopsij vzorcev tkiv ali celic. Laserska ablacija z masno spektrometrijo z induktivno sklopljeno plazmo (LA-ICP-MS) je instrumentalna analizna tehnika, ki se uporablja za kvantitativno določitev elementne sestave vzorcev in slikanje oz. mapiranje prostorske porazdelitve kovin ter polkovin v tankih rezinah vzorcev tkiv živalskega ali rastlinskega izvora. Vse bolj je vključena tudi v medicinske predklinične raziskave in napredno klinično diagnostiko ter zdravljenje.

V disertaciji je predstavljena uporaba LA-ICP-MS za biološko slikanje platine (Pt), ki je prisotna v kemoterapevtiku cisplatin v različnih vzorcih tumorjev. Velika občutljivost določitve in možnost pridobitve kvantitativnih slik s 3D rekonstrukcijo vzorcev nam je omogočila, da smo z LA-ICP-MS določili kvantitativno porazdelitev Pt v tumorskih sferoidih HT29, ki smo jih tretirali s cisplatinom (CDDP) ali fluorescenčno označenim Texas Red cisplatinom (TR-CDDP). S skrbno optimizacijo instrumentalnih parametrov merjenja smo pridobili slike z veliko prostorsko ločljivostjo in nizkimi mejami zaznave določitve Pt. Za kvantitativno določitev Pt smo uporabili standarde želatine in/ali analize razredčitve izotopov, ki so se po svoji osnovi in koncentracijskem območju Pt ujemale z analiziranimi vzorci. Analiza slik, ki smo jih pridobili z LA-ICP-MS, je pokazala, da je bila Pt v tumorskih sferoidih, ki smo jih tretirali s CDDP, prisotna večinoma na zunanjem obodu sferoidov in le v manjši meri v globljem sloju ter nekrotičnem jedru. Sferoidi, ki smo jih tretirali s TR-CDDP, so imeli zaradi steričnih učinkov 2,2-krat nižje koncentracije Pt kot tisti, ki smo jih tretirali s CDDP. Pt je tudi v tem primeru bila večinoma porazdeljena na zunanjem obodu sferoidov. Slike, ki smo jih pridobili z LA-ICP-MS, smo nato primerjali s tistimi, ki smo jih pridobili s konfokalno fluorescenčno mikroskopijo. Uporaba slednje je v onkoloških raziskavah zelo pogosta. Primerjava je potrdila dobro ujemanje med tehnikama tako pri določitvi prostorske porazdelitve TR-CDDP kot med intenzivnostjo fluorescence in koncentracijami Pt.

Metodo, ki temelji na LA-ICP-MS, smo nadalje uporabili še za proučevanje porazdelitve in privzema CDDP v tumorje rakavih celičnih linij B16F10 in 4T1. Potem ko smo odmerek CDDP injicirali na dva različna načina, smo sledili prostorski porazdelitvi Pt v tumorjih. Rezultati so pokazali, da so bile koncentracije CDDP v tumorskem tkivu v primeru intratumorske aplikacije CDDP znatno višje kot v primeru intravenozne. Po intratumorski aplikaciji se CDDP najprej kopiči v tumorskem tkivu, nato se sčasoma sprosti v tumorsko okolje in krvni obtok. Pri intravenozni aplikaciji pa se CDDP nespecifično veže tudi na DNA in beljakovine v organizmu in je njegova koncentracija v ciljnem tumorskem tkivu nižja. Za dosego enakih koncentracij CDDP v tumorjih zato intratumorsko injiciramo manjši odmerek kot pri intravenoznem injiciranju. To omogoča bolj ciljno usmerjen pristop tretiranja z manj stranskimi učinki.

Uporabnosti metode, ki temelji na LA-ICP-MS, za trdne rastlinske vzorce smo na koncu raziskave preverili z določitvijo prostorske porazdelitve Cr v listih regrata (Taraxacum officinale).

Contents

List of Figures

List of Tables

Abbreviations

2D	...	Two dimensional
3D	...	Three dimensional
4T1	...	Murine mammary carcinoma cells
AMEM	...	Advanced Minimal Essential Medium
ARIS	...	Aerosol Rapid Introduction System
B16F10	...	Murine melanoma cell line
CDDP or cisplatin	...	Cis-diaminedichloro-platinum (II)
Cps	...	Counts per second
CRM	...	Certified reference material
CT	...	Computed tomography
Cts	...	Counts
DNA	...	Deoxyribonucleic acid
DW	...	Dwell time
EDTA	...	Ethylenediaminetetraacetic acid
ESI	...	Electrospray ionization
ESID	...	Electronically switchable illumination and detection module
EU	...	European Union
FBS	...	Fetal bovine serum
HPLC	...	High-performance liquid chromatography
HT29	...	Human colon adenocarcinoma cells
ICP	...	Inductively coupled plasma
ICP-MS	...	Inductively coupled plasma mass spectrometry
ID	...	Isotope dilution
LA	...	Laser ablation
LA-ICP-MS	...	Laser ablation inductively coupled plasma mass spectrometry
LOD	...	Limit of detection
LOQ	...	Limit of quantification
m/z	...	Mass to charge ratio
MALDI-MS	...	Matrix-assisted laser desorption/ionization mass spectrometry
MC	...	Multicollector
MCTS	...	Multicellular tumour spheroids
MRI	...	Magnetic resonance imaging
MS	...	Mass spectrometry
Nd:YAG	...	Neodymium-doped yttrium aluminium garnet
NIST	...	National Institute of Standards and Technology
PBS	...	Phosphate-buffered saline
RM	...	Reference material
RSD	...	Relative standard deviation
SC	...	Singlecollector
SI	...	International System of Units
SPS-SW1	...	Surface water reference materials

SRM	. . .	Standard reference material
TOF	. . .	Time of flight
TR	. . .	Texas red
US	. . .	Ultrasound
UV	. . .	Ultra violet

Symbols

^{194}Pt	...	Platinum isotope with mass number of 194
^{195}Pt	...	Platinum isotope with mass number of 195
Ar	...	Argon
CO_2		Carbon dioxide
Cr	...	Chromium
C_S	...	Sample concentration
C_{Std}	...	Standard concentration
d_S	...	Sample density
EDTA		Ethylenediaminetetraacetic acid
F		Fluorine
h	...	Height
H_2O_2		Hydrogen peroxide
HCl		Hydrochloric acid
He	...	Helium
HNO_3		Nitric acid
Ir		Iridium
K	...	Mass bias factor
MF_S	...	mass flow
m_S	...	Sample mass
m_{Std}	...	Standard mass
Ni		Nickel
Pt	...	Platinum
Rh		Rhodium
t	...	Time
V_S	...	Sample volume
x	...	Ablation line diameter
y	...	Laser scanning speed

Chapter 1

Introduction

1.1 Cancer

Cancer is a disease that results from complicated oncogene function factors, loss of tumour suppressor gene functions and environmental influences, all of which contribute to a genetic mutation [1], [2]. There are various combinations of mutated cancer genes, which can result in different cancer types. Cancerous tissues are complex and are made up of neoplastic (cancer) cells together with many other normal tissue cells, connective tissues and components (e.g., immune cells, endothelial, fibroblast) depending on the location and the type of cancer. Even the same type of cancer can have different characteristics and responses to treatment from patient to patient because of its different morphological and biological characteristics [3]. The tumour microenvironment is the cellular environment in which tumours or cancer stem cells exist. It has a huge influence on tumorigenesis because it contains tumour cells that interact with surrounding cells and tissues through the circulatory and lymphatic systems to influence the development and progression of cancer. In addition, non-malignant cells in the tumour microenvironment play critical roles in all stages of carcinogenesis by stimulating and facilitating uncontrolled cell proliferation [4]. As a consequence, multiple zones form within the tumour microenvironment, each with its own unique morphological and biological conditions [5].

Cancer is the second leading cause of mortality in EU countries after cardiovascular diseases. Every year, 2.6 million people are diagnosed with the disease and it kills another 1.2 million [6]. Therefore, there is an urgent need for constant improvements in current cancer diagnosis and treatment. Modern cancer diagnostics and therapies require an ever-increasing number of questions about the disease to be answered before the proper treatment for the patient is selected [7]. The earlier such information is available, the more likely the treatment is to be successful, while the number of questions that can be answered about a tumour can be limited by the sample that is available for testing and the accessibility to reliable analytical techniques that allow for the early detection of a tumour-specific biomarker and monitoring of the transport, distribution and metabolism of the drug used. The quantitative analysis of pathology images is becoming a necessity for the diagnosis and clinical treatment of cancer, but also for different research applications where it is used, for example, to understand the biological mechanisms of the disease process or for evaluating the efficacy of anticancer drugs [8]. The imaging of cancer usually includes a wide range of radiology-, microscopy- and spectroscopy-based techniques [9].

1.1.1 *In vitro and in vivo* cancer models

Two-dimensional (2D) cell cultures growing on plastic are the simplest *in vitro* cancer models used in preclinical trials. Such traditional monolayer cultures are, as an example, routinely used in cancer research, when evaluating the effectiveness of potential anti-cancer drugs [10]. The drug's mechanisms of action need to be understood and tested in order to determine its safety, effectiveness and toxicity. Usually, this is performed in 2D multi-well plates with relevant cell cultures of both targeted and healthy tissues [11]. While relevant, the distribution and kinetic data for these types of tests do not represent a "real-world" scenario, since the model lacks the complexity and conditions present in the patient's body [12]. Therefore, laboratory three-dimensional (3D) models, which more realistically simulate physiological conditions, are of great importance [13]–[15].

The use of mouse models for human cancer research has been a staple model for some time now due to the physiological and genomic similarity, relatively easy preparation, and good repeatability when compared to other types of *in vivo* animal models [16], [17]. These properties allow for a similar tumour environment that mimics basic cancer development and the response to treatment [16]. Yet, these models can still lack the complexity and heterogeneity present in human cancerous tissue and there is also an ethical dilemma about their use [18]. With the advancement of genetic engineering, transgenic mice with incorporated genes of another species have seen wide application in research. These newer models allow for much more representative conditions for research with a more representative microenvironment and patient variability [19], [20]. In addition to the use of animals, there is a constant search for newer, more representative *in vitro* models. Ideally, they should be easy to prepare, perfectly simulate real conditions, and do not raise any ethical concerns.

Models that are close to the above-mentioned requirements are 3D multicellular tumour spheroids (MCTS) . They are cell clusters formed by cell growth, which at a diameter of 200 µm or more form different proliferating zones that reflect those in real solid tumours [21]. Each zone possesses its own distinctive stiffness, porosity and topology, reflecting different pathophysiological phenomena, such as drug gradients. In comparison to 2D models of the same cell line, MCTS have shown higher drug resistance to chemo and radio therapy [15], [22]. Poor vascularization of the MCTS limits the nutrient and oxygen transportation to the core and also the penetration of drugs, which is consequently solely reliant on diffusion [23]. This can result in necrotic cores, the poorly vascularized, hypoxic parts of the tumours, made up of dead nutrient-deprived cells (usually in spheroids larger than 500 µm) [21]. The necrotic core also serves as a nutrient reservoir for the surrounding layers of the MCTS. Surrounding the necrotic core is the intermediate layer, which is located beneath the outer rim and is formed because of the limited access to oxygen, nutrients and metabolites [24]. The outer rim cells in the external proliferating zone represent cells close to the blood vessels and thus have the best access to nutrients, possibly hindering drugs from penetrating deeper into the MCTS [25]. Another possibility, besides using a single cell line for MCTS development, is the use of the combination of different cells, extracellular matrix and cancer stem cells, all of which are present *in vivo*, in order to significantly improve the model in a manner that it mimics the tumour microenvironment more closely [10].

1.2 Chemotherapy

Chemotherapy is defined as the use of chemicals to treat diseases [26]. The discovery of cancer chemotherapy has significantly influenced the treatment and survival of cancer

patients [27]. In the early 20th century, it was noticed that exposure to certain chemicals affects the number of blood cells and severe exposure results in anaemia and leukopenia [28]. Soon after, research in drug discovery and the treatment of cancer started on the basis of previous observations. In chemotherapy, different cancer cells show different responses to a given drug, and effective destruction of the cancer tumour may cause significant danger to the patient [29]. Hence, drugs with targeted action should be used in chemotherapy, and their dosage carefully selected in order to avoid severe side effects [7]. In recent years, a lot of effort has been concentrated on the development of specific and targeted drugs and carriers for the drug [30], [31]. In order to effectively develop and understand the mechanism of the drug, it is necessary to determine its distribution throughout the organism [32]. The dose of chemotherapeutics applied, its schedule and route of administration are determined after studying its pharmacokinetic factors, such as drug absorption, metabolism and elimination [28].

The discovery of different families of antitumor drugs such as antibiotics, antimitotic nucleoside analogues and nucleobases, cisplatin, and others led to chemotherapy in which the combination of drugs that have different mechanisms of action is applied [26], [28]. Chemotherapy is also frequently used together with radiotherapy and surgery as a complementary technique to remove microtumours [29].

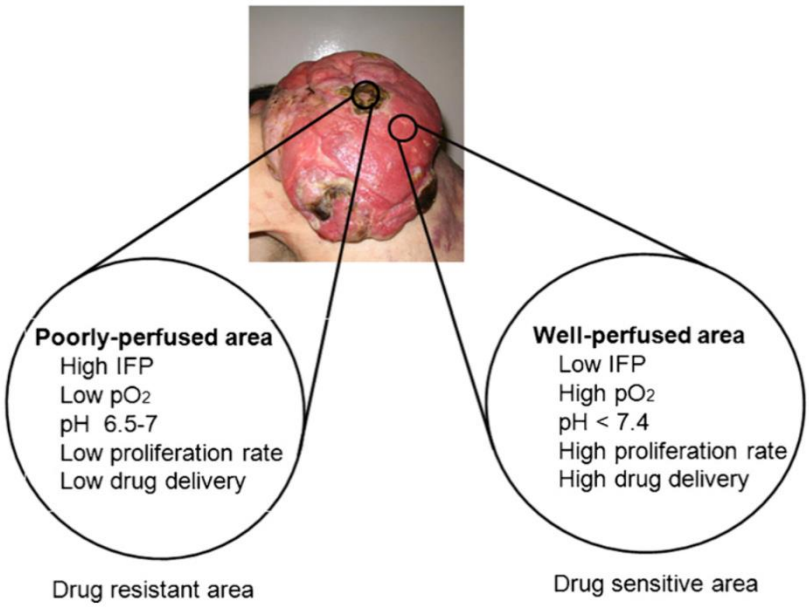

Figure 1: Causes of tumour drug resistance. Resistance to chemotherapy is due to extracellular and intracellular factors. Reproduced from Galmarini et al. (2012) [28] with permission from Elsevier.

The method of drug delivery is of vital importance. Ideally, the full dose would bind to the cancerous tissue without damaging the healthy tissue and have a long period of action. The most common way of administering the drug is intravenous [33]. In order to achieve the necessary concentration and time of exposure to the drug, the therapeutic dosage of the drug is usually applied in smaller doses, several times, to maximise its effectiveness [34]. There are other possibilities for drug application, like intratumoral injections [35]. This method has the benefit of higher local concentrations, and as such smaller amounts of the drug need to be administered for the same (optimal) dosage in the tumour. However, it cannot be applied in a lot of cases, and there is still significant drug leaching from the

targeted area. Another possibility is an application with electroporation or a combination of the previously mentioned methods [36]–[38].

1.2.1 Cisplatin

Cisplatin (cis-diaminedichloro-platinum (II); CDDP) is a chemotherapeutic drug used to cure different types of cancers including bladder, oesophageal, cervical, lung, ovarian, testicular, (non-)small-cell lung, head and neck cancers. It was discovered in 1965 during an experiment with *Escherichia coli* in electric field using a Pt electrode. In this experiment the bacteria stopped dividing and grew abnormally even after the electric flow was stopped. It was discovered that CDDP was formed, and it was decided to test it as a possible chemotherapeutic [39]. In the trials, it showed promising results, and in 1978 it was approved by the Food and Drug Administration for the treatment of testicular cancer. CDDP is the first metal-based chemotherapeutic, and as such, it is commonly used as a benchmark for the comparison and testing of newly developed metal-based drugs [40]. The treatment using cisplatin can have severe side effects, like neurotoxicity, nephrotoxicity, ototoxicity and emesis [41], [42] as a result of unspecific binding. Usually, it is injected intravenously, but in some cases, intratumorally [43]. The cytotoxicity of cisplatin comes from Pt's high affinity to bind to the DNA, and this results in crosslinked DNA with an altered double-helical structure [44]. As a result of the DNA damage, cellular processes like transcription and replication are altered, and they trigger cellular death by apoptosis or necrosis. Besides binding to the DNA, it also binds to proteins and becomes inactive [40], [44], [45]. In order to improve the efficiency of CDDP and supress its side effects, it is necessary to understand the distribution and behaviour of the CDDP at therapeutically relevant levels [46]–[48].

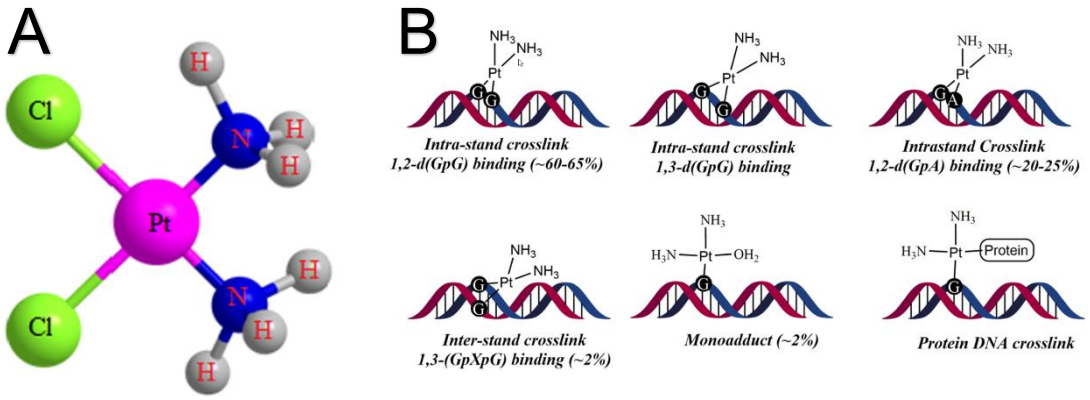

Figure 2: A) Structure of cisplatin B) DNA adduct formation. Reproduced from Ghosh (2019) [39] with permission from Elsevier.

1.3 Cancer Imaging Techniques

Modern medicine relies on imaging techniques, as they provide valuable data for diagnosing and treating diseases and injuries. These techniques have rapidly progressed in recent years and significantly impacted on the developments in medicine. However, they still have limits and sometimes lack crucial information needed for their proper assessment [49]. Currently, non-invasive or minimally invasive imaging techniques are the most commonly used in cancer diagnosis and therapy. For example, ultrasound, computed tomography and magnetic resonance imaging are used for both preclinical investigations and applied at the

clinical level [37]. In clinical practice, histopathological image analysis of tissue or cell samples taken directly from tumours remains the best option for diagnosing almost all types of cancer [50]. Frequently applied in preclinical research are fluorescence imaging techniques, including confocal microscopy, which has been employed for *in vitro* and *in vivo* monitoring of the delivery and distribution of many drugs, including chemotherapeutics [46], [51]. Among them, CDDP marked with the fluorophore dye Texas Red (TR) was frequently used in fluorescence imaging [46], [52].

Quantitative analyses of pathology images is becoming a necessity, not only for a diagnosis and clinical treatment of cancer, but also for different research applications where it is used, for example, to understand the biological mechanisms of the disease process or for evaluating the efficacy of anticancer drugs [53]. Quantifying analytes of interest with subcellular resolution is critical to many applications ranging from biomarker discovery, pharmaceutical research, systems biology, to disease treatment planning [54]. Quantification is also needed for the comparison of images generated by different imaging techniques. For this purpose, techniques that allow quantification at the low-ppb level for bio-species in micro-sections of complex biological sample matrices, such as in tumour tissues, are required [55]. There are several imaging techniques that make it possible to track the spatial distribution in the target tissues when metallodrug (e.g., CDDP) is used [56], [57]. When the anticancer drug contains a non-physiological atom, imaging is possible with different ion beam and mass spectrometry based analytical techniques such as micro-X-ray fluorescence, matrix-assisted laser desorption/ionization mass spectrometry (MALDI) and laser ablation inductively coupled plasma mass spectrometry (LA-ICP-MS) [58]–[60].

1.4 Laser Ablation Hyphenated to Inductively Coupled Plasma Mass Spectrometry

LA-ICP-MS is a hyphenation of multiple instruments that allows for the spatially resolved microanalysis of solid samples. The first published application was in 1985, one year after the first commercial ICP-MS was released [61]. Since its conception, this method has been widely accepted and used in geological research and analysis. However, the capabilities of this method have been tested in other fields and at the time of writing, are gaining a significant foothold in the field of metallomics as an important bio-imaging tool [62]. The number of publications with LA-ICP-MS is now large, and its unique abilities are being applied in fundamental medical research as a reliable semi-quantitative or quantitative imaging method [58].

Since the first published application, the development of the new LA-ICP-MS instrumental set-up has rapidly accelerated. Due to its high sensitivity and spatial resolution down to, at least, the cellular level, modern LA-ICP-MS is frequently applied in medical imaging [58]. Its main advantage is the possibility to provide a quantitative image of the elemental spatial distribution [60]. It is used for imaging metals and metalloids in biological tissues in a selected area of interest or in a complete thin tissue section [58], [63]. For such applications, there is a need for the development of validated methods to determine the quantitative distribution of the analytes relevant for cancer diagnosis and therapy in tumour models or cancer tissue at a low concentration of ng g^{-1} [57]. Reliable imaging procedures based on LA-ICP-MS can significantly contribute to modern research in oncology as they provide the quantitative data needed to evaluate the drug's efficacy and the selected therapy's effectiveness [48]. In addition to the growing interest in LA-ICP-MS imaging, imaging using two or more different complementary techniques on the same sample provides a deeper insight into evaluating the spatial distribution of the elements in

biological samples [64]. In this way, it is possible to image samples prepared for the visualization of metal-based drug distributions in tissue samples with fluorescence microscopy and LA-ICP-MS. However, such a multimodal imaging approach was rarely applied in oncology research.

Because of tumour sample complexity, there are several requirements for reliable LA-ICP-MS imaging of tumour spheroids and tissues. LA-ICP-MS imaging can provide essential data, but there are also some limitations, as follows:

- The sample morphology should not be changed when preparing the sample for imaging, as this will directly alter the drug's distribution in the image.
- Higher resolution of the acquired concentration images provides a better insight into the distribution and effect of the metal-based drug selected for analysis.
- The 3D image provides the most accurate data on the whole system, while a 2D image created from a single cryo-sectioned slice can give misleading data about the distribution and the concentration.
- *In vitro* studies (such as tumour spheroids) provide a valuable insight and are easier to interpret, but can still lack the complexity of a living organism.

Therefore, it was hypothesized in the presented work that a quantitative analytical method based on LA-ICP-MS could successfully overcome some of the challenges mentioned above and provide a high-resolution (at a cellular level) quantitative image of the selected metal's spatial distribution at a low ng g^{-1} level.

The essential components of LA-ICP-MS are shown in Table 1.

Table 1: LA-ICP-MS components.

Instrument	Components
Laser Ablation (LA)	Laser (light source)
	Beam control system (power control, power monitor, homogenisation, beam steering, focusing)
	Sample observation camera
	Sample cell (movable stages)
	Transport tubing
Inductively Coupled Plasma (ICP)	Ion source
Mass Spectrometer (MS)	Vacuum system
	Interface and ion lenses
	Analyser
	Detector

Hyphenating the LA sample introduction system to the ICP-MS creates a powerful analytical tool that combines all the advantages of both instruments. This instrumental set-up allows for a multi-elemental sample mapping with a high spatial resolution (down to a 1 μm pixel size at the time of writing) [8]. The exact capabilities and applications depend on the available instrumentation. The new instrumentation has made it possible to couple the laser to other types of ICP-MS detectors, such as TOF (time of flight) and MC (multicollector - sector field), unlocking their full potentials [65]. The capabilities provided by this instrumentation have an extensive application area and are seeing increasing use with time.

Direct analysis of a solid sample using LA-ICP-MS has advantages over the solution-based nebulization ICP-MS technique. There is a smaller risk of introducing impurities and interferences with reagents, sample consumption is reduced, LA-ICP-MS has the ability to map and investigate the spatial distribution of elements in a sample with high spatial resolution, and in most cases, the preparation of the sample is less laborious [66]. Traditionally, to measure the content of elements in solid samples, the sample had to be digested or ashed in order to create a solution. This results in the loss of the spatial distribution information and the species of elements in the analysed sample, resulting in an average element content in the whole mass of the sample and thus losing very important information in clinical research [67].

Preparation and measurement of the sample are relatively easy, but LA-ICP-MS requires the use of standards prior to the analysis in order to quantify the analyte. For a map of the quantitative distribution of elements to be accurate, rigorous preparation and analysis of the calibration standards must be carried out [68]. The way of approaching the measurement depends on the nature, structure and composition of the sample. The efficiency of the ablation and the generated aerosol characteristics depend on the analysed sample's mechanical and optical properties [67]. With the development of ablation cells with a low “dead” volume and a fast signal washout interface, faster ablation with lower resolution and high clarity has become possible [69].

The main drawback to the method is that there are no universally accepted and applied methods and certified reference materials, which is a consequence of every sample having a unique matrix, and difficulties in the analysis [70]. Internal standards would solve many of these issues, as in regular solution nebulization analysis, but it is impossible to spike a solid sample evenly throughout the entire volume and retain information about its spatial distribution.

In order to overcome some of the difficulties and quantify the analyte, many methods have been proposed and tested. In the case of solid standards for quantification, homogeneity and an even distribution and thickness of the analytes are desirable characteristics, if not mandatory [71].

1.4.1 LA-ICP-MS fundamentals

Elemental imaging with LA-ICP-MS is susceptible to image degradation as a result of selecting unsuitable instrumental parameters. This degradation can crate image artefacts such as blur, smearing, aliasing and signal noise [72]. They result from fast scanning, low or high repetition laser rates, unsynchronised ICP-MS dwell times, long signal washout times, inadequate spot size, low analyte concentration, etc. Many measurement parameters and optimisations have been reported in literature, but so far, no standard approach to setting up instrumental parameters has been widely accepted to address all of the previously mentioned artefacts [73].

With the advances in instrumentation, the analysis time per given area has advanced significantly due to the modern LA systems containing low-volume, fast-washout ablation cells, which reduce the flow turbulence and significantly reduce the “dead space” of the cell [74]. Additionally, the hyphenation tubing has become shorter and has a smaller diameter, which reduces the washout and aerosol travel times. In the last 10 years, the potential analysis speed has increased 100 times [75]. However, this advancement is constrained by conventional quadrupole ICP-MS, which measures each m/z sequentially, and thus a lot of information can be lost while the ICP-MS is measuring other m/z values or during instrument's “dead time”, when the ICP-MS is switching between different m/z values. This problem can be solved by using the recently introduced time of flight mass spectrometry (ICP-TOFMS), which has the capability to measure the whole m/z spectra

simultaneously with extremely fast integration times (more than capable of measuring at the fastest ablation parameters) [76], albeit with a more than ten-times decrease in sensitivity.

Optimal measuring conditions would minimally degrade the image with blur, aliasing, noise and smear, while having high sensitivity, high resolution and a short time of analysis with the parameter synchronisation between both instruments.

1.4.2 Data handling and image creation

The amount of data produced by LA-ICP-MS can be large, especially in the imaging application [77], [78]. In this case it can be in the range of hundreds of thousands of values per image. In order to process this amount of data, some kind of data-reduction scheme is normally used [79], [80]. In order to create an image, a program usually synchronises the data from both instruments and assigns a value for the ICP-MS to a stage position reported by the LA. There is a large number of programs that are able to do this (e.g., HDIP, ImageJ, Iolite). However, all of these programs have their own approach to data handling, so each has its advantages depending on the use case. For example, HDIP by Teledyne Photon Machines (Bozeman, MT, USA) was designed explicitly for the imaging use case and offers a large number of options and configurations, including 3D imaging.

1.4.3 Inductively coupled plasma mass spectrometry

ICP-MS is an instrumental technique for elemental analysis. It is used to measure elements rather than molecules and compounds. ICP-MS consists of the ion source (ICP), a mass spectrometer analyser (the MS is usually a quadrupole mass filter), and a detector (electron multiplier). The ICP is at atmospheric pressure, while the MS and detector are in a vacuum chamber [81].

Samples are nebulised in the sample introduction system, creating a fine aerosol that is transferred to the argon plasma. The high-temperature plasma atomises and ionises the sample, generating ions, which then go into a set of electrostatic lenses called ion optics. The ion optics focuses and guides the ion beam into the mass analyser. The mass analyser then separates the ions according to their mass-charge ratio (m/z), and these ions are then measured at the detector [82].

ICP-MS can measure virtually every element and their isotopes. The only elements that ICP-MS cannot measure are H and He (below the mass range of the mass spectrometer), Ar, N, and O (which are present at a high level from the plasma and air), and F and Ne (which cannot be ionized in argon plasma) [83].

The reason ICP-MS is so widely used is that it provides extremely low detection limits for nearly all the elements that it can measure. ICP-MS can detect many elements at levels below 0.1 part per trillion (ppt). However, ICP-MS can also measure elements at high concentrations, up to one thousand ppm (0.1%), and the concentration range from 0.1 ppt to 0.1% covers ten orders of magnitude. No other technique has such a broad elemental coverage, low detection limits, and a wide measurement range [83]. Because of the powerful capabilities of ICP-MS, it was initially used for the total quantification of trace metals in liquid samples. However, by hyphenating different sample introduction techniques and mass separators, the instrument has matured into a versatile and a popular method. The possibility to accurately measure heteroatoms in compounds with a wide range of introduction techniques has made the ICP-MS a staple instrument in environmental and life sciences [83].

Depending on the type of mass analyser, there are multiple versions of ICP-MS instruments, each type with its own capabilities. The most commonly used mass analyser

is a quadrupole analyser. This type of mass analyser was also installed in the first commercially available ICP-MS instrument [84]. It functions by applying a complex field of electrical current on four metal rods. The most significant advantages of this type of analyser are its low cost, good sensitivity and robust measuring conditions. It measures each *m/z* ratio independently, but the switching time between different *m/z* ratios (dead time) can be fast, especially on the newer models [85]. However, when hyphenated with LA, this is still a significant limitation because, if multiple elements are measured, a lot of information can be lost and we could end up with an unrepresentative value in an inhomogeneous sample (all real samples) for a given area (pixel). The most significant disadvantage of quadrupole ICP-MS is its low mass resolution, which is inadequate for precise isotope ratio measurements [61], [86].

A time of flight (TOF) analyser is a newer type found in ICP-MS instruments. It offers simultaneous measurements of all the possible *m/z* values of generated ions (it measures the majority of the periodic table simultaneously) [87]. This is achieved by simultaneously firing all the *m/z* values (with an ion pulser) through a vacuum tube with ion mirrors (reflectron) onto a detector. Depending on the time it takes for an ion to travel from the pulse to the detector, an *m/z* value can be assigned. This can be extremely useful for imaging and screening purposes [61], [88]. Moreover, the flicker noise present in quadrupole ICP-MS is removed by simultaneous sampling. ICP-TOFMS is capable of measuring the whole spectra of elements tens of thousands of times per second, which is much faster than the fastest commercially available LA system is capable of firing. The most significant disadvantage of ICP-TOFMS is its relatively low sensitivity (around two orders of magnitude lower than quadrupole ICP-MS) and its low mass resolution [89].

Sector field analysers are based on curving the flight path of a high-velocity ion in a magnetic field (sector field) [90]. By adjusting the strength of the magnetic field and the potential of the ions, it is possible to separate the *m/z* values and to guide the targeted ion onto a detector (a Faraday cup in the case of a multicollector ICP-MS, for example). The most significant advantage of the sector field analyser is its good sensitivity, with an excellent mass resolution, which makes it perfect for high-precision isotopic analysis [91]. The main disadvantages are the high price and slow *m/z* shift (high dead time) of the analyser [91]. Depending on the instrument's configuration and the number of detectors, the sector field analyser can be classified into two groups: singlecollector (SC) and multicollector (MC) [92]. Hyphenated to LA, ICP-SCMS has good sensitivity and excellent mass resolution, but it is limited in practise to monitoring one *m/z* value in imaging applications due to the complexity of the mass shifting (changing the *m/z* value) [8], [86], which can cause artefacts (aliasing, blurring) on the final image [61]. ICP-MCMS has, like the ICP-SCMS, good sensitivity and excellent mass resolution, but can measure multiple m/z values simultaneously [93], [94]. This makes it perfect for high-precision isotope ratio measurement in a heterogenous sample (all real solid samples). This is due to the fact that MC has multiple detectors, and the amount of *m/z* values that can be monitored is dependent on the manufacturer. The biggest drawback to his method is that the instrument is limited to a specific number of *m/z* values depending on the number of faraday cups it has. Because *m/z* switching is even slower than in the SC ICP-MS, this makes it impractical for LA application while switching [61].

Table 2: ICP-MS configurations based on the type of mass analyser.

	Quadrupole	Time of flight	Singlecollector	Multicollector
Speed	Fast	Very fast	Slow	Slow
Sensitivity	Medium to high	Low	High	High
Application	General	High-speed scanning of all m/z values simultaneously	General and isotopic analysis	Isotopic analysis with high precision

All the possible ICP-MS systems can be used with the LA sample introduction system. No best option exists; it is dependent on the application and the price.

Sensitivity is the signal strength the instrument detects per unit of concentration. Besides the signal strength, the linearity of the signal is essential. High linearity allows for a precise measurement over a wide concentration range [81]. Obviously, a stronger signal is always better as it allows for lower detection limits and background interference. The instrument's sensitivity is tuned with a defined standard prior to the measurement in order to optimise or maximise the sensitivity [95]. For LA-ICP-MS, sensitivity is especially important, as it is the main limiting factor for high-resolution imaging. The amount of analyte that is ablated in this case (laser spot - pixel diameter <5 µm) is extremely low (orders of femtograms per pulse or even less), and concentrations that would typically be detected without any issues are very hard to measure and are unreliable.

The background is the signal noise that comes from the instrument or sample matrix (polyatomic interference, memory effect). It can be determined by measuring a blank sample, and then subtracting it from the signal to remove it. LA-ICP-MS is less susceptible to background noise when compared to conventional "wet plasma" ICP-MS, as only a concentrated sample is introduced, so contaminations introduced by the sample preparation are far less likely [70].

The detection limit is the ratio between the signal strength and the background noise [96]. Low limits of detection are always better. Higher sensitivity and lower background noise produce lower detection limits, and vice versa increases the detection limits.

The dwell time is the time the instrument takes to measure one signal (m/z). This can usually be adjusted, and lower is always better, as it allows for smaller pixels while imaging and more information is gained [97].

The dead time is the time it takes the detector to switch between two measurements. It cannot be adjusted and is in some cases one of the main limiting factors for the measurement speed, the number of m/z measured and the sensitivity [97].

The acquisition time is the time it takes the ICP-MS to measure all the m/z ratios and to switch between them. It is the sum of all the dwell and dead times. This time multiplied by the laser scanning speed is what defines the length of a pixel.

Drift is the change in sensitivity during a measurement. It is especially important as it is impossible to predict and thus requires extra steps during the measurement (measuring a standard at defined intervals) to compensate for. Normally, an internal standard is used to correct the instrument drift and the sample introduction efficiency, but in the case of solid samples, it is impossible to evenly spike the sample without destroying its spatial characteristics, which is the main reason for the LA-ICP-MS measurement [98].

1.4.4 Laser ablation sampling system

LA is an instrumental sample introduction method that allows the direct analysis of solid samples. LA is based on the firing and focusing of a high-power pulsed laser beam on a prepared sample placed in an air-tight cell [75]. A solid sample is irradiated by a high-energy pulse of photons that vaporises (boils) the sample as a fine, dense sub-micrometre particle size aerosol, and a gas stream (usually He) carries the created sample aerosol to the ICP-MS [99]. Because of the potential danger while working with a high-power beam, a high-magnification camera is required to operate the instrument. The main advantage of LA as a sample intake method is its ability to analyse solid samples with high spatial resolution, which makes it possible to selectively analyse regions of interest in the sample (unlike the commonly used digestion method, which measures the average concentration in the sample). LA can fire photon beams with adjustable frequency, beam diameters, and beam energy. Adjusting these parameters allows almost any solid material to be ablated [63].

There are many components in a LA system that are important for the quality of the ablation and sample transport.

The laser is the fundamental component of the LA sample introduction system. Any laser with high enough energy to ablate the sample can be used. However, more robust lasers with adjustable energy are preferred. The energy is measured in milli Joules (mJ), but the energy delivered to the sample is in irradiance (J/area). Besides the energy, the essential parameters are the shooting frequency (most modern LA systems have 300–500 Hz maximum), and pulse width [100]. The pulse width is the length of time that the beam is fired, and it affects the ablation quality, as lower lengths reduce the sample melting and fractionation effect. Conventional, commonly used lasers are nanosecond pulse lasers, but newer and far more expensive options are femtosecond lasers, which have far greater potential for stability and control [101]. There is a wide variety of lasers types, two of the most commonly used lasers types are Nd:YAG (neodymium-doped yttrium aluminium garnet - 1064 nm base, 532 nm, 266 nm, 213 nm and 193 nm available) and ArF excimer (193 nm), with the latter having more energy and wider possible applications. The 193 nm laser allows for the ablation of almost any solid material (even quartz, which is transparent to UV light, can be ablated to some extent) with minimal sample melting or splintering [102].

When the laser beam is fired, it is first guided by an optical system, which can adjust the energy, homogenise the beam and focus it on the sample. The sample cell is airtight, preferably with as little as possible dead volume, with a high-efficiency sample transport system. The cell is mounted on movable stages, which move the sample while the laser beam is stationary. Recently, there has been a heavy emphasis on sample cell design, as it directly influences the transport speed, efficiency and washout time [103]. Helium is preferably used as the carrier gas, as it improves the aerosol formation. The sample aerosol is carried through an inert tube to the ICP-MS (shorter and small-diameter tubing allows for faster imaging conditions).

When using lasers with a lower wavelength, the ablation is more efficient and the produced aerosol particles are smaller and are more efficiently transported and ionised in the plasma [94]. The wavelength has an important role since the reflectivity and absorption of the beam depend directly on the wavelength. For example, 193 nm lasers have a higher energy per photon than higher wavelength lasers, and at that wavelength, the absorption is far more efficient, and there is less reflection. On the other hand, wavelengths below 193 nm are more difficult to use since they will be absorbed by the air and thus not practical in this use case [102].

A shorter laser pulse duration increases the ablation efficiency, lowers sample melting and cracking with more efficient energy delivery (reduces elemental fractionation), forms a finer aerosol and creates a more regular crater [104].

Laser energy and frequency can be adjusted and have to be optimised for each sample type. By adjusting the energy dosage (energy, frequency and stage movement), it is possible to minimise the sample melting and fractionation [105]. Lower dosages produce incomplete ablation with elemental fractionation (volatile elements are evaporated, while non-volatile elements remain in the sample), while high dosages result in excess melting of the crater walls (which also introduce elemental fractionation) and sample cracking. Both cases create sub-optimal particle sizes [73].

Depending on the use case, the sample cell design, transport efficiency, and dynamics are of crucial importance [74]. In the ideal case, the cell would have no "dead" volume, and transport efficiency through the tubing would be 100% with an even, laminar gas flow. However, this is impossible to achieve, but modern cell design has significantly reduced the volume, and the tubing is much shorter and smaller in diameter [69]. This has resulted in a highly efficient, concentrated sample delivery with each laser pulse being resolved from each other (washout time), which is especially useful in imaging applications since it reduces the blurring and increases the potential speed of analysis by a couple of orders of magnitude [103].

Besides optimising each instrument individually, it is crucial to synchronise the parameters between both instruments, as inadequate conditions will lead to measuring artefacts, the most important of which is aliasing [75], [106]. Therefore, in order to reduce the number of artefacts and to obtain a stable sample signal, the acquisition time on the ICP-MS and the shooting frequency on the LA need to be synchronised. To achieve this, the laser has to fire a set number of times per ICP-MS acquisition time without oscillation (if multiple m/z values are measured, the same applies to individual dwell times) [72], [100], [107].

1.4.5 Analyte quantification using LA-ICP-MS

If a measurement gives a result that depends on the sample composition and physical characteristic, then the technique exhibits a matrix effect. LA-ICP-MS is an example of a technique that exhibits a very strong matrix effect [108]. While the conventional ICP-MS also suffers from a matrix effect, it can be corrected by matrix matching the standards, internal standardisation and determining the spike recoveries in the sample. In the case of LA-ICP-MS, it is a lot more complicated. The most significant problem resulting from the matrix effect can be observed in the LA sample introduction system. Due to the significant difference between samples, available standards and within the sample itself, the ablation efficiency differs by a large amount during the measurement [109]. This results in a variable amount of sample aerosol being delivered to the plasma, depending on how well the sample ablates [110]. The matrix effect deriving from ICP-MS while coupled to LA is almost negligible because only a small amount of sample is delivered to the plasma, making the ionisation very efficient, and without solvents, the oxide levels and interferences are very low. All of the above-mentioned solutions for conventional ICP-MS, except for matrix-matched standards, cannot be applied to LA-ICP-MS because there is no way to use them without destroying the sample. The problem of variable sample delivery is the first issue to solve if we want reliable quantification and imaging. Conventionally, accuracy is determined with a reference material (RM) analysis. However, this is difficult to achieve using LA-ICP-MS, as there is a limited number of reference materials certified on the micro-scale. The most commonly used RM is NIST 610 and NIST 612 glass, but due to the significant difference in matrix composition, it is not easily applicable for bioanalysis.

The most common quantification strategy in LA-ICP-MS is an external calibration that includes matrix-matched standards [111], [112]. Gelatine, which has a similar elemental composition to the tissue samples, was suggested for preparing matrix-matched standards [113]. Besides an external calibration, the isotope dilution (ID) technique can be used as an alternative technique for quantification [114]. ID is a definitive quantification method that is traceable to SI units and can be used to accurately quantify elements that possess at least two stable isotopes [115]. As the isotope standard mixes with the sample aerosol, the ablation efficiency that is influenced by the matrix effect, which limits the use of external standards, is avoided.

1.4.5.1 External calibration with solid standards

To successfully quantify the analyte with a solid standard, the ICP-MS needs mass calibration for the signal response, and a correction for the ablation yield [116]. In order to solve the issue of ablation yield, it is necessary to match the matrix of the RM and the sample. Another way is to have a known low sample and a standard thickness, and ablate both completely in their z-axis (depth). However, a possible drawback to this method is that the samples have to be very thin.

Because the ICP-MS instrument is relatively unstable (due to its complexity), it is necessary to recalibrate every couple of hours during the measurement to correct the instrumental signal drift.

1.4.5.2 External calibration with a reference material

Calibration with a RM can be reliable and easy to perform. However, because of the different ablation yields that arise from the difference in the matrix composition and the limited number of RMs that are homogeneous on the micro-level, this method is only applicable to a handful of sample types (almost all are geological samples) [117].

It is possible to create a pellet from a RM that is sold in powder form and is matrix matched to the sample, but the physical properties of such a standard are different from the sample, which affects the ablation yield.

1.4.5.3 External calibration with matrix-matched standards

If there is a lack of RM applicable to the sample type, in-house, matrix-matched standards can be created by spiking the powdered material (usually the same type of material as the sample) with the analyte, homogenising it and pressing it into a pellet (or some other way) to compact the powder [68], [84]. This method is widely used in the analysis of biological samples with LA-ICP-MS. However, it is extremely labour intensive and prone to measurement difficulties.

1.4.5.4 External calibration with gelatine or agar standards

To avoid using spiked biological materials as in-house, matrix-matched standards, easy to prepare standards that mimic matrices of the sample have been suggested and tested. For animal tissue, spiked gelatine gels made from animal gelatine have been used for the preparation of standards [113], [116], [118], while for plant tissue, spiked agarose gels are used [119]. The advantage of this method is the easy preparation and optimization. However, this method also suffers from some drawbacks. Usually, standards prepared in this way exhibit a severe ″coffee stain″ effect, since they are applied as a droplet on a glass slide and left to dry, which results in an uneven thickness of the standard. The ″coffee stain″ effect results from capillary flow to the edges of the standard while drying and results in elevated concentrations of the analyte on the edges of the standard. In order to avoid

the effect, it is possible to freeze the standard and dry it by sublimating. However, this results in a porous, frail standard that is susceptible to cracking. Luckily, several elements bind to some gel standards (such as Pt^{2+} in porcine gelatine), which results in an even distribution throughout the gel volume. Using moulds for gels, in order to obtain an even thickness, has been suggested. Hence, with careful preparation, it is possible to obtain a gel standard of even thickness and analyte distribution [116].

1.4.5.5 External calibration with a filter standard

When measuring plant materials, it is possible to spike filter papers and use them as matrix-matched calibration standards [120], [121]. However, this method suffers from a severe ″coffee stain″ effect, and cellulose fibres that make up the filter are usually unevenly distributed (due to filter porosity), resulting in an unreliable method.

1.4.5.6 External calibration with wet aspiration of analyte

External calibration using a nebulised analyte solution has been widely used. Usually, the analyte mist is carried by Ar gas and mixed with ablation cell carrier gas [70]. However, during the sample measurement, it is necessary to nebulise a blank solution, which removes the sensitivity and interference benefits of using dry plasma [119]. Also, the difference in the particle size and the matrix composition of the ablation and standard aerosol can influence the sensitivity between the two.

1.4.5.7 Quantification using online ID-LA-ICP-MS

Isotope dilution (ID) is a quantification technique based on measuring the elemental isotope ratio in a sample with a known addition of an isotopically enriched elemental standard. This can be used to accurately quantify elements that possess at least two stable isotopes [115]. By changing the natural isotopic composition with a known quantity of isotopes and measuring them, many of the usual measuring problems are avoided, albeit at a higher cost and a longer time of preparation. Using this technique, it is also possible to quantify compounds [61].

Usually, the isotopic spike is mixed with the sample prior to the analysis or aspirated simultaneously during the analysis. For time-resolved analysis (e.g., chromatography, speciation, LA-ICP-MS), usually, the spike is aspirated continually (online) in order to quantify the entire time of measurement (in some cases the measurement can last for hours) [92]. This is especially true in the case of ID-LA-ICP-MS imaging, since it is impossible to add an isotopic spike to a solid sample without altering its composition. Some other techniques were tried, like printing isotopically spiked ink and sputter depositing the isotopic spike evenly onto or below the sample. However, they have considerable drawbacks [122]. In order to precisely quantify the analyte using the online aspiration approach, a known amount of isotope must be aspirated with a stable and continuous flow. Using this method, instrumental drift can be annulled, since it is based on the isotope ratio and not the signal strength. However, it has a major drawback, i.e., the quantification range is limited to about a factor of 10 (for a quadrupole MS) [25]. Exceeding this can result in an unreliable measurement and overestimating the concentration. This presents a problem in the case of imaging because the concentration range in the sample can vary a lot.

Chapter 2

Aims and Hypothesis

At present, the most commonly used methods for cancer diagnosis in oncology are imaging techniques (US, CT, MRI). These methods are also used to evaluate a selected therapy's efficacy. Among the new imaging techniques used in pre-clinical research is LA-ICP-MS. This technique can provide 2D or 3D high-resolution images of the quantitative distribution of the analytes relevant for cancer diagnosis and therapy in samples like tumour spheroid models or tumour tissue at a low ng/g concentration. Quantitative images provided by LA-ICP-MS can help us to better understand the pharmacological characteristics (kinetics and mode of action) of the metal-based drugs used in therapy. The spatial distribution and concentration values shown in the images are of crucial importance, as they are directly responsible for the efficiency of the selected cancer therapy.

Pt-based chemotherapeutics are widely used in cancer therapy. After application, information about their quantitative spatial distribution in tumours or sections of tumour tissues can be provided by LA-ICP-MS. In this work, CDDP, one of the oldest chemotherapeutics, which is still commonly used in cancer therapy, was chosen for the Pt distribution imaging by LA-ICP-MS. Tumour spheroids and tumour tissue samples were analysed. Additional reasons for the selection of CDDP were the extensive published literature on the use of this chemotherapeutic at the pre-clinical and clinical level (better interpretation and comparison of the results with those published) and the fact that Pt is not normally present in tissues (making imaging easier).

In this regard, the purpose of the doctoral research was to develop a versatile imaging method based on the use of LA-ICP-MS for the quantitative determination of Pt in tumour spheroids and tumour tissues. The developed method represents a new tool that supports established analytical methodologies in oncological studies. The possibility of using the developed LA-ICP-MS for the localization of metals in plant tissue was further demonstrated, extending the possibilities of its application in the other branches of natural science.

The main goal of the doctoral dissertation was to develop a reliable analytical method for the quantitative bioimaging of Pt-based chemotherapeutic drugs in tumour spheroids and tumour tissues by LA-ICP-MS. The specific goals were:

- To optimize and synchronize the parameters of the LA-ICP-MS set-up for stable, sensitive and repeatable measurements with a high spatial resolution of the images created.
- To develop reliable quantification methods for the imaging of Pt in tumour spheroids and tumour tissues treated with CDDP. For this purpose, matrix-matched standards, which are homogeneous, uniform and have known thickness, were used. Alternatively, the ID technique was used for the quantification.

- To compare the spatial distribution of the Pt in tumour spheroids treated with CDDP and TR-CDDP. The comparison was based on quantitative images created by LA-ICP-MS. The ID technique was applied for the quantification.
- To compare the distribution of the TR-CDDP in the tumour spheroids analysed first by confocal fluorescence microscopy and then by LA-ICP-MS, with the ID technique applied for the quantification of the Pt.
- To provide 3D images of spheroids treated with cisplatin or TR-cisplatin using ID-LA-ICP-MS.
- To describe the drug distribution and kinetics in tumour samples by assessing the data from the created images.
- To extend the applicability of the developed LA-ICP-MS method for other solid biological samples, plant leaves were chosen as an example.

Chapter 3

Materials and Methods

3.1 Reagents and Material

Ultrapure water (18.2 MΩ cm) was obtained from a Direct-Q 5 Ultrapure water system (Millipore Watertown, MA, USA). Merck (Darmstadt, Germany) stock Pt solution (1000 mg L^{-1} ± 10 mg L^{-1} in 8% HCl) was used for the preparation of the calibration standard solutions for the determination of Pt concentrations in the analysed samples. Cisplatin was obtained from Medoc (Hamburg, Germany). Texas Red cisplatin (TR-CDDP) was supplied by Ursa BioScience™ LLC (Abingdon, MA, USA). Platinum enriched in the ^{194}Pt isotope (Pt metallic plate, 15 mg) was obtained from Oak Ridge National Laboratory (Oak Ridge, TN, USA). It was dissolved in 1 mL of *aqua regia* and diluted to 10 mL with an appropriate amount of HCl, so that the final concentration of HCl was 8%. The declared composition of the enriched Pt plate was 96.45% ± 0.05%, 2.46% ± 0.05%, 0.87% ± 0.02%, 0.18% ± 0.01%, 0.03% ± 0.00% and 0.01% ± 0.00% for the isotopes 194, 195, 196, 198, 192 and 190, respectively. The concentration of the ^{194}Pt standard was determined with reverse ID-ICP-MS. A stock standard solution of Cr(III)-nitrate (1000 ± 2 mg L^{-1} in 5% HNO_3), from Merck (Darmstadt, Germany), was used for the preparation of the calibration standards. Nitric acid (HNO_3, 65%), hydrochloric acid (HCl, 37%), hydrogen peroxide (H_2O_2, 30% solution in water) of suprapure grade and ethylenediaminetetraacetic acid (EDTA) of pro analysis grade were obtained from Merck. Rhodium (1000 ± 2 mg L^{-1} Rh in 8% HCl) and iridium 1000 ± 8 mg L^{-1} Ir in 7% HCl) stock solutions purchased from Merck were used as internal standards in the ICP-MS determinations. Tris(hydroxymethyl)aminomethane (Tris) ultrapure from Goldbio (St. Louis, Missouri, USA) was used for buffer preparation. Working standard solutions were prepared daily by appropriate dilution with ultrapure water. Gelatine from porcine skin (gel strength 300, Type A) and agarose was purchased from Sigma-Aldrich (Steinheim, Germany). Grace Bio-Labs HybriWell™ adhesive chamber sealing systems (9.8 mm × 20 mm × 0.25 mm, 50 µL, ports diameter 1.5 mm) (Sigma-Aldrich) were used to manufacture gelatine and agar standards. Advanced Minimal Essential Medium (AMEM), fetal bovine serum (FBS) and L-glutamine (GlutaMAX) were obtained from Thermo Fisher Scientific (Waltham, MA, USA). Penicillin was purchased from Grünenthal (Aachen, Germany), gentamicin from Krka (Novo mesto, Slovenia), Mycoplasma Detection kit (MycoAlert™) from Lonza (Basel, Switzerland), trypsin from Gibco, Life Technologies Corporation (Grand Island, NY, USA) and phosphate-buffered saline (PBS) from Sigma-Aldrich. Human colon adenocarcinoma cells (HT29), murine melanoma cell line (B16F10) and murine mammary carcinoma cells (4T1) were obtained from American Type Culture Collection (ATCC, Manassas, VA, USA) and cultured in 75 cm^2 flasks (Corning®, Corning, NY, USA). Spheroids were prepared and cultured in round-bottom 96-well plates (Corning®). Tissue-tek® O.C.T.™ Compound (Sakura Finetek,

Tokyo, Japan) was used as an embedding medium for cryosectioning. Frozen sections were stored on glass slides SuperFrostPlus™ (Thermo Fisher Scientific, Waltham, MA, USA). SPS-SW1 Quality Control Material for Surface Water Analysis purchased from SPS Spectrapure Standards AS (Oslo, Norway), the certified reference materials CRM 320R Trace Elements in River Sediment, Community Bureau of Reference (Geel, Belgium) and SRM 1573a Tomato leaves purchased from the National Institute of Standards and Technology (NIST), (Gaithersburg, MD, USA) were used to check the accuracy of the total Cr determinations in plants. The stability check and tuning of the LA-ICP-MS measurement were performed with SRM 612 Trace Elements in a Glass standard reference material obtained from NIST. 0.45 µm nitrocellulose filters (25 mm diameter) obtained from Sartorius were used to prepare calibration standards in the LA-ICP-MS procedure. SuperFrost Microscope Slides for fixing the sample and calibration standards were obtained from VWR (Radnor, PA, USA).

3.2 Instrumentation

For the sample imaging, Analyte G2 193 ArF excimer laser ablation with a HelEx II low-dispersion ablation cell (Teledyne Photon Machines Inc., Bozeman, MT, USA) was coupled to an Agilent 8800 ICP-QQQ-MS (Agilent Technologies Inc., Tokyo, Japan) via an Aerosol Rapid Introduction System (ARIS), (Teledyne Photon Machines). HDIP imaging software (Teledyne Photon Machines) was used to create and calculate the elemental distributions of the sample. For the determination of the total concentrations in the samples and standards, Agilent 7900 ICP-MS (Agilent Technologies) was used. For tumour sample preparation, two centrifuges were used (Centrifuge 5430; Eppendorf, Hamburg, Germany and Kendro Heraeus Multifuge®1S-R; Thermo Electron Corporation, Waltham, MA, USA). The cryostat (Leica CM1850, Wetzlar, Germany) was used to cut frozen sections. Representative photographs of the spheroid sections were captured using an LSM 800 Confocal Microscope (Zeiss Confocal LSM 800, Zeiss, Oberkochen, Germany). A Mettler Toledo MS104 (Zürich, Switzerland) analytical balance was used for the weighing. The pH was measured with a WTW pH meter 3110 (Weilheim, Germany).

3.3 Sample Preparation

The sample preparation strategies in LA-ICP-MS greatly depend on the type of tissue being examined [64], [123]–[126]. During the sample preparation, the chemical composition and the distribution of the analyte within the sample must be preserved [124], [126]. For LA-ICP-MS imaging, the tumour and tissue samples are usually embedded in an appropriate matrix for cryostat sectioning (e.g., Tissue-Tek composed of water-soluble glycols and resins, or paraffin blocks) [59], [108]. Biological samples are primarily prepared as cryo-sections on glass slides, with the tissue thickness ranging from 5 to 20 µm [125], [127]–[129].

3.3.1 Preparation of cell cultures

HT29, B16F10 and 4T1 cells were cultured in AMEM supplemented with 5% FBS, 10 mM L-glutamine, 100 U mL^{-1} penicillin and 50 mg mL^{-1} gentamicin under standard conditions (5% CO_2 humidified incubator at 37 °C). Cells were tested with a mycoplasma detection kit and found to be mycoplasma negative.

3.3.2 Preparation of multicellular tumour spheroids

The procedure from this chapter was published by the author in Marković et al. (2021) [25].

For the spheroid production, HT29 cells were harvested from culture flasks with 80% confluency. Specifically, cells were trypsinized, washed once with PBS buffer, counted, and 1500 HT29 cells in 200 µL of AMEM per well were seeded in round-bottom 96-well plates. After centrifugation (2 minutes, 1000 rpm), the plate was incubated for 3 days under standard culturing conditions. The resulting spheroids with a diameter of 250–300 µm contained an outer rim, intermediary layer and necrotic core. Then, the medium was removed, and the spheroids were treated by adding 100 µL of AMEM with the appropriate drug concentration to each well so that the final concentration of CDDP (100 µM or 500 µM) or TR-CDDP (100 µM) in the spheroid medium was obtained. After 1 h of incubation under standard culturing conditions, spheroids were washed twice with PBS, embedded in Tissue-Tek, frozen in liquid nitrogen and stored at -20 °C. For the LA-ICP-MS measurements, samples were cryo-sectioned into consecutive slices of 20 µm thickness with a cryostat, placed onto glass slides, air dried and stored, protected from light, at 4 °C until analysis.

3.3.3 Preparation of mice tumour samples

At 80% cell confluence, trypsinization was performed with 0.25% trypsin/EDTA, and the cells were washed using AMEM with FBS and collected by centrifugation. The cells were routinely checked for the presence of Mycoplasma. The tumours were induced on the back of the mice with the injection of 100 µL of B16F10 or 4T1 cell suspension containing one million cells. Female C57Bl/6JOlaHsd mice (Envigo RMS SrL, San Pietro al Natisone, Italy), 7 weeks old, weighing 18–20 g, were housed under specific pathogen-free conditions at a temperature of 20–24 °C and with a relative humidity of 55 ± 10%, a 12-hour light/dark cycle, and were provided with food and water. All the procedures were performed according to the guidelines for animal experiments in the EU directive (2010/63/EU). Regulatory approval was issued by the Veterinary Administration of the Ministry of Agriculture and the Environment of the Republic of Slovenia (No. U344011/2015/38). The tumours were first allowed to grow, and then they were exposed to the CDDP drug with an intravenous or intratumoral injection, all with a dose of 4 mg/kg [130]. After a specific amount of time, shown in Table 3, the mice were humanely sacrificed, and the tumours were removed. One half was embedded in Tissue-Tek, frozen in liquid nitrogen and cryo-sectioned into slices of 10 µm thickness with a cryostat, placed onto glass slides, air dried and stored, and protected from light at 4 °C until LA-ICP-MS analysis. The other half was transferred into pre-weighed plastic tubes and then weighed again. 0.2 mL H_2O_2 and 0.2 mL HNO_3 were added to tubes containing the tumour samples. The tubes were closed with plastic caps and sealed with Teflon tape. The samples were left at 80 °C for 24 h to digest. The digested samples were diluted with ultrapure water and weighed. The Pt concentration in the digested samples was determined by ICP-MS using ^{193}Ir as an internal standard.

Table 3: Time of tumour removal after the CDDP injection's administration.

Intravenous		Intratumoral	
B16F10	4T1	B16F10	4T1
3 min	1 min	1 min	1 min
10 min		5 min	5 min
		10 min	10 min
		20 min	

3.3.4 Dandelion sampling and preparation for LA-ICP-MS Cr mapping

The procedure from this chapter was published by the author in Marković et al. (2022) [131].

Dandelion (*Taraxacum officinale*) plants grown in field soil with high Cr content at village Vranja Peč (municipality of Kamnik) were collected in plastic vessels. The field soil in Vranja Peč was for 17 years treated with tannery waste, while dandelion sampling was performed 37 years after the last tannery waste application. The dandelion leaves were washed with ultrapure water to remove soil and dust, left for an hour to dry and attached to a glass slide using double-sided scotch tape so that the leaf was completely flat on the tape. The leaf was then left to dry at room temperature for one week.

3.4 Preparation of Pt Calibration Standards

3.4.1 Preparation of gelatine calibration standards

The procedure from this chapter was mostly published by the author in Marković et al. (2021) [25].

Gelatine standards for tumour spheroids analysis were prepared using gelatine from porcine skin. Gelatine from porcine skin was selected since it exhibits cross-linking structures and thus immobilizes the Pt and prevents leaching (the "coffee-stain" effect). 500 mg of gelatine was dissolved in 5 mL of 100 mM Tris-HCl + 10 mM EDTA buffer solution (pH 7.4) with the Pt standard added in different concentrations. The addition of buffer prevented denaturation of proteins and maintained the integrity of gelatine after the addition of the acidic Pt standard solution. Gelatine was heated to 55 °C on a hotplate until it was liquefied and homogenized. Then, it was pipetted into heated HybriWell chambers connected by adhesion on a glass slide. HybriWell sealing system was used as a mould enabled to prepare gelatine standards with a uniform thickness. Gels were rapidly frozen and left at -24 °C for 30 min, enabling the preservation of their shape and thickness when removing the mould for drying. After the mould was removed, frozen gels remained on a glass slide and were left overnight to dry at room temperature. After drying, the gels retained their original shape and size, but their thickness shrank tenfold from 250 to ~25 µm.

Gelatine standards for the analysis of tumours grown on mice were prepared in an almost identical procedure as described previously for tumour spheroids, except that a larger amount of gelatine was prepared with a wider Pt concentration range, and instead of the hotplate, a microwave was used for the gelatine liquefication and homogenisation (faster and easier preparation). The spiked gelatine was then pipetted into preheated Grace Bio-Labs hybridization chambers with preheated pipette tips. The gels were left at -24 °C

for 30 min, the mould was removed, and the gels were left to dry overnight at room temperature.

In order to determine the Pt concentration, the gelatine standards for tumour spheroids and tumours were pipetted into a premeasured plastic cylinder, weighed again, filed with ultrapure water to 10 mL, closed and weighed again, and then left for 48 h at 80 °C in the oven to dissolve the gelatine. Total Pt concentrations in the gelatine were determined by the ICP-MS. To determine the standard homogeneity, standards were measured using LA-ICP-MS with parallel line scans applying the same measurement conditions as used in the samples.

3.4.2 Preparation of gelatine droplet as a standard for quantification

Gelatine standards with added Pt were prepared in the same way as previously described, but without pouring the standard into the HybriWell sealing system, a single drop from each Pt concentration range was placed onto a glass slide. The glass slide was air dried at room temperature and then stored until the analysis.

3.4.3 Preparation of single cells as a quantification standard

HT29 cells cultured in the same way as for the spheroid samples. The cells were taken from the flask and mixed with CDDP in AMEM with different drug concentrations for each well. After incubation, the cells were washed with PBS. With the use of the citospin deposition method, cells from each concentration level were deposited on a glass slide. The cells were then left to air dry and stored, protected from the light, at 4 °C until analysis.

3.4.4 Preparation of filter paper calibration standards

The procedure from this chapter was partialy described by the author in Marković et al (2022) [131].

The calibration standards were prepared using 0.45 µm nitrocellulose paper filters with a 25 mm diameter. 20 µL of Pt standard in five different concentrations were pipetted into the centre of the filters and allowed to air dry for 5 h. Six spiked filters (blank and five Pt standards) were weighed and transferred to a 10 mL graduated polyethylene tube. The filters were dissolved by adding 0.5 mL of HNO_3 and 0.5 mL of H_2O_2. The tubes were sealed with caps and Teflon tape. The samples were left at 80 °C overnight to digest the contents. Each tube was then filled to 5 mL with ultrapure water and weighed, and the Pt concentration in the dissolved filters was determined by ICP-MS. Parallel aliquots of the filters for each Pt concentration level were attached on a glass slide using a double-sided Scotch tape so that all the Pt calibration standards were present on one glass slide. To determine the standards' homogeneity, the standards were measured by LA-ICP-MS with parallel lines scan, applying the same measurement conditions as used for the tumour spheroid samples.

3.5 Analytical Procedures for Tumour Sample Imaging

3.5.1 Analytical procedure for laser ablation imaging of tumour spheroids

The procedure from this chapter was published by the author in Marković et al. (2021) [25].

The procedure was optimized for a high resolution and a short analysis time while maintaining an adequate Pt sensitivity. It should be emphasised that the high resolution and a short analysis time applies for the LA technique. The laser beam was 5 µm square-shaped spot, which provided an even energy delivery with 2.5 J cm^2 fluence. Its repetition rate was 100 Hz, while the scan speed was 40 µm s^{-1} with connected parallel lines. The total dwell time on the ICP-MS was 0.1 s per cycle for measuring both the ^{195}Pt or the ^{194}Pt and ^{195}Pt isotopes. ARIS was used for rapid analysis with good signal retention. The washout time of a single laser pulse was determined to be 58 ms with the above-described measurement parameters. A helium carrier gas was used (0.45 L min^{-1}) to introduce a sample aerosol into the ICP. Argon make up gas (0.95 L min^{-1}) was introduced through the ARIS mixing bulb. If used, each level of the gelatine calibration standard was ablated with three lines before and after sample ablation with identical line parameters as the sample. HDIP software was used for the LA-ICP-MS imaging with a convolution factor of two, which allowed an enhancement of the spatial resolution of imaging to 2.0 µm × 2.5 µm per pixel.

The LA parameters are presented in Table 4.

Table 4: Laser operating parameters.

Instrument	Analyte G2
Parameter	Type/Value
Wavelength	193 nm
Sample chamber	HelEx-II
Laser energy (Fluence)	2.5 J cm^{-2}
Laser beam size	5 µm × 5 µm (square)
Scanning speed	40 µm s^{-1}
Repetition rate	100 Hz
Carrier gas flow (He)	0.45 L min^{-1}

The ICP-MS parameters are presented in Table 5.

Table 5: ICP-MS operating parameters.

Method	LA-ICP-MS	ID-LA-ICP-MS	ICP-MS
ICP-MS instrument	Agilent 8800	Agilent 8800	Agilent 7900
Parameter	Type/Value Elemental analysis	Type/Value Elemental analysis	Type/Value Elemental analysis
Aerosol introduction	ARIS	ARIS + Micromist nebulizer	Micromist nebulizer
Spray chamber	/	Scott	Scott
Skimmer and sampler	Ni	Ni	Ni
Forward power	1600 W	1600 W	1600 W
Plasma gas flow (Ar)	15.0 L min^{-1}	15.0 L min^{-1}	15.0 L min^{-1}
Carrier gas flow (He)	0.45 L min^{-1}	0.45 L min^{-1}	/
Carrier gas flow (Ar)	0.95 L min^{-1}	0.95 L min^{-1}	1.05 L min^{-1}
Dilution gas flow (Ar)	/	/	/
Make up gas flow (Ar)	/	/	0.10 L min^{-1}
Total carrier gas flow	1.30 L min^{-1}	1.30 L min^{-1}	1.15 L min^{-1}
Oct bias	-85 V	-85 V	-115 V
Cell entrance	-40 V	-40 V	-30 V
Cell exit	-50 V	-50 V	-50 V
Deflect	12.0 V	12.8 V	13.8 V
Plate bias	-50 V	-50 V	-35 V
Data acquisition parameters			
m/z of isotopes monitored	^{194}Pt, ^{195}Pt	^{194}Pt, ^{195}Pt	^{194}Pt, ^{195}Pt

3.5.2 Analytical procedure for laser ablation imaging of mice tumours

Prior to the sample analysis, a mosaic image of the sample was taken with an LA integrated camera. Since the sample area varied widely, the following LA parameters were chosen as a compromise between the highest achievable resolution and time of analysis for all of the samples.

The laser beam was set to a 10 µm square-shaped spot, which provided an even energy distribution of 3.5 J cm^2 fluency. The laser beam repetition rate was set to 100 Hz, while the scan speed was 100 µm s^{-1} with connected parallel lines, but without overlapping. The total dwell time on the ICP-MS was 0.1 s per cycle, and only 195 *m/z* was measured. The aerosol of the ablated sample was carried by a helium carrier gas (0.6 L min^{-1} flow, 6.0 purity) to the ICP through the ARIS. Argon make-up gas (0.95 L min^{-1} flow, 5.0 purity) was introduced through the ARIS mixing bulb. The optimal parameters resulted in a spatial resolution of 10 µm x 10 µm (x 10 µm depth – thickness of the tumour samples) per pixel. The LA-ICP-MS system was tuned daily using NIST 612 standard reference material. The same parameters applied to the tumour samples were used on the matrix-matched gelatine calibration standards. Each level of the gelatine calibration standard was

ablated with three lines before and after the sample ablation with identical line parameters. HDIP software was used for the LA-ICP-MS imaging.

The LA parameters are presented in Table 6.

Table 6: Laser operating parameters.

Instrument	Analyte G2
Parameter	Type/Value
Wavelength	193 nm
Sample chamber	HelEx-II
Laser energy (Fluence)	3.5 J cm^{-2}
Laser beam size	10 µm × 10 µm (square)
Scanning speed	100 µm s^{-1}
Repetition rate	100 Hz
Carrier gas flow (He)	0.6 L min^{-1}

The ICP-MS parameters are presented in Table 7.

Table 7: ICP-MS operating parameters.

Method	LA-ICP-MS	ICP-MS
ICP-MS instrument	Agilent 8800	Agilent 7900
Parameter	Type/Value Elemental analysis	Type/Value Elemental analysis
Aerosol introduction	ARIS	Micromist nebulizer
Spray chamber	/	Scott
Skimmer and sampler	Ni	Ni
Forward power	1550 W	1550 W
Plasma gas flow (Ar)	15.0 L min^{-1}	15.0 L min^{-1}
Carrier gas flow (He)	0.60 L min^{-1}	/
Carrier gas flow (Ar)	0.95 L min^{-1}	1.05 L min^{-1}
Dilution gas flow (Ar)	/	/
Make up gas flow (Ar)	/	0.10 L min^{-1}
Total carrier gas flow	1.55 L min^{-1}	1.15 L min^{-1}
Oct bias	-8.0 V	-8.0 V
Cell entrance	-40 V	-26 V
Cell exit	-50 V	-50 V
Deflect	12.6 V	15.8 V
Plate bias	-50 V	-50 V
Data acquisition parameters		
m/z of isotopes monitored	^{195}Pt	^{195}Pt

3.5.3 Procedure for fluorescence microscopy imaging of TR-CDDP treated HT29 spheroids

The procedure from this chapter was published by the author in Marković et al. (2021) [25].

The TR-CDDP treated spheroids were imaged using a confocal microscope with a 20× Plan-Apocromat objective and a numerical aperture of 0.8. For visualization of the TR-CDDP, a laser providing excitation light at a wavelength of 561 nm was used. The emitted light was collected with a gallium arsenide phosphide (GaAsP) detector via a variable dichroic at 576–700 nm. Additionally, for the detection of spheroids, the electronically switchable illumination and detection module (ESID) was used, which combines transmitted light illumination and detection. Images of the spheroid slices were acquired by tile scanning and were processed by stitching.

3.6 Quantification Procedure

3.6.1 External calibration with a solid standard

In order to quantify the analyte in the sample, besides the signal intensity, several parameters must be considered. First, the mass of the ablated sample and the standard need to be calculated. For this, the area of the ablation per pixel is calculated. In the case of a square spot, the size of the spot (e.g., 5 µm) is multiplied by the ablation line speed (e.g., 50 µm s^{-1}) and multiplied by the time for a pixel's acquisition (e.g., 0.1 s), resulting in the sample area (total area of this example is 25 $µm^2$). To calculate the volume, the area is multiplied by the ablation depth. Since it is almost impossible to control the depth of the laser beam's penetration, the sample or standard must have a small thickness, enabling complete sample ablation. To convert it to mass, the pixel volume is multiplied by the density. Equation (1) is presented below:

$$m_S = d_S \; V_S = d_S \; h \; x \; y \; t \tag{1}$$

Where m_S is the sample mass, d_S is the sample density, V_S is the sample volume per pixel, which in turn was calculated by multiplying the height of the sample (h), the ablation line diameter (x), the laser scanning speed (y) and the time of pixel acquisition (t).

By ablating standards in different concentrations, a calibration curve is fitted with the elemental signal response per standard concentration. The result can then be converted to the sample concentration by applying the difference of the mass factor (equation (2)).

$$C_S = \frac{C_{Std} \; m_{Std}}{m_S} \tag{2}$$

Where C_S is the concentration of the sample, C_{Std} is the concentration of the standard resulting from the sample signal intensity fitted to the calibration curve and m_{Std} is the mass of the standard (calculated in the same way as the sample mass (m_S)).

3.6.2 Isotope dilution

The procedure from this chapter was published by the author in Marković et al. (2021) [25].

During the sample ablation, isotopically enriched ^{194}Pt (150.18 ng L^{-1}) was nebulized into the spray chamber through a Micromist nebulizer connected to a 0.25 mm tube, submerged in an isotopic solution. The negative pressure created from the Ar flow (0.95 L min^{-1}, set as carrier gas on ICP-MS) pumped the isotopic standard into the ICP without the assistance of a peri pump. The HelEx II sample chamber of the LA was coupled to the ICP-MS via ARIS tubing connected to a dilution gas inlet, using helium (0.45 L min^{-1}) as the carrier gas. The position of the ARIS tubing was optimized in such a way that the maximum sensitivity and stability of the signal throughout multiple days of measurement were ensured. In order to re-create the image areas in the sample with high and low Pt concentrations, the signal-to-noise ratio was adjusted so that the areas with low analyte concentrations could be detected. For this purpose, the enriched isotopic ^{194}Pt solution was appropriately diluted with ultrapure water, enabling the detection of the areas with low Pt contents in the sample analysed in the presence of the background signal arising from the enriched isotopic ^{194}Pt solution, which contained $2.46\% \pm 0.05\%$ of ^{195}Pt. Namely, lower concentrations of enriched ^{194}Pt solution provide the minimum ^{195}Pt background signal.

For the calculation of areas with Pt content, the mass flow of Pt was plotted versus time throughout the ablation period. To determine the mass flow, an enriched ^{194}Pt solution was aspirated during the ablation period via the Micromist nebulizer and the waste was collected. To account for nebulization efficiency, the mass of ^{194}Pt solution aspirated, reduced by the mass of waste collected, corresponded to the mass introduced into the ICP. When the mass introduced into the ICP was divided by the mass of ^{194}Pt solution aspirated, nebulization efficiency was obtained and determined to be 15%. Based on twelve measurements, the Pt solution nebulisation mass flow was determined to be 0.0274 mL min^{-1} with an RSD of 3.15%.

To calculate the Pt content in the sample by online ID-LA-ICP-MS, the instrument mass bias factor (K) was first determined (equation (3)).

$$K = \frac{\frac{R_m}{R_n} - 1}{\Delta m} \tag{3}$$

K was calculated as a ratio from the measured signal ratio R_m (^{195}Pt/^{194}Pt) of the standard with the natural abundance of isotopes introduced into the plasma in the same way as the enriched ^{194}Pt isotopic spike solution during the online ID analysis and the natural abundance ^{195}Pt/^{194}Pt ratio R_n, corrected for the mass difference between the masses of the measured isotopes ^{195}Pt and ^{194}Pt (Δm).

Corrected Pt isotopic ratios (R_{corr}) were obtained using a linear equation for mass bias correction (equation 4).

$$R_{corr} = \frac{R_m}{(1+K\Delta m)} \tag{4}$$

In order to determine the Pt concentration in the sample (C_S), the mass flow (MF_S) was calculated using equation (5) adapted from [115]:

$$MF_S = C_{Sp}\, f_{Sp}\, t \frac{AW_S^a}{AW_{Sp}^b} \frac{A_{Sp}^b}{A_S^a} \left(\frac{R_m\text{-}R_{Sp}}{1\text{-}R_m R_S}\right) \tag{5}$$

Where C_{Sp} is the concentration of the spike, f_{Sp} is the flow rate of the spike introduced into the plasma, t is the time of the pixel acquisition, AW_S^a is the molar mass of the sample (^{195}Pt), AW_{Sp}^b is the molar mass of the spike (^{194}Pt), A_{Sp}^b is the isotopic abundance of the spike (^{194}Pt), A_S^a is the isotopic abundance of the sample (^{195}Pt), R_m is the isotope ratio a/b

in the mixture, where a is the ^{195}Pt isotope in the sample and b is the ^{194}Pt isotope in the spike, R_S is the isotope ratio b/a in the sample and R_{Sp} is the isotope ratio ^{195}Pt/^{194}Pt in the spike.

To determine the sample mass, equation (1) from paragraph 3.6.1 was used. Finally, equation (6) is used to calculate the Pt concentration (C_S) in the sample.

$$C_S = \frac{MF_S}{m_S} \tag{6}$$

Each pixel is calculated independently, with MF_S as the only variable between the pixel values under the same measurement conditions.

3.7 Analytical Procedures for Dandelion Leaf Imaging

The procedures from this chapter were mostly described by the author in Marković et al (2022) [131].

3.7.1 Analytical procedure for laser ablation imaging of the dandelion leaf

The laser beam was 35 µm square-shaped spot, which provided an even energy delivery with 3.5 J cm^2 fluency. Its repetition rate was 50 Hz, while the scan speed was 200 µm s^{-1} with connected parallel lines. The total dwell time on ICP-MS was 0.2 s per cycle. ARIS was used for rapid analysis with good signal retention. Helium carrier gas (0.6 L min^{-1}) was used to introduce a sample aerosol into the ICP. Argon make-up gas (1.05 L min^{-1}) was introduced through the ARIS mixing bulb. The LA-ICP-MS system was tuned daily using NIST 612 standard reference material. HDIP software was used for the LA-ICP-MS imaging.

The LA parameters are presented in Table 8.

Table 8: Laser operating parameters.

Instrument	Analyte G2
Parameter	Type/Value
Wavelength	193 nm
Sample chamber	HelEx-II
Laser energy (Fluence)	3.5 J cm^{-2}
Laser beam size	35 µm × 35 µm (square)
Scanning speed	200 µm s^{-1}
Repetition rate	50 Hz
Carrier gas flow (He)	0.60 L min^{-1}

The ICP-MS parameters are presented in Table 9.

Table 9: ICP-MS operating parameters.

Method	LA-ICP-MS
ICP-MS instrument	Agilent 8800
Parameter	Type/Value
Aerosol introduction	ARIS
Spray chamber	/
Skimmer and sampler	Ni
Plasma conditions	
Forward power	1550 W
Plasma gas flow (Ar)	15.0 L min^{-1}
Carrier gas flow (He)	0.6 L min^{-1}
Carrier gas flow (Ar)	1.05 L min^{-1}
Dilution gas flow (Ar)	/
He collision gas flow	2.5 mL min^{-1}
Total carrier gas flow	1.65 L min^{-1}
QP bias	-2.0
Oct bias	-18.0 V
Cell entrance	-40 V
Cell exit	-50 V
Deflect	-5.0 V
Plate bias	-50 V
Data acquisition parameters	
m/z of isotopes monitored	^{52}Cr

3.7.2 Preparation of filter paper calibration standards for LA-ICP-MS Cr mapping

The calibration standards were prepared using 0.45 µm nitrocellulose paper filters with a 25 mm diameter. 20 µL of Cr standard in five different concentrations were pipetted into the centre of the filters and allowed to air dry for 5 h. After drying, a 5 mm circle was cut from the centre of the filter paper with a hollow-hole puncher. This was done to minimize the uneven distribution of Cr throughout the filter paper due to the "coffee stain" effect caused by drying. Six cut-outs (one blank and five Cr standards) were weighed and transferred to a 10 mL graduated polyethylene tube. The cut-outs were dissolved by adding 0.2 mL of HNO_3 and 0.2 mL of H_2O_2, the tubes were then sealed with caps and Teflon tape. The samples were left at 80 °C overnight to digest the contents. Each tube was then filled with 2 mL of ultrapure water and weighed, and the Cr concentration in the dissolved filters was determined by ICP-MS. Parallel aliquots of a further six filter cut-outs for each Cr concentration level were attached to a glass slide using double-sided Scotch tape so that all the Cr calibration standards were present on one glass slide. To determine the standard homogeneity, standards were measured on LA-ICP-MS with parallel line scans with the same measurement conditions used on the applied sample.

3.7.3 Preparation of agarose calibration standards for LA-ICP-MS Cr mapping

The Cr agarose standards for the LA-ICP-MS analysis of dandelion leaves were prepared in a similar way to that described previously for Pt gelatine standards. Cr solutions with different Cr concentrations were prepared in 10 mM EDTA and 100 mM Hepes buffer (pH 6.5). Agarose was added in different amounts in the prepared Cr solutions so that its final concentration was 2%. Microwaves were used for the agarose gel liquefication and homogenisation. However, in the highest concentration of Cr standard, the pH had dropped to 3.2. Homogenised agarose was pipetted into the preheated Grace Bio-Labs hybridization chambers and left at -24 °C for 30 min to freeze. The mould was removed, and gels were left overnight to dry at room temperature. The total Cr concentrations in the agarose standards were determined by ICP-MS. To determine the standard homogeneity, the standards were measured by LA-ICP-MS with parallel line scans with the same measurement parameters used on the dandelion leaf samples (Tables 8 and 9).

3.7.4 Preparation of CRM 1573a as a standard for LA-ICP-MS Cr mapping

Certified reference material 1573a Tomato leaves was used for the quantification of the dandelion leaves samples. Since this CRM is in powder form, a pellet press was used to create a flat, solid pellet, which should provide even ablation. Since the CRM was pressed without deformation, no filler (like paraffin or epoxy) was used.

Chapter 4

Results and Discussion

4.1 Optimization of the Ablation Procedure

Optimisation and synchronisation of the ablation and measuring parameters are crucial steps in the development of the LA-ICP-MS analysis. A poorly optimised method introduces signal degradation, which leads to artefacts such as blur, smearing, aliasing and signal noise. The optimised parameters are a compromise between the signal strength, the image resolution and the time of analysis. Since the tumour spheroids have a small diameter, ranging from 200 µm to 600 µm, the time of analysis was not an issue, and optimisation was a compromise between the sensitivity and resolution. To achieve the best parameters for the ablation procedure, the following parameters were optimised:

- Sensitivity – ICP-MS tuning parameters were adjusted in such a way as to provide the maximum signal response while ablating a gelatine standard containing Pt.
- Gas flow – He flow from LA and Ar flow from ICP-MS were adjusted to reduce sample trailing and achieve high sensitivity (the addition of the ARIS sample introduction system significantly reduced the sample trailing by reducing the sample washout time and allowed images to be generated faster and more clearly).
- ICP-MS acquisition time and LA frequency – these two parameters were synchronised to avoid image degradations (such as aliasing) in such a way as to have no variation of LA pulses per one ICP-MS acquisition cycle.
- Laser energy – was adjusted to achieve complete ablation without visible sample melting, which could induce elemental fractionation.
- Laser scanning speed – was adjusted, taking into account the size of the pixel and the sensitivity, while trying to maintain the square shape of the image pixel.
- Laser spot size – was adjusted to achieve the highest possible resolution while maintaining a signal strength sufficient for good resolution of the low-concentration differences within the sample.

All of the parameters were tested in different settings. The optimised parameters are presented in Section 3.5.1. To demonstrate the importance of the parameters' optimisation, different ablation procedures and their influence on the results are shown in Figure 3. The images in Figure 3 are from HT29 tumour spheroids, similar in size and concentration.

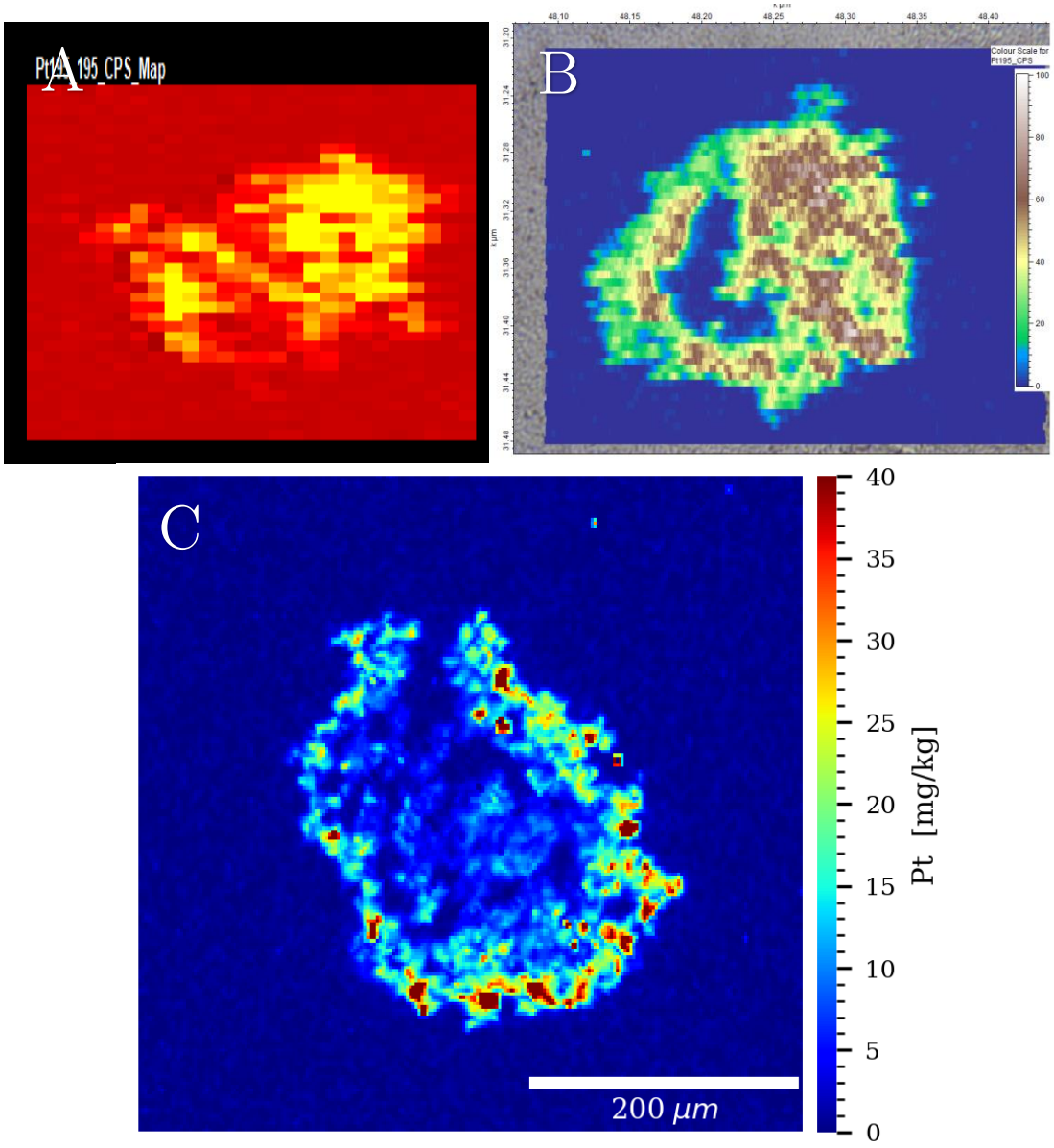

Figure 3: Optimization timeline for the measuring parameters on HT29 tumour spheroids A) Measurements with low resolution and sensitivity B) Improved parameters C) Optimal parameters.

The data from Figure 3 A demonstrate that a measurement with low resolution and sensitivity results in visible blurring. Improved measurement parameters (Figure 3B) provide better resolution and sensitivity, but with blurring still present, while under the optimized parameters (Section 3.5.1, Figure 3C), significantly better resolution and sensitivity without image burring are obtained.

4.2 Quantification Approaches for Imaging of Tumour Spheroids by LA-ICP-MS

For a reliable quantification of the analyte using LA-ICP-MS, it is necessary to know the amount of sample and the standard intake per one cycle of the ICP-MS. The lack of this knowledge makes the measurements semi-quantitative.

Different quantification approaches were tested to obtain a reliable method for quantifying the Pt in tumour spheroids.

4.2.1 Quantification of Pt using spiked filter paper

The Pt spiked filter paper standard was prepared according to the procedure described in Section 3.4.4. The filter paper was ablated using identical parameters to the tumour spheroid samples. The signal intensities are shown in Figure 4.

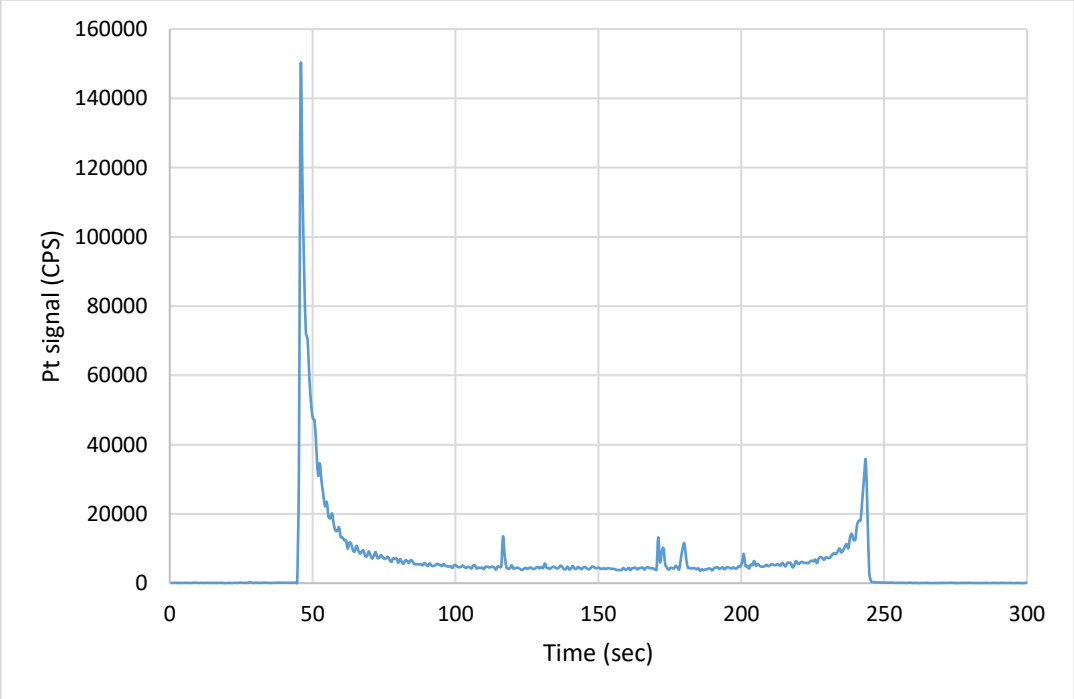

Figure 4: Signal intensities obtained from the ablation of the filter paper spiked with Pt standard.

As can be seen from Figure 4, the signal sampled with a straight line across the entire diameter of the filter is not stable. The signal intensity is significantly higher at the beginning of ablation and drops as the line progress across the standard, until it reaches the end where it rises again. This is related to the "coffee stain" effect. Such inhomogeneous analyte distribution in a calibration standard makes it useless for quantification. Additionally, the filter standard was too thick for the laser beam to penetrate it entirely under the same measuring parameters. It would require much stronger beam parameters for through ablation. Therefore, it is not possible to know how much Pt from standard enters the plasma. These problems and the difference in matrix composition between the standard and the sample make this calibration approach unreliable for Pt quantification in tumour samples. However, if "coffee stain" effect issue is solved, such calibration could be applied in samples with similar matrix composition as the filter paper.

4.2.2 Quantification of Pt using spiked HT29 cells

In order to avoid the time consuming work of growing a large amount of cells to produce enough tissue samples for spiking and to prepare them as the matrix-matched standard, a single cell standard, produced with CDDP spiked cells of the same line as the spheroid samples, was tested. The standard was prepared as described in Section 3.4.3. This matrix-matched quantification approach is possible if the volume of the ablated cell is determined by its diameter or a signal of an essential element (such as P), and by measuring Pt and correlating its signal with multiple concentration ranges of cells. However, using both the cell diameter or P signal for correlation yielded unreliable results, due to the measurement error and the differences between the different cells at the same Pt concentration level, being as high as 100% (Figure 5). Most likely, the cell morphology and growth state differed significantly, which resulted in different CDDP uptake by the cells. Due to the preparation complexity and unreliable results, this method was not used.

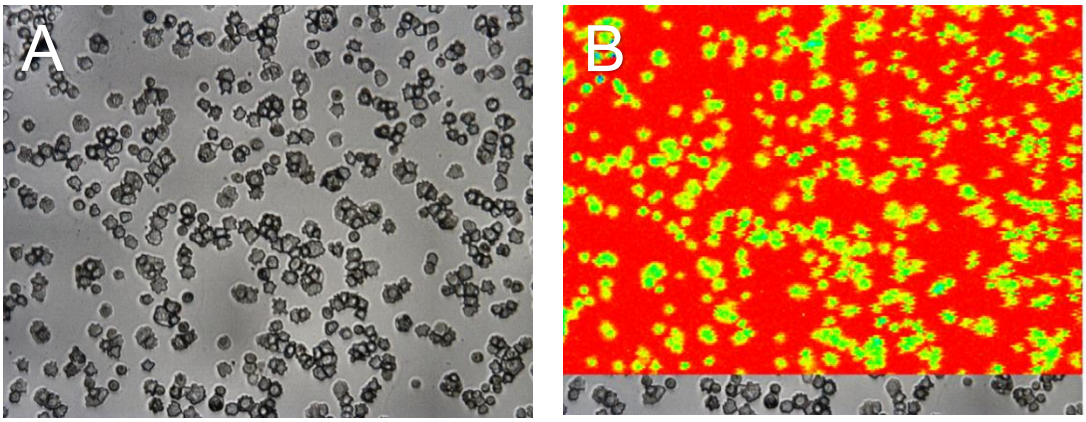

Figure 5: Citospin HT29 treated by CDDP cells images by A) Integrated LA camera (microscope) B) LA-ICP-MS distribution of Pt (red is a low signal intensity, while green is the highest signal intensity).

4.2.3 Quantification of Pt using spiked gelatine from porcine skin

Gelatine standards were prepared as described in Sections 3.4.1. and 3.4.2. There were two different methods of gelatine application to a glass slide. The first used a gelatine droplet on a glass slide, while the second used HybriWell moulds attached to a glass slide. The first method resulted in the uneven application of gelatine, while the second provided a flat surface of even and known thickness (Figure 6).

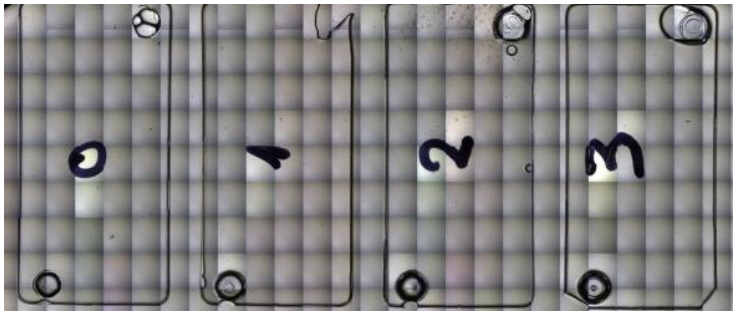

Figure 6: Four different levels of Pt spiked gelatine standards on a glass slide moulded by HybriWell. The image was taken with an integrated LA camera (microscope).

A gelatine droplet provided an uneven Pt signal, while the gelatine from the HybriWell mould provided a stable signal (Figure 7).

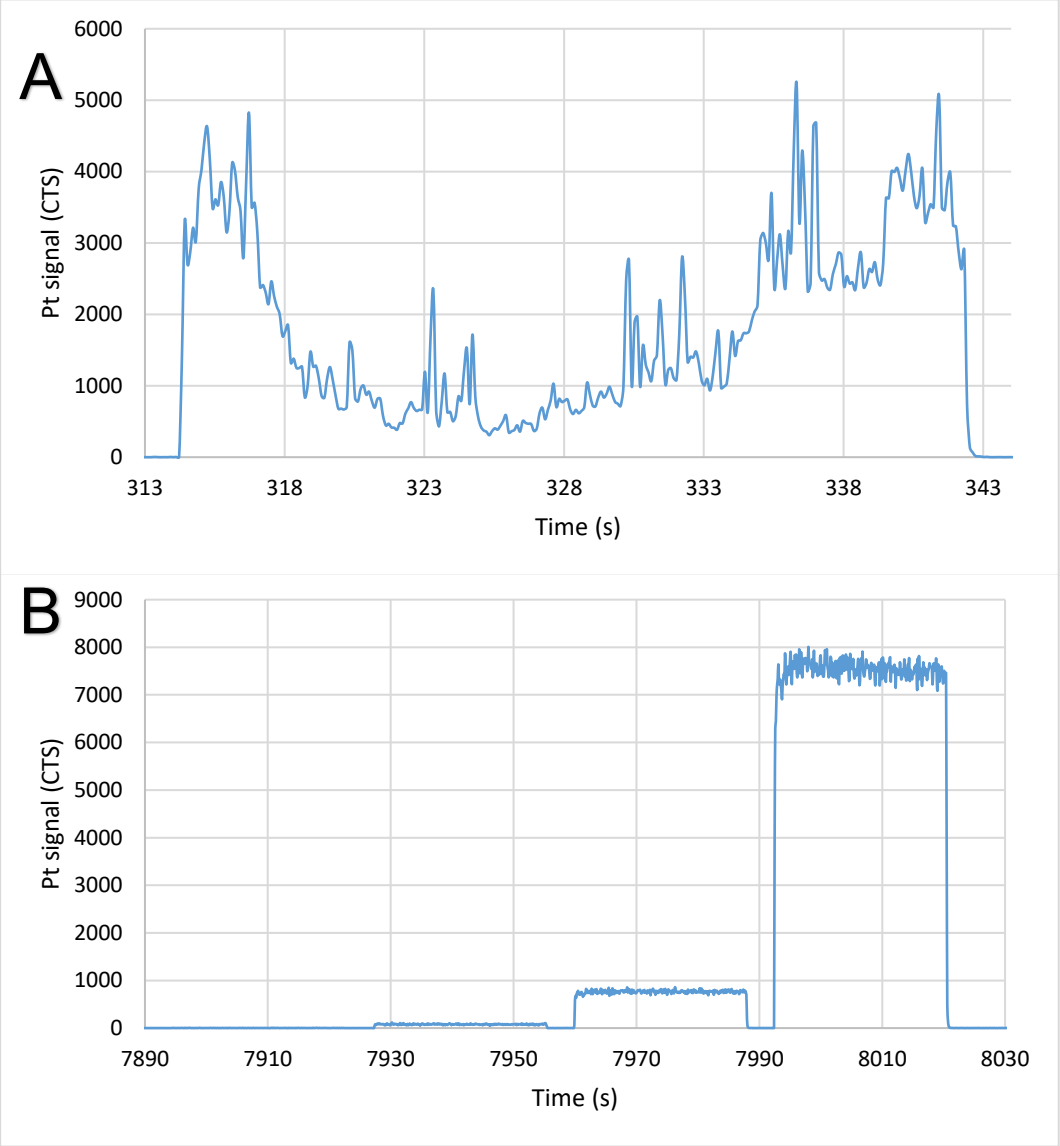

Figure 7: Pt signal intensities obtained from the ablation of gelatine standards prepared by A) droplet procedure and B) HybriWell mould procedure.

For this reason, quantification using the gelatine droplet standard was not used, while the gelatine mould standard was considered appropriate.

4.3 Quantitative Bioimaging of Pt in Tumour Spheroids Using LA-ICP-MS

The results from this chapter were published by the author in Marković et al. (2021) [25].

To obtain a high resolution, a short analysis time and a sufficient Pt sensitivity, the instrumental parameters were used as described in paragraph 3.5.1. Quantification and

distribution of the Pt in the HT29 tumour spheroids treated with CDDP were performed with LA-ICP-MS using matrix-matched gelatine standards and an online ID approach.

Gelatine calibration standards were used for multiple measurements under the same LA-ICP-MS operating parameters as the spheroid samples (Tables 4 and 5). During the analysis, each standard was ablated three times before and after each sample.

Since there are no certified reference materials available, the accuracy of the quantitative determination of Pt in the spheroids was checked with a comparative analysis by applying the simultaneous quantification of Pt in the same spheroid samples using a matrix-matched calibration and online ID-LA-ICP-MS procedure.

The limit of detection (LOD) and the limit of quantification (LOQ) for the tumour spheroid samples using two quantification approaches were calculated as the concentration that provided a signal equal to *3 s* or *10 s* of the blank sample, respectively. To calculate the LOD and LOQ applying a simultaneous analysis of the Pt using online ID-LA-ICP-MS and matrix-matched gelatine standards (^{194}Pt isotopic spike solution was aspirated), 10 blank samples (gelatine fixed on a glass slide) were analysed. The LOD and LOQ expressed on a dry mass basis (of gelatine) for the ID-LA-ICP-MS analysis were found to be 0.78 mg kg^{-1} and 2.60 mg kg^{-1} Pt, while for the gelatine standards, it was 0.66 mg kg^{-1} and 2.20 mg kg^{-1} Pt, respectively. When only gelatine standards were used for the calibration in the analysis of Pt in the tumour spheroids, the ^{194}Pt isotopic spike solution was not aspirated. Consequently, the background signal was reduced, and lower LOD and LOQ were obtained, 0.39 and 1.30 mg kg^{-1} Pt, respectively. The signal intensities of the Pt in the blank gelatine calibration standard during the simultaneous analysis using online ID-LA-ICP-MS and matrix-matched gelatine standards, and the analysis of Pt using matrix-matched gelatine standards without aspiration of ^{194}Pt, are presented in Figure 8.

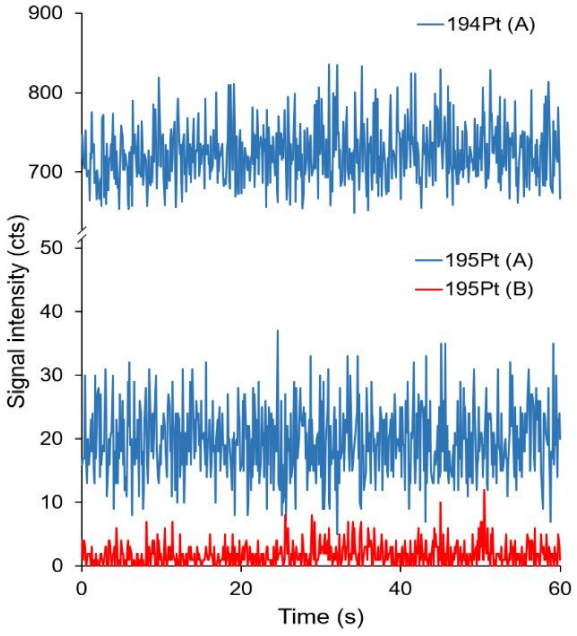

Figure 8: Signal intensities obtained by ablation of a blank gelatine standard (A) during aspiration of ^{194}Pt (150.18 ng L^{-1}) applying simultaneous analysis by on-line ID and matrix-matched standards, and (B) Pt signal using matrix-matched standards without aspiration of ^{194}Pt.

The data from Figure 8 show that the background signal of the ^{195}Pt is higher when the ^{194}Pt isotopic spike solution (150.18 ng L^{-1}) is aspirated online during the analysis, since it corresponds to the instrumental background of the ^{195}Pt and the contribution of the ^{195}Pt

from the isotopically enriched ^{194}Pt (2.46%). The background signal of the ^{195}Pt without the aspiration of the ^{194}Pt is lower because it only corresponds to the instrumental background of the ^{195}Pt. Consequently, lower LODs and LOQs are obtained.

To determine the Pt concentration in the gelatine calibration standards, known amounts of gels were dissolved in an appropriate amount of ultrapure water and analysed by ICP-MS. To verify the accuracy of the Pt concentrations in the gelatine standards determined by ICP-MS, comparative analysis using online ID-LA-ICP-MS were performed. The results, which represent an average of six independent analyses by ICP-MS and ID-LA-ICP-MS, are presented in Table 10.

Table 10: Pt concentration in the gelatine calibration standards (average of six replicates with corresponding RSD) determined by ICP-MS and online ID-LA-ICP-MS.

Sample	ICP-MS		ID-LA-ICP-MS	
	Pt concentration (mg kg^{-1})	RSD (%)	Pt concentration (mg kg^{-1})	RSD (%)
Standard 1(blank)	<0.21	/	<0.78	/
Standard 2	4.06	1.5	4.04	2.0
Standard 3	44.7	1.2	46.2	1.6
Standard 4	460	1.0	*	/

*Out of the measuring range

The results from Table 10 show good agreement between the two different quantification approaches, confirming the accurate determination of the Pt concentrations in the gelatine calibration standards. The relative standard deviations (RSDs) of the measurements, which are better than 2%, further indicate the good homogeneity of the prepared gelatine standards. The homogeneity of the gelatine standards was a result of the even distribution and the immobilization of Pt in the gelatine. The buffering of the acidic Pt standard solution to pH 7.4, prior to mixing with gelatine further prevents the denaturation of gelatine proteins, while the use of the HybriWell sealing system as a mould preserved the gelatine's thickness when removing the mould to dry the gelatine standards. The linear response using gelatine standards for the calibration was obtained from 1.30 to 460 mg kg^{-1} Pt, with a correlation coefficient (R^2) better than 0.9997.

When the ID-LA-ICP-MS approach was used for the quantification of Pt, the concentration of the ^{194}Pt isotopic spike solution was optimized in such a way as to provide a signal intensity similar to 10 mg kg^{-1} Pt in the gelatine standard. This enabled a reliable determination of low Pt concentrations in the gelatine standards and extended the applicability of the ID quantification approach to Pt concentrations up to 100 mg kg^{-1}. Therefore, it was not possible to reliably determine higher Pt concentrations.

4.3.1 Quantitative bioimaging of Pt with a high spatial resolution in tumour spheroids treated with CDDP by LA-ICP-MS

The results from this chapter were published by the author in Marković et al. (2021) [25].

To examine the applicability of the two quantification approaches for the determination of Pt in tumour spheroids, HT29 spheroids were incubated with CDDP and prepared for the analysis as described in paragraph 3.3.2. Since LA is a destructive technique, the only way to compare two quantification approaches on the same sample was a simultaneous analysis

of the Pt using the matrix-matched calibration and online ID-LA-ICP-MS procedure. The quantitative Pt distribution in an HT29 spheroid incubated for 1 h with 500 µM CDDP in different cryo-cut slices of the same spheroid, obtained using two quantification approaches, is presented in Figure 9.

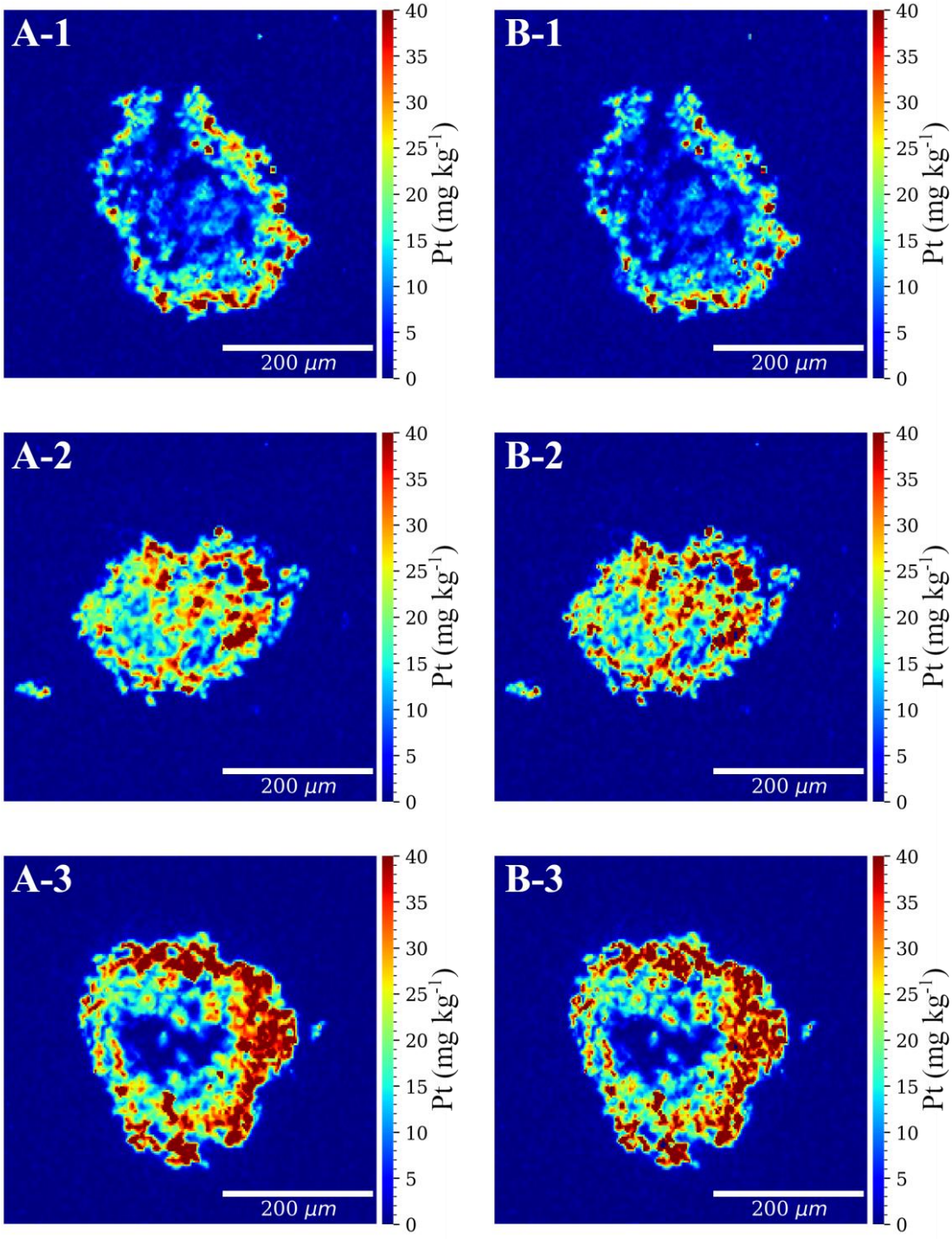

Figure 9: Quantitative Pt distribution in HT29 spheroid incubated for 1 h with 500 µM CDDP. Spheroid slices were analysed with LA-ICP-MS and quantified simultaneously by A) the use of matrix-matched gelatine standards and B) isotope dilution. Samples 1–3 are different cryo-cut slices of the same spheroid.

The data from Figure 9 shows that the Pt from the CDDP in spheroid slices 1 and 3 is accumulated in areas of the outer rim, while lower Pt concentrations are observed in the intermediary layer and the necrotic core. In slice 2, Pt is distributed mainly between the outer rim and the intermediary layer. Theiner et al. (2016), who treated tumour spheroids with different Pt(IV) complexes for 96 h, found that the Pt was accumulated in the outer rim of the spheroids as well as in the necrotic core. By careful optimization of the measurement parameters, highly sensitive Pt bioimaging was achieved (LOD <0.78 mg kg^{-1} Pt) with a high spatial resolution for pixel dimensions of 2.0 µm × 2.5 µm. Highly sensitive imaging made it possible to follow the accumulation of CDDP in the tumour spheroids at concentrations relevant for clinical practice [48].

Figure 9 further indicates that the Pt concentration in most of the pixels does not exceed 40 mg kg^{-1}. To check the agreement between the two quantification approaches, a comparative analysis of 10 slices of the same spheroid were performed. Data showed that the differences in the Pt concentrations usually did not exceed 4% when comparing the average Pt concentration, confirming the good agreement between the results obtained using the matrix-matched calibration and the online ID quantification approach. It should be noted that in the areas with Pt concentrations above 100 mg kg^{-1} (less than 0.05% of cases), the ID quantification approach provides false-negative results since the ratio between the signal intensity of the ^{195}Pt from the ablated sample and the intensity of the ^{194}Pt isotopic spike solution exceeded a factor of ten, leading to an unreliable Pt determination [115].

Namely, the concentration of the ^{194}Pt isotopic spike solution was optimized as a compromise to achieve good sensitivity with a high spatial resolution and to determine the majority of the Pt concentrations in the spheroids (more than 99.5%) within the optimal measurement range for the ID quantification approach.

Table 11: Summation of all Pt (mg kg^{-1}) values on parallel slices of the same HT29 spheroid treated with 500 µM CDDP for 1 h.

Sample	LA-ICP-MS	ID-LA-ICP-MS
Quantification method	Gelatine standards	Isotope dilution
	Sum of Pt values	Sum of Pt values
Slice 1	3.68E+04	3.71E+04
Slice 2	4.12E+04	3.93E+04
Slice 3	3.65E+04	3.87E+04
Slice 4	2.55E+04	2.54E+04
Slice 5	4.94E+04	5.00E+04
Slice 6	5.38E+04	5.62E+04
Slice 7	7.52E+04	7.16E+04
Slice 8	2.66E+04	2.74E+04
Slice 9	6.80E+04	6.47E+04
Slice 10	5.75E+04	5.75E+04
Total	4.70E+05	4.68E+05

Data from Table 11 shows the summation of all Pt concentrations of individual pixels from slices of HT29 spheroid and total concentration summation for all 10 sample slices by two different quantification approaches. While the individual results per slice may vary, the difference is in the range of measurement and instrumental error. However, when the

total sum of slices is considered, the concentration variation is significantly lower on the scale of the whole sample. This can be explained by the measuring uncertainty (typical deviation for LA-ICP-MS measurement is up to 10%) reducing with measuring repetition of a larger set of data and increasing the accuracy of the results. It should be noted that in this case, the amount of data measured per a single slice is in the range of hundreds of thousands of values, depending on the sample size with said measurement parameters.

The choice of quantification approach depends on the number of samples, the concentration range of the Pt in the spheroids to be analysed, and the time needed to prepare the calibration standards. In the case when a large number of spheroid samples with long-time of analysis and a wide concentration range of Pt needs to be analysed, the matrix-matched calibration using gelatine standards is the quantification method of choice. If only a few spheroid samples are analysed and the Pt concentration mostly fits the optimal measurement range for the ID analysis, the ID quantification procedure is a better choice. In addition, when using ID, fewer steps are needed in the analytical procedure, which reduces the number of possible operational mistakes.

4.3.2 Quantitative bioimaging of Pt with a high spatial resolution in tumour spheroids treated with CDDP or TR-CDDP by online ID-LA-ICP-MS

The results from this chapter were published by the author in Marković et al. (2021) [25].

Since TR is a common fluorescent agent used in oncological research, the imaging of Pt was compared in spheroids incubated for 1 h with 100 µM CDDP or 100 µM TR-CDDP. For this purpose, three different cryo-cut slices of the CDDP and TR-CDDP treated spheroids taken from the central region of the spheroid were analysed using online ID-LA-ICP-MS. The results are presented in Figure 10.

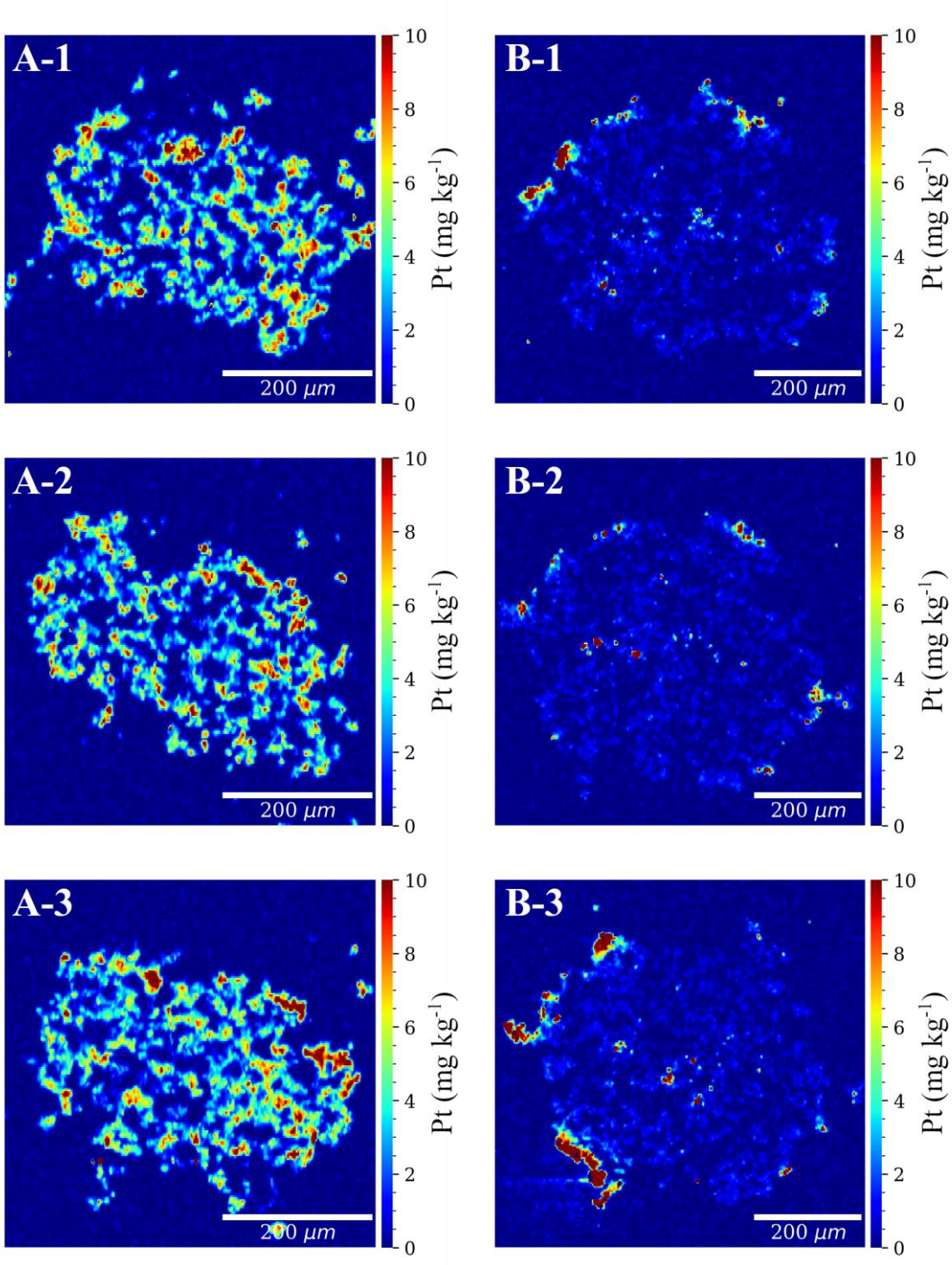

Figure 10: Quantitative Pt distribution in two HT29 spheroids incubated for 1 h with A) 100 µM CDDP and B) 100 µM TR-CDDP. Spheroid slices were analysed with ID-LA-ICP-MS. Samples 1–3 are different cryo-cut slices of the same spheroid.

Although the images shown in Figure 10 do not indicate Pt concentrations in the same spheroid (since simultaneous imaging of the same spheroid treated with CDDP and TR-CDDP using LA-ICP-MS is only possible if the CDDP or TR-CDDP is marked with the enriched Pt isotope), it is evident that the TR-marked CDDP exhibits a significantly different spatial distribution than the CDDP treated spheroids. This phenomenon is related

to the different physicochemical properties of the TR-CDDP and to the steric hindrance that obstructs its penetrations across cellular membranes [46]. Consequently, the Pt concentration in slices of TR-CDDP treated spheroid is notably lower and mainly accumulated in the outer rim of the spheroid. The results suggest that the TR bound to the CDDP could impact the intra-spheroid distribution and thus not necessarily reflect the real distribution of CDDP in the tumour tissue. It is likely that the difference is more evident when short incubation times are applied (in our study, the incubation time was 1 h). For example, Chu et al. (2016) [46] found no difference in the uptake and cytotoxicity of CDDP and TR-CDDP when cochlear hair cells were incubated for longer times (24 h).

For a more detailed demonstration of the steric effects caused by TR-marked CDDP, thin sections (20 µm) of spheroid slices were overlaid, one over another, to reconstruct the entire spheroid, forming 3D images of the CDDP and TR-CDDP treated spheroids. Each spheroid was reconstructed from 20 slices. The 3D images of CDDP and TR-CDDP treated spheroids are presented in Figure 11.

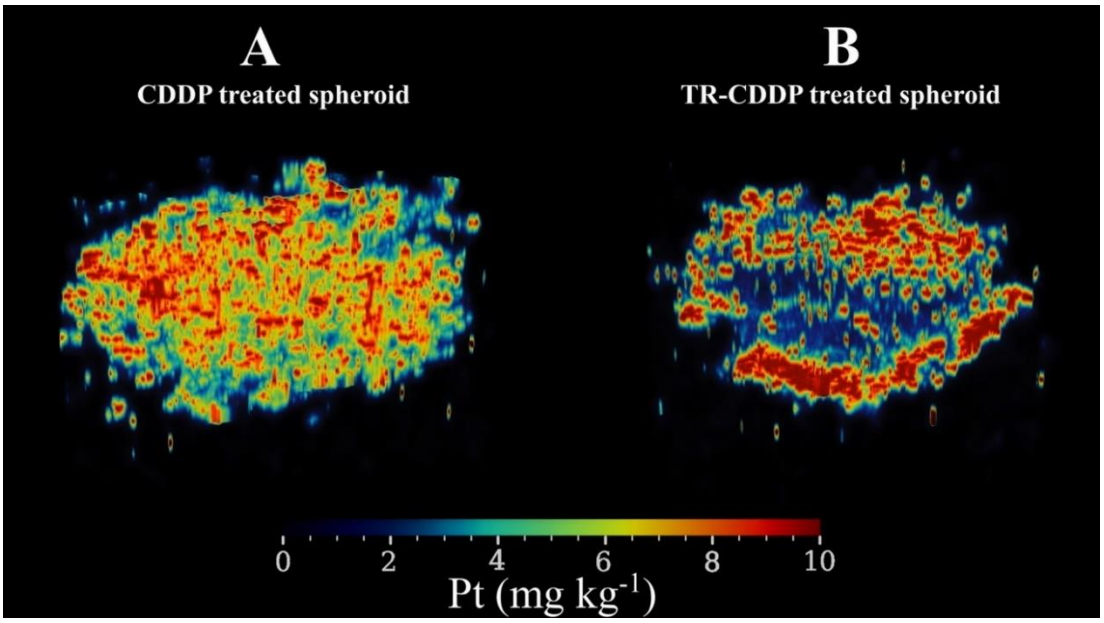

Figure 11: 3D images of Pt distribution from two HT29 spheroids obtained by ID-LA-ICP-MS after incubation for 1 h with A) 100 µM CDDP and B) 100 µM TR-CDDP.

3D images of the CDDP and TR-CDDP treated spheroids further confirmed the observations from Figure 10. While a video of 3D images can be assessed at this link (https://drive.google.com/file/d/1H8WHpTR_wT8QIkvsmnYJo-ZLb5BNq1IT/view).

4.3.3 Bioimaging of Pt in tumour spheroids treated with TR-CDDP by confocal fluorescence microscopy and online ID-LA-ICP-MS

The results from this chapter were published by the author in Marković et al. (2021) [25].

Confocal fluorescence microscopy is widely used in preclinical investigations. To compare the distribution of the TR-CDDP in spheroids, the same slices of spheroid incubated for 1 h with 100 µM TR-CDDP were first analysed by confocal fluorescence microscopy and then by LA-ICP-MS using ID for the quantification of the Pt. This was possible since the preparation of the slices for the two imaging techniques was the same and because microscopy is a non-destructive analytical technique. The images of the TR-CDDP

distribution obtained by the confocal fluorescence microscopy and Pt using online ID-LA-ICP-MS analysis are presented in Figure 12.

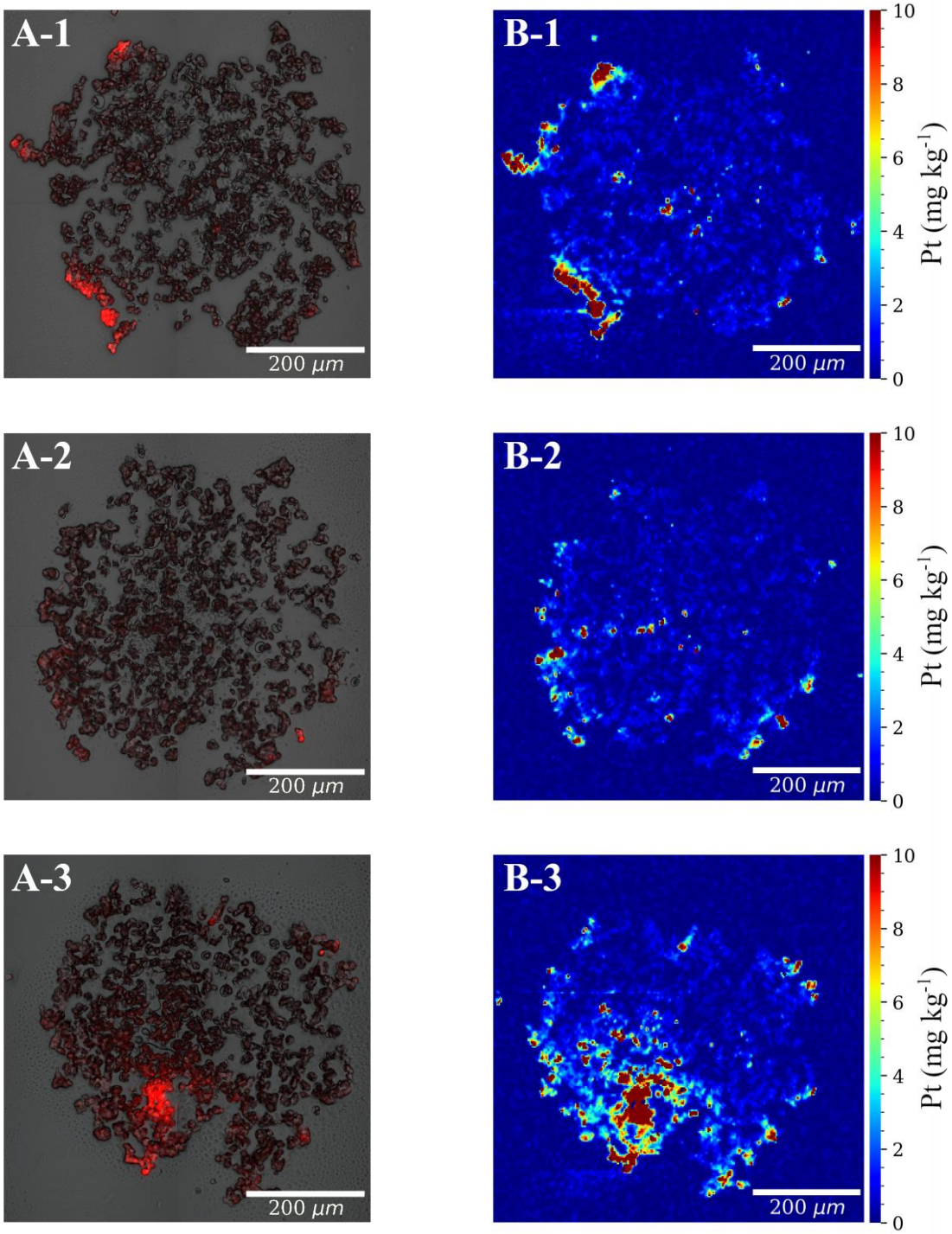

Figure 12: Imaging of TR-CDDP in HT29 spheroid incubated for 1 h with 100 µM TR-CDDP. Spheroid slices were analysed first with A) confocal fluorescence microscopy and then by B) LA-ICP-MS using ID for quantification of Pt. Samples 1–3 are different cryo-cut slices of the same spheroid.

The images in Figure 12 demonstrate a good agreement of the TR-CDDP distribution inside the tumour spheroids obtained using two high-resolution techniques. Although

confocal microscopy is a semi-quantitative technique, the intensity of the TR-CDDP fluorescence matches well with the Pt concentrations determined using online ID-LA-ICP-MS. In comparison with LA, fluorescence imaging is a rapid procedure. However, ID-LA-ICP-MS enables quantitative imaging with high sensitivity and high resolution. Its great advantage is that CDDP, which is used in clinical practice, can be followed in tumour spheroids with a more representative Pt distribution than that obtained using TR-CDDP (see data from Figure 10). Nevertheless, TR-CDDP can be used for the rapid screening of the Pt distribution when this information is sufficient for a rough estimation of the Pt accumulation in tumour spheroids.

4.4 Bioimaging of Pt in Mice Tumours Treated with CDDP by LA-ICP-MS

In order to study the CDDP uptake and distribution in mice tumours, Pt spiked gelatine standards were selected as the quantification method most suited for this application. They were chosen as an optimal solution from the previously tested procedures on tumour spheroids. Their wide concentration range and stability made them an ideal solution for long measuring times and the wide CDDP concentration range expected in the samples. To determine the Pt concentration in the prepared gelatine calibration standards, known amounts of gels were dissolved in an appropriate amount of ultrapure water and analysed by ICP-MS. The results are averages of ten replicate standards presented in Table 12.

Table 12: Pt concentration in the gelatine calibration standards (average of ten replicates with corresponding RSD) determined by ICP-MS.

Sample		
	Pt concentration (μg g^{-1})	RSD (%)
Standard 1	0.008	21.9
Standard 2	1.02	1.1
Standard 3	11.1	1.6
Standard 4	124	2.4
Standard 5	1268	1.8

The gelatine calibration standards were used for multiple measurements under the same LA-ICP-MS operating parameters as the tumour samples (Tables 6 and 7). During the analysis, each standard was ablated three times before and after each sample. The LOD and the LOQ for the tumour samples were calculated as the concentration that provided a signal equal to *3 s* or *10 s* of the blank sample, respectively. The LOD and LOQ of the LA-ICP-MS measurements expressed on a dry mass basis (of gelatine) were found to be 0.078 μg g^{-1} and 0.260 μg g^{-1} of Pt.

The instrumental parameters used in the ablation of the tumour spheroids were modified for the tumour analysis so as to increase the speed of the measurement, by increasing the pixel dimension and the scanning speed. These instrumental parameters are described in Section 3.5.2.

The tumours were scanned with parallel lines directly adjacent and ablated from left to right. The set parameters allowed for the total ablation of both the tumour samples and the gelatine standards, enabling a reliable external calibration. The imaging of the quantitative Pt distribution by LA-ICP-MS in two B16F10 tumour slices 3 and 10 min

after intravenous injection of the CDDP (4 mg per kg of body mass) is presented in Figure 13.

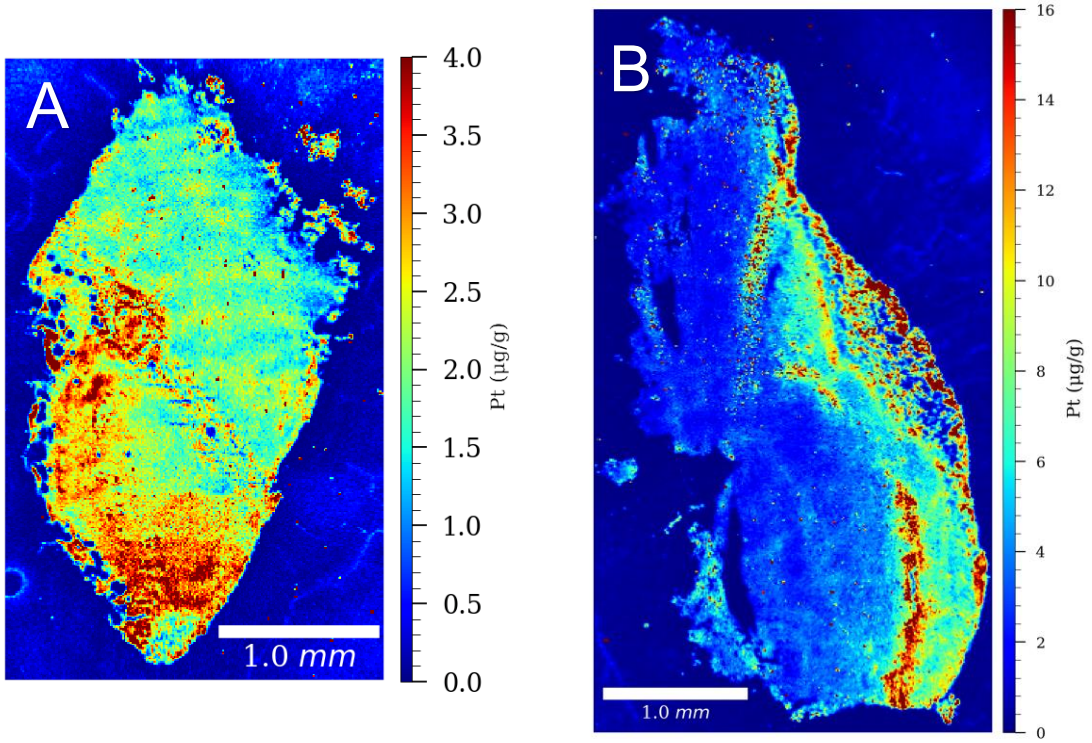

Figure 13: Quantitative Pt distribution in two B16F10 tumour slices analysed with LA-ICP-MS. Mice were injected with an intravenous dose of 4 mg per kg of body mass. Tumours were removed and fixed after A) 3 min B) 10 min of incubation with CDDP.

The data from Figure 13 show that the Pt in the B16F10 slices is in a relatively low concentration after the intravenous administration of the CDDP. Image B of the sample exposed for 10 min to the drug has a higher Pt content than the sample in image A, which was exposed for 3 min. This was expected. However, a significantly higher heterogenic distribution of Pt in sample B can be attributed to the different sample morphology and proliferation.

The quantitative Pt distribution images were deemed to be of satisfactory quality. As a regular method of CDDP treatment, intravenous injections were used as a starting benchmark for a comparison. Intratumoral injected tumours were then analysed to compare the difference between these two drug administration methods. Representative images of the intratumoral injected tumours can be assessed in Figure 14.

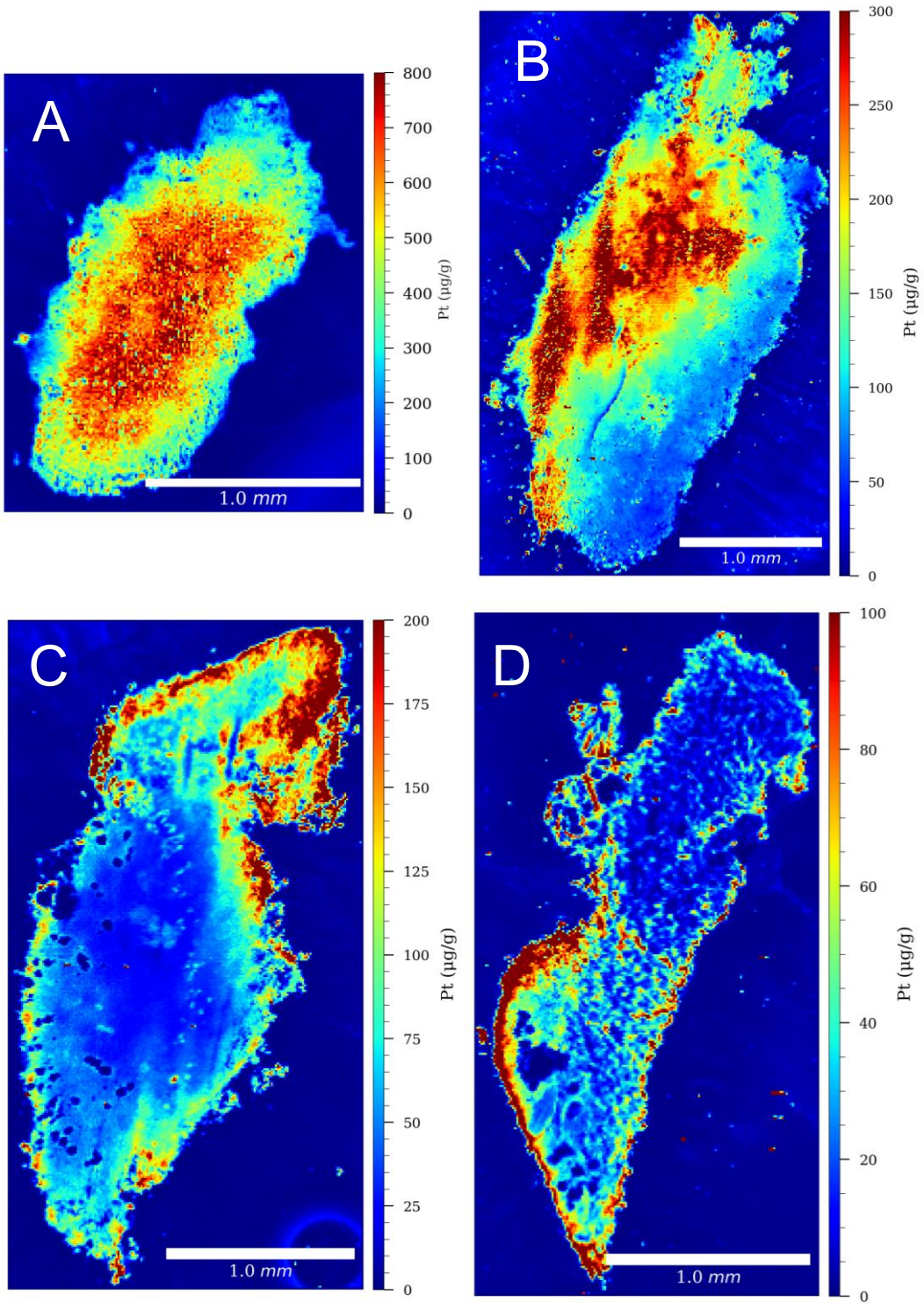

Figure 14: Quantitative Pt distribution in B16F10 tumour slices analysed with LA-ICP-MS. Mice were injected with an intratumoral dose of 4 mg per kg of body mass. Tumours were removed and fixed after A) 1 min B) 3 min C) 10 min D) 20 min after injection.

When comparing the intratumoral samples, the most obvious conclusion is that the Pt concentration is reduced over time. As expected, the high dosage of CDDP injected (same for intravenous and intratumoral application) into the small volume of the tumour is oversaturating the tumour tissue, entering into the tumour environment and bloodstream. Sample A from Figure 14, which was exposed for 1 min to CDDP, has a significantly higher

concentration of Pt than the samples with a longer exposure time. Sample D, which was incubated for 20 min, still shows a significantly higher concentration of Pt than the intravenous application. At longer exposure times, tumour tissue necrosis can be observed, which could be related to the cell apoptosis induced by the high CDDP concentration [132]. Cell death was only noticed in the intratumoral samples that were exposed for a longer period of time.

The same tumour preparation and analysis procedures were applied for the 4T1 tumour samples. Similar trends were observed as in the B16F10 tumour line, except no cell necrosis was present and there was a higher Pt concentration than with the B16F10 samples. However, the experiment with the 4T1 tumour was only measured after 1 min of exposure with the intravenous injections and up to 10 min with an intratumoral injection. The difference between these two experiments is probably related to the different tumour morphology. It is also worth pointing out that a smaller number of 4T1 tumours than B16F10 tumours were analysed by LA-ICP-MS. The 4T1 tumour images can be seen in Figure 15.

The intravenous CDDP administration provides a more even distribution throughout the tumour, although at lower concentrations. When injected intravenously, CDDP binds unspecifically to the DNA and proteins throughout the whole organism, causing side effects. Consequently, a lower CDDP concentration is delivered to the targeted tumorous tissue.

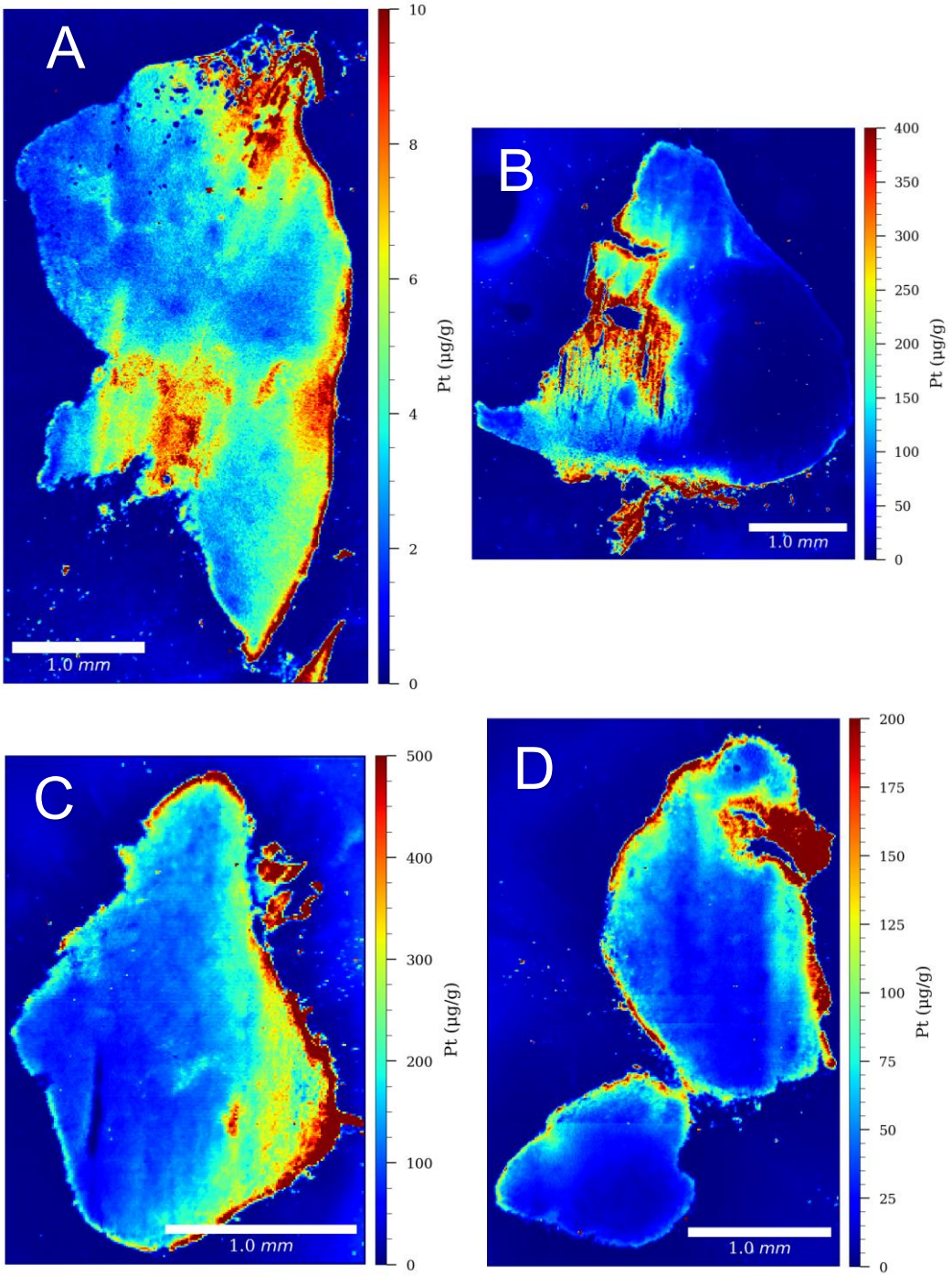

Figure 15: Quantitative Pt distribution in four 4T1 tumour slices analysed with LA-ICP-MS. Mice were injected with a dose of 4 mg per kg of body mass. The dose was injected intravenously in image A) and intratumorally in images B) C) D). Tumours were removed and fixed A) 1 min B) 1 min C) 5 min D) 10 min after injection.

To compare the results obtained using LA-ICP-MS with those analysed for total Pt content, Tissue-Tek fixed tumours obtained at different times after intratumoral or intravenous injections were sliced in half. For each time point in the experiments three tumours were prepared. The first half was digested with acids prior to Pt content determination using ICP-MS, while the other half was cryosliced (10 µm thickness) and analysed directly using LA-ICP-MS. The total tumour area in the images was integrated

and divided by the total number of integrated pixels. To determine the total Pt concentration by LA, up to eight slices from each B16F10 tumour sample were analysed. Each time point represents the average of all three tumours prepared under the same conditions. The results of these experiments are presented in Figure 16.

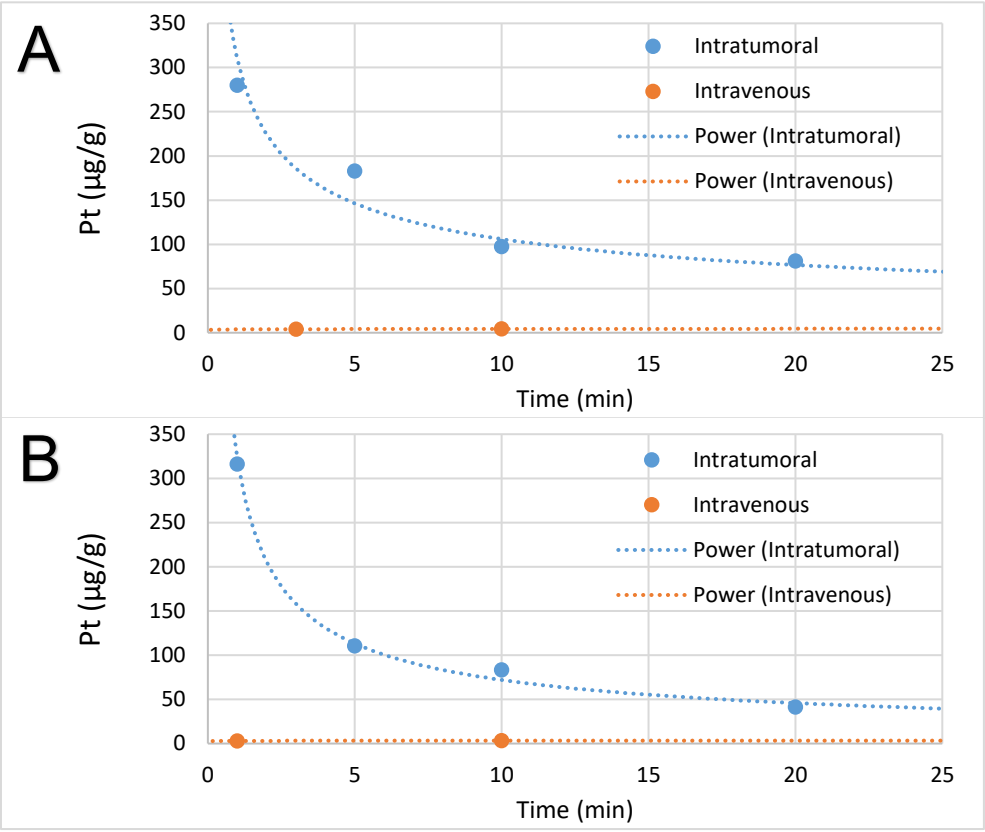

Figure 16: Time-resolved average Pt concentration of intratumoral and intravenous CDDP injections in B16F10 tumours determined A) after sample digestion and Pt measurement by ICP-MS and B) by integration of tumour area in LA-ICP-MS quantitative Pt images.

It is worth mentioning that half of the tumour that was digested was fixed in Tissue-Tek, which made it impossible to determine the exact mass of the tumour. This led to a higher uncertainty in the determination of the Pt concentration using ICP-MS. The LA-ICP-MS data from the images of the other tumour half was averaged. LA-ICP-MS imaging did not include the Tissue-Tek area in the calculation of the Pt concentration. From graphs A and B in Figure 16, it is evident that intratumoral CDDP administration results in a significantly higher drug concentration. The differences between the Pt concentrations at the same time points obtained by two quantification methods are most likely the result of the uneven application in intratumoral samples, tumour morphology and the relatively small number of samples. However, the trendlines of the Pt concentrations between both application methods show similar patterns. From these trendlines it can be concluded that due to the CDDP leaching from the intratumoral samples, the Pt concentration in the tumours is reduced over time, but it is still higher than in the intravenous injection treatment. Therefore, to achieve the same drug concentration in the targeted tissue, a smaller dosage is needed with intratumoral administration. This allows for a more targeted approach with reduced side effects from the treatment.

In order to evaluate the distribution and homogeneity of the CDDP in the intratumoral samples in relation to the time of incubation, quantitative data from the LA-ICP-MS

images of B16F10 tumours for each pixel was extracted. Depending on the concentration of the pixel, they were sorted into 50 groups, each containing 2% of the total Pt concentration range in the sample. The pixels in each group were then counted, normalised to the group with the largest number of pixels (1 on the y axis) and compared. The results are presented in Figure 17.

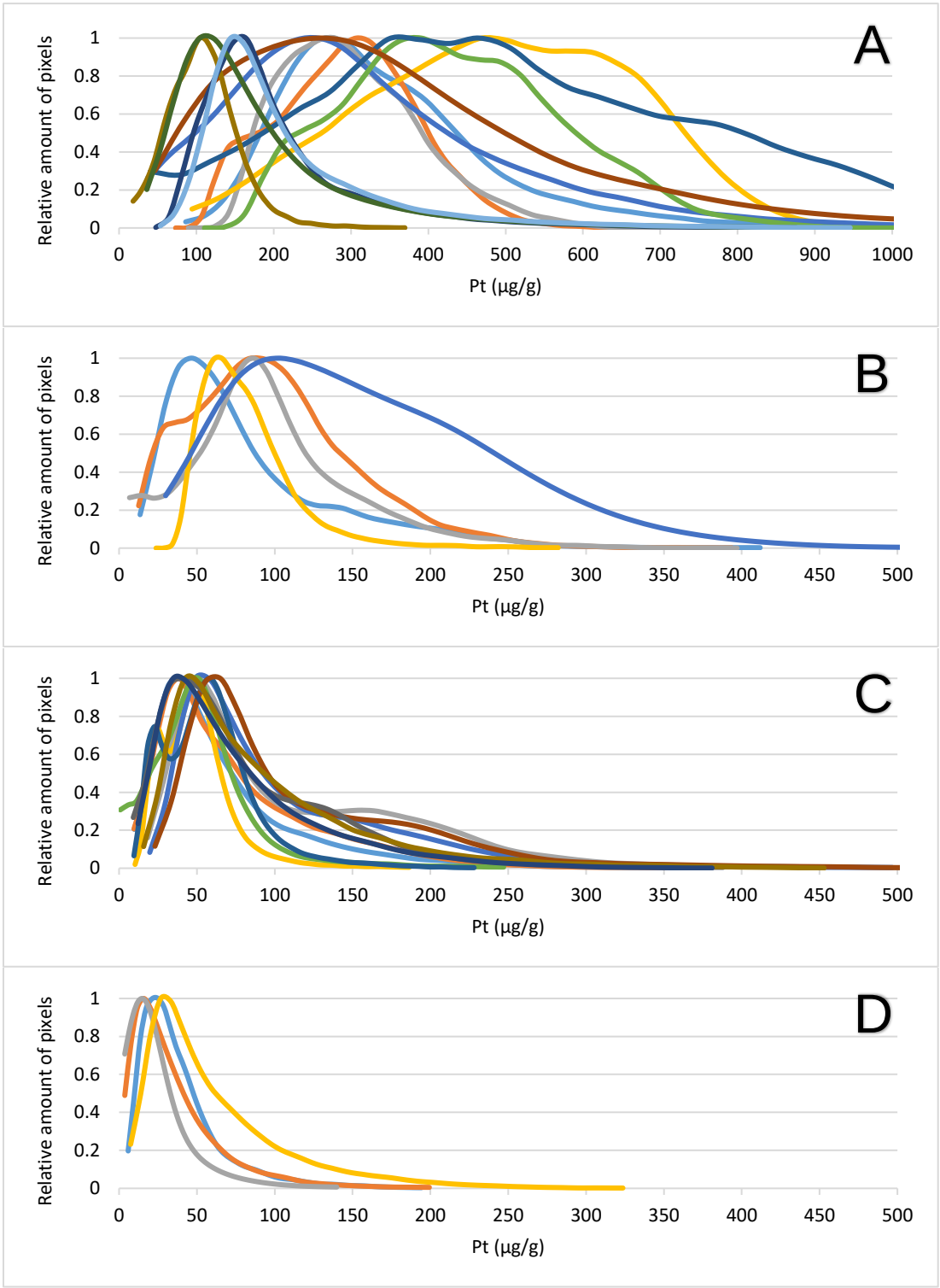

Figure 17: Intratumoral CDDP concentration in B16F10 tumours determined by LA-ICP-MS correlated to the relative pixel amount in A) 1 min exposure B) 5 min exposure C) 10

min exposure D) 20 min exposure. Colours represent different slices of B16F10 tumours prepared under the same conditions.

Data from Figure 17 show that the considerable variation of concentration and homogeneity in the intratumoral samples is gradually distributed over time, resulting in a relatively even CDDP distribution, similar to the intravenous samples. The variation in graphs A and B is most likely caused by uneven drug application using the syringe. It is localised at the injection location and quickly distributed throughout the tumour, so the distribution is more even by the 10^{th} min, as seen in graph C.

To summarise, the quantitative data obtained using the LA-ICP-MS technique provide additional information to the traditional methods and allow for a deeper insight into the treatment planning and drug development.

4.5 Localization of Cr in Dandelion Leaves Using LA-ICP-MS

Some of the results from this chapter were published by the author in Marković et al. (2022) [131].

The potential of bioimaging with LA-ICP-MS was also demonstrated by ablating plant tissue samples [133]–[136].

In order to localize the Cr in a dandelion leaf, imaging was performed by LA-ICP-MS using the procedure described in Section 3.7.1. To reduce the number of analyses in relation to the large leaf area, parameters for the LA-ICP-MS imaging were adjusted to achieve a good resolution, while maintaining a reasonable analysis time and adequate sensitivity. For this purpose, a spatial resolution of 40 µm x 35 µm per pixel was achieved with the laser beam parameters set to a square spot of 35 µm x 35 µm and a scanning speed adjusted to 200 µm s^{-1}. Due to the uneven thickness of the leaf sample, laser fluence was set to 3.5 J cm^{-2} with a 50 Hz firing rate to achieve total sample ablation. The total dwell time per cycle was set to 200 ms. However, due to the thickness of the leaf veins and the laser focus, some parts of the veins were not completely ablated (in most cases a small amount of the primary leaf vein remained).

Three different calibration approaches were tested, shown in Figure 18.

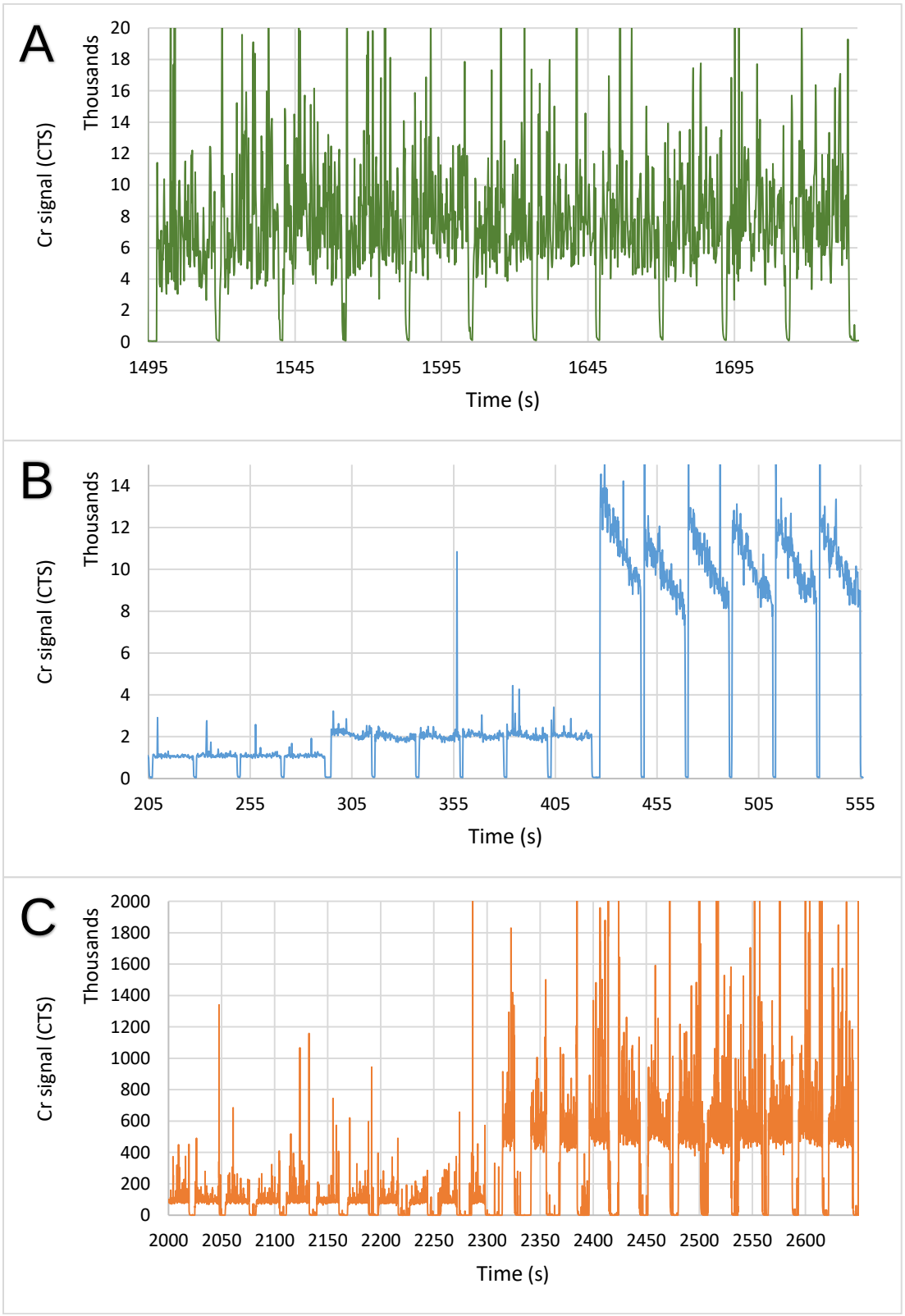

Figure 18: Chromium signal intensities were obtained by LA-ICP-MS analysis of A) NIST 1573a pressed pellet B) Cr spiked agarose gels C) Cr spiked filter paper cut-outs.

The pressed NIST 1573a CRM (Figure 18 A) pellet with a similar sample composition was used as a matrix-matched standard. Due to the thickness of the pressed pellet, the

ablation crater penetrated the whole sample. Consequently, the amount of standard intake per measuring cycle could not be determined. Another consequence of the sample thickness is the difficulty of focusing the laser beam on the surface of the standard, since the thick standard is not transparent. Therefore, graph A (Figure 18) shows an unstable signal with the standard crumbling. For this reason, a calibration using the 1573a CRM was not used.

The Cr spiked agarose gels (Figure 18 B) were tested based on the results of previous experience with Pt spiked gelatine standards. Agarose was chosen since the matrix is more similar to plant tissues than the gelatine from porcine skin. However, the preparation was challenging. 2% agarose gels were used, but they proved almost impossible to manipulate due to the viscosity and a tendency to solidify. Agarose standards shrank to around ~5 µm. The resulting gels were deformed, and a visible "coffee stain" effect was present on the gels with the highest spiked Cr concentration. The Cr signal (Figure 18 B) shows a potentially usable method with more effort involved in the preparation. Ten different glass slides with calibration standards were prepared, but due to the difficult preparation, only two slides contained all six calibration points , but with a visible deformation (see Figure 19) and a low yield. For these reasons, this calibration method was also not used. The quality of agarose standards was visibly worse than the gelatine standards

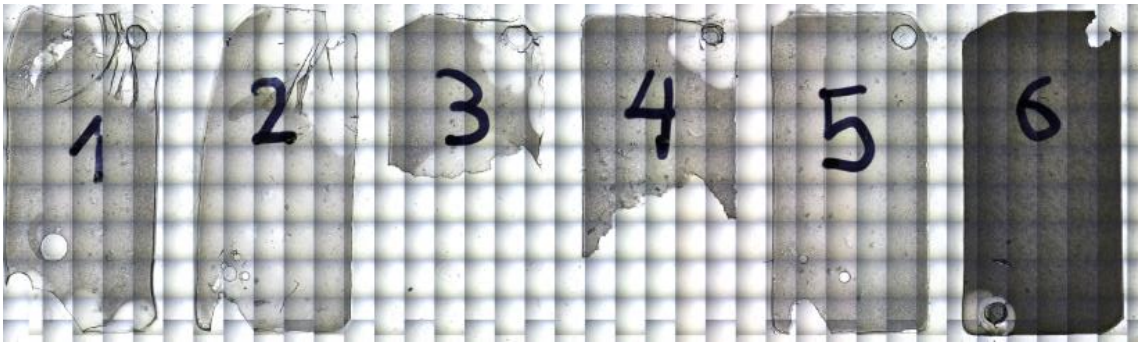

Figure 19: Cr spiked agarose standards on a glass slide moulded by HybriWell. The image was taken using an integrated LA camera (microscope).

0.45 µm nitrocellulose filters with added Cr standard solution were then tested as a calibration standard (Figure 18 C). These filters were chosen because of their similar composition to the plant matrix, easy and fast preparation, surface smoothness (even and total ablation), known thickness, ability to absorb the Cr standard solution, and by cutting the central part out, avoiding the "coffee stain" effect caused by drying of the filter. The signal instability was localised at the edges of the filter. By cutting out and using only the central part of the filter, repeatable concentrations were obtained for parallel standards. The total Cr concentration of the digested filter calibration standards (average of six replicates) measured using ICP-MS is shown in Table 13. For these reasons, Cr spiked filter paper cut-outs were chosen as a satisfactory calibration standard for the plant imaging.

Table 13: Total Cr concentration of the digested filter calibration standards (average of six replicates with corresponding RSD) measured by ICP-MS.

Sample	Cr concentration (mg kg^{-1})	RSD (%)
Standard 1	0.904	15.6
Standard 2	1.70	4.7
Standard 3	6.0	11.6
Standard 4	16.3	7.8
Standard 5	60.1	3.9

In the filter standards, the even Cr distribution was confirmed with LA-ICP-MS (Figure 18 C), by ablation and measurement of Cr in parallel lines running across the entire length of the filter cut-outs. Filter paper crumbling can be seen as spikes in the signal strength (Figure 18 C). This phenomenon is most likely caused by the harsh ablation parameters with a high laser beam strength and a large spot size, which resulted in lose, fine particles crumbling away from the filter.

During the leaf sample preparation, its thickness had shrunk while drying, but the leaf veins remained protruding from the leaf. However, due to the uneven thickness, and lack of thickness information for each part of the leaf sample, the quantification was not feasible. The resulting quantification approach is semi-quantitative, and Cr concentration is given as the total Cr amount in the pixel area (40 µm x 35 µm).

The calibration standards were measured multiple times, during the Cr mapping of the dandelion leaf. After fifty ablation lines of the dandelion sample, each standard was ablated once with the same instrument parameters. Knowing the concentration and mass of the ablated calibration material per pixel, we were able to determine the total Cr mass in the pixel of the leaf sample from the signal intensity.

After the filter ablation, we observed that a small number of filter particles were still crumbling from the ablation crater about a minute after ablation, which contributed to slightly higher concentration lines that can be seen on the Cr map in the leaf image.

The LA-ICP-MS image of a dandelion leaf from Vranja Peč showing the relative distribution of Cr is presented in Figure 20.

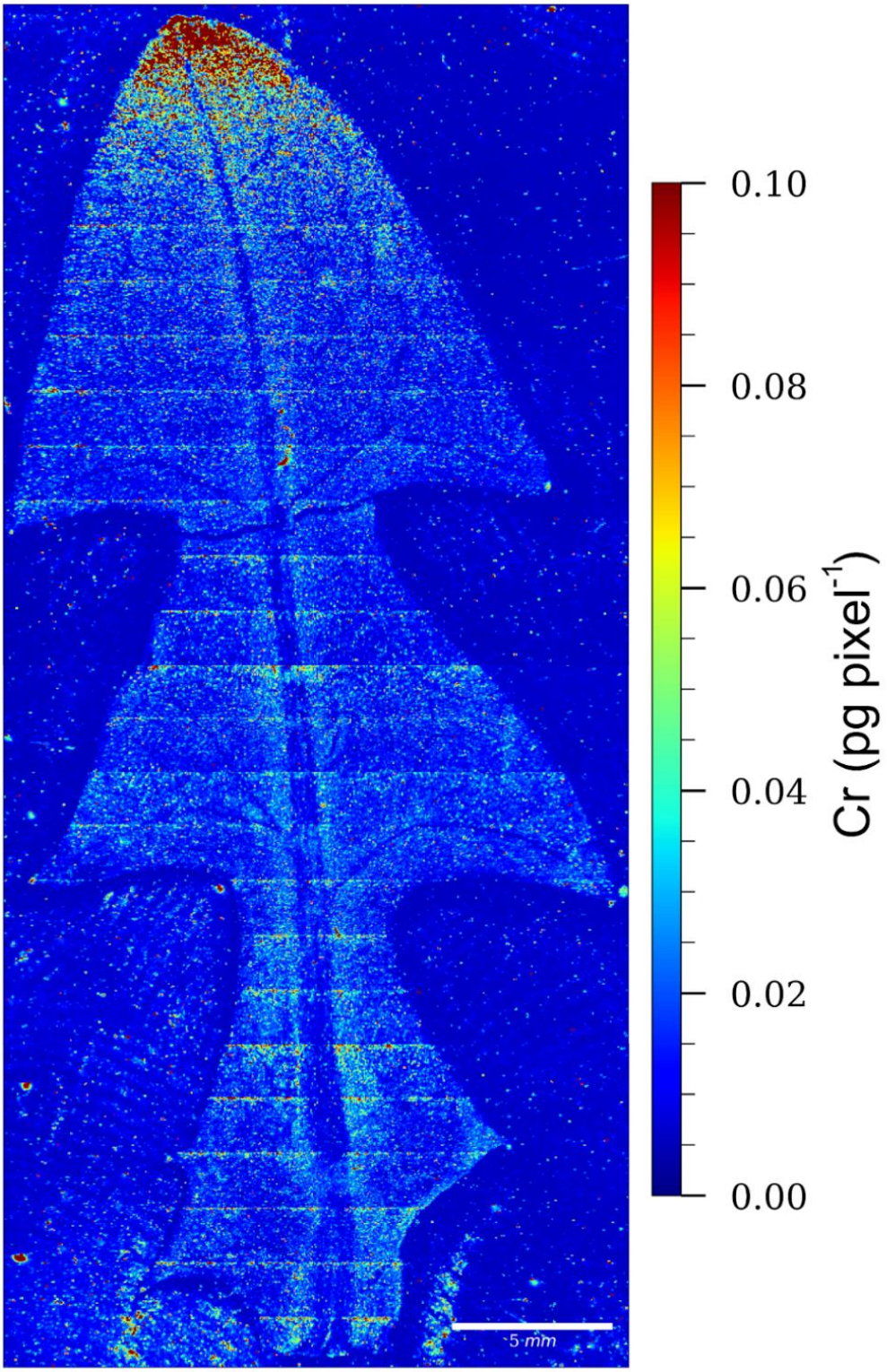

Figure 20: LA-ICP-MS image of a dandelion leaf from Vranja Peč, showing the relative distribution of Cr.

From the relative distribution of Cr and the intensity of the red colour, which indicates the highest Cr concentration, it is evident that Cr in the leaf of dandelion growing in Cr rich soil is localized mainly at the apex of the leaf and a smaller amount surrounding the leaf midrib.

Chapter 5

Conclusions

The analytical method using LA-ICP-MS was developed to study the distribution of CDDP and TR-CDDP in tumour spheroids and tumour tissues. Different quantification approaches were tested to obtain a reliable method for quantifying the Pt in tumour spheroids. The selection was made on the basis of quantification applicability, easy preparation and good reproducibility. The optimized measurement parameters for the LA-ICP-MS enabled highly sensitive, quantitative Pt bioimaging with a high spatial resolution, applying matrix-matched gelatine standards and/or online ID-LA-ICP-MS. The results from these two quantification approaches were in good agreement, e.g., the differences in the Pt concentrations did not exceed 4%. The Pt from the CDDP treated spheroids was accumulated in areas of the outer rim, whereas lower Pt concentrations were observed in the intermediary layer and the necrotic core. A comparison of the CDDP and TR-CDDP treated spheroids analysed using online ID-LA-ICP-MS demonstrated a different Pt distribution, which was related to the steric effects of the TR-CDDP that obstruct its penetration into the cells. In the TR-CDDP treated spheroids, the Pt was almost entirely accumulated in the outer rim, while its concentration was notably lower than in the CDDP treated spheroids. Since fluorescence imaging is widely used in clinical investigations, the distribution of the TR-CDDP in the spheroids was compared using complementary confocal fluorescence microscopy and the online ID-LA-ICP-MS techniques. Although confocal fluorescence microscopy is a semiquantitative technique, the intensity of the TR-CDDP fluorescence matched well with the Pt concentrations determined using LA-ICPMS, which is a quantitative technique. The advantage of LA-ICP-MS, i.e., measuring unmarked CDDP, which is used in clinical practice, allows for more representative bioimaging of the Pt.

Data on the concentrations and the spatial distribution of the Pt in CDDP treated tumours obtained by LA-ICP-MS using gelatine gel standards revealed that the drug's application method influences the Pt concentration and distribution in the tumour. The dosage of CDDP injected (same for intravenous and intratumoral application) into the small volume of the tumour is oversaturating the tumour tissue, entering into the tumour environment and bloodstream. Although the intratumorally injected samples release CDDP with time, the CDDP concentration in the targeted tumour tissue was significantly higher than in the intravenous drug injection. Intravenous CDDP administration provides a more even distribution throughout the tumour. Consequently, a lower CDDP concentration is delivered to the tumorous tissue. This finding is of clinical relevance since it enables the targeted injection of the drug into the tumorous tissue. Consequently, the same drug's effectiveness is achieved at a lower dosage, which is beneficial in reducing the drug's side effects. It was also shown that the considerable variation of concentration and homogeneity in intratumoral samples is gradually reduced over time, resulting in a relatively even CDDP

distribution, similar to intravenous samples. After the application of the CDDP, the Pt is localised at the injection location and quickly distributed throughout the tumour, so the distribution is more even 10 min after the drug's administration. The LA-ICP-MS method was also optimized to study the localization of Cr in dandelions (Taraxacum officinale) grown in Cr-rich soil. Quantification with Cr spiked filter cut-out calibration standards provided semi-quantitative data for the Cr distribution in the dandelion leaf. The LA-ICP-MS data showed that the Cr in the leaf of the dandelions was localized mainly at the apex of the leaf.

To summarise, quantitative data provided by the LA-ICP-MS technique provides valuable additional information to the traditional methods, allowing for a deeper insight into the analyte's distribution in the sample.

References

[1] C. M. Croce, "Oncogenes and Cancer," *The New England Journal of Medicine*, p. 10, 2008.

[2] C. R. Thoma, M. Zimmermann, I. Agarkova, J. M. Kelm, and W. Krek, "3D cell culture systems modeling tumor growth determinants in cancer target discovery," *Advanced Drug Delivery Reviews*, vol. 69–70, pp. 29–41, Apr. 2014, doi: 10.1016/j.addr.2014.03.001.

[3] R. Baghban *et al.*, "Tumor microenvironment complexity and therapeutic implications at a glance," *Cell Commun Signal*, vol. 18, no. 1, p. 59, Dec. 2020, doi: 10.1186/s12964-020-0530-4.

[4] B. Arneth, "Tumor Microenvironment," *Medicina*, vol. 56, no. 1, p. 15, Dec. 2019, doi: 10.3390/medicina56010015.

[5] A. I. Minchinton and I. F. Tannock, "Drug penetration in solid tumours," *Nat Rev Cancer*, vol. 6, no. 8, pp. 583–592, Aug. 2006, doi: 10.1038/nrc1893.

[6] European Commission, "EU policy on cancer," 2021. [Online]. Available: https://ec.europa.eu/health/non-communicable-diseases/cancer_en

[7] M. Rowland and T. N. Tozer, *Clinical pharmacokinetics and pharmacodynamics: concepts and applications*, 4th ed. Philadelphia: Wolters Kluwer health - Lippincott William & Wilkins, 2011.

[8] J. S. Becker, A. Matusch, and B. Wu, "Bioimaging mass spectrometry of trace elements – recent advance and applications of LA-ICP-MS: A review," *Analytica Chimica Acta*, vol. 835, pp. 1–18, Jul. 2014, doi: 10.1016/j.aca.2014.04.048.

[9] A. R. Kherlopian *et al.*, "A review of imaging techniques for systems biology," *BMC Syst Biol*, vol. 2, no. 1, p. 74, 2008, doi: 10.1186/1752-0509-2-74.

[10] M. F. Gencoglu *et al.*, "Comparative Study of Multicellular Tumor Spheroid Formation Methods and Implications for Drug Screening," *ACS Biomater. Sci. Eng.*, vol. 4, no. 2, pp. 410–420, Feb. 2018, doi: 10.1021/acsbiomaterials.7b00069.

[11] H. J. Bowers, E. E. Fannin, A. Thomas, and J. A. Weis, "Characterization of multicellular breast tumor spheroids using image data-driven biophysical mathematical modeling," *Sci Rep*, vol. 10, no. 1, p. 11583, Dec. 2020, doi: 10.1038/s41598-020-68324-4.

[12] G. Mehta, A. Y. Hsiao, M. Ingram, G. D. Luker, and S. Takayama, "Opportunities and challenges for use of tumor spheroids as models to test drug delivery and efficacy," *Journal of Controlled Release*, vol. 164, no. 2, pp. 192–204, Dec. 2012, doi: 10.1016/j.jconrel.2012.04.045.

[13] S. Breslin and L. O'Driscoll, "Three-dimensional cell culture: the missing link in drug discovery," *Drug Discovery Today*, vol. 18, no. 5–6, pp. 240–249, Mar. 2013, doi: 10.1016/j.drudis.2012.10.003.

[14] R. Edmondson, J. J. Broglie, A. F. Adcock, and L. Yang, "Three-Dimensional Cell Culture Systems and Their Applications in Drug Discovery and Cell-Based Biosensors," *ASSAY and Drug Development Technologies*, vol. 12, no. 4, pp. 207–218, May 2014, doi: 10.1089/adt.2014.573.

[15] K. Stock *et al.*, "Capturing tumor complexity in vitro: Comparative analysis of 2D and 3D tumor models for drug discovery," *Sci Rep*, vol. 6, no. 1, p. 28951, Jul. 2016, doi: 10.1038/srep28951.

[16] L. Zitvogel, J. M. Pitt, R. Daillère, M. J. Smyth, and G. Kroemer, "Mouse models in oncoimmunology," *Nat Rev Cancer*, vol. 16, no. 12, pp. 759–773, Dec. 2016, doi: 10.1038/nrc.2016.91.

[17] D. S. Chulpanova, K. V. Kitaeva, C. S. Rutland, A. A. Rizvanov, and V. V. Solovyeva, "Mouse Tumor Models for Advanced Cancer Immunotherapy," *IJMS*, vol. 21, no. 11, p. 4118, Jun. 2020, doi: 10.3390/ijms21114118.

[18] N. Gengenbacher, M. Singhal, and H. G. Augustin, "Preclinical mouse solid tumour models: status quo, challenges and perspectives," *Nat Rev Cancer*, vol. 17, no. 12, pp. 751–765, Dec. 2017, doi: 10.1038/nrc.2017.92.

[19] U. Lampreht Tratar, S. Horvat, and M. Cemazar, "Transgenic Mouse Models in Cancer Research," *Front. Oncol.*, vol. 8, p. 268, Jul. 2018, doi: 10.3389/fonc.2018.00268.

[20] L. Yin, X.-J. Wang, D.-X. Chen, X.-N. Liu, and X.-J. Wang, "Humanized mouse model: a review on preclinical applications for cancer immunotherapy," p. 17.

[21] F. Hirschhaeuser, H. Menne, C. Dittfeld, J. West, W. Mueller-Klieser, and L. A. Kunz-Schughart, "Multicellular tumor spheroids: An underestimated tool is catching up again," *Journal of Biotechnology*, vol. 148, no. 1, pp. 3–15, Jul. 2010, doi: 10.1016/j.jbiotec.2010.01.012.

[22] S. C. Brüningk, I. Rivens, C. Box, U. Oelfke, and G. ter Haar, "3D tumour spheroids for the prediction of the effects of radiation and hyperthermia treatments," *Sci Rep*, vol. 10, no. 1, p. 1653, Dec. 2020, doi: 10.1038/s41598-020-58569-4.

[23] S. J. Han, S. Kwon, and K. S. Kim, "Challenges of applying multicellular tumor spheroids in preclinical phase," *Cancer Cell Int*, vol. 21, no. 1, p. 152, Dec. 2021, doi: 10.1186/s12935-021-01853-8.

[24] G. Lazzari, P. Couvreur, and S. Mura, "Multicellular tumor spheroids: a relevant 3D model for the in vitro preclinical investigation of polymer nanomedicines," *Polym. Chem.*, vol. 8, no. 34, pp. 4947–4969, 2017, doi: 10.1039/C7PY00559H.

[25] S. Marković *et al.*, "High spatial resolution imaging of cisplatin and Texas Red cisplatin in tumour spheroids using laser ablation isotope dilution inductively coupled plasma mass spectrometry and confocal fluorescence microscopy," *Analytica Chimica Acta*, vol. 1162, p. 338424, Jun. 2021, doi: 10.1016/j.aca.2021.338424.

[26] V. T. DeVita and E. Chu, "A History of Cancer Chemotherapy," *Cancer Res*, vol. 68, no. 21, pp. 8643–8653, Nov. 2008, doi: 10.1158/0008-5472.CAN-07-6611.

[27] B. A. Chabner and T. G. Roberts, "Chemotherapy and the war on cancer," *Nat Rev Cancer*, vol. 5, no. 1, pp. 65–72, Jan. 2005, doi: 10.1038/nrc1529.

[28] D. Galmarini, C. M. Galmarini, and F. C. Galmarini, "Cancer chemotherapy: A critical analysis of its 60 years of history," *Critical Reviews in Oncology/Hematology*, vol. 84, no. 2, pp. 181–199, Nov. 2012, doi: 10.1016/j.critrevonc.2012.03.002.

[29] M. Hejna, M. Pruckmayer, and M. Raderer, "The role of chemotherapy and radiation in the management of biliary cancer: a review of the literature," *European Journal of Cancer*, vol. 34, no. 7, pp. 977–986, Jun. 1998, doi: 10.1016/S0959-8049(97)10166-6.

[30] C. Carlier *et al.*, "Nanoscopic tumor tissue distribution of platinum after intraperitoneal administration in a xenograft model of ovarian cancer," *Journal of Pharmaceutical and Biomedical Analysis*, vol. 131, pp. 256–262, Nov. 2016, doi: 10.1016/j.jpba.2016.09.004.

[31] V. Schirrmacher, "From chemotherapy to biological therapy: A review of novel concepts to reduce the side effects of systemic cancer treatment (Review)," *INTERNATIONAL JOURNAL OF ONCOLOGY*, p. 13, 2019.

[32] A. I. Minchinton and I. F. Tannock, "Drug penetration in solid tumours," *Nat Rev Cancer*, vol. 6, no. 8, pp. 583–592, Aug. 2006, doi: 10.1038/nrc1893.

[33] W. Jiang, J. Chen, C. Gong, Y. Wang, Y. Gao, and Y. Yuan, "Intravenous delivery of enzalutamide based on high drug loading multifunctional graphene oxide nanoparticles for castration-resistant prostate cancer therapy," *J Nanobiotechnol*, vol. 18, no. 1, p. 50, Dec. 2020, doi: 10.1186/s12951-020-00607-4.

[34] R. Tziortzioti, "Anti-tumor Effect of Intravenous Administration of CRM197 for Triple-negative Breast Cancer Therapy," *ANTICANCER RESEARCH*, p. 7, 2016.

[35] E. P. Goldberg, A. R. Hadba, B. A. Almond, and J. S. Marotta, "Intratumoral cancer chemotherapy and immunotherapy: opportunities for nonsystemic preoperative drug delivery," *Journal of Pharmacy and Pharmacology*, vol. 54, no. 2, pp. 159–180, Feb. 2010, doi: 10.1211/0022357021778268.

[36] A. Groselj *et al.*, "Bleomycin Concentration in Patients' Plasma and Tumors after Electrochemotherapy. A Study from InspECT Group," *Pharmaceutics*, vol. 13, no. 9, p. 1324, Aug. 2021, doi: 10.3390/pharmaceutics13091324.

[37] G. Sersa, K. Ursic, M. Cemazar, R. Heller, M. Bosnjak, and L. G. Campana, "Biological factors of the tumour response to electrochemotherapy: Review of the evidence and a research roadmap," *European Journal of Surgical Oncology*, vol. 47, no. 8, pp. 1836–1846, Aug. 2021, doi: 10.1016/j.ejso.2021.03.229.

[38] A. Vižintin, S. Marković, J. Ščančar, and D. Miklavčič, "Electroporation with nanosecond pulses and bleomycin or cisplatin results in efficient cell kill and low metal release from electrodes," *Bioelectrochemistry*, vol. 140, p. 107798, Aug. 2021, doi: 10.1016/j.bioelechem.2021.107798.

[39] S. Ghosh, "Cisplatin: The first metal based anticancer drug," *Bioorganic Chemistry*, vol. 88, p. 102925, Jul. 2019, doi: 10.1016/j.bioorg.2019.102925.

[40] T. C. Johnstone, K. Suntharalingam, and S. J. Lippard, "The Next Generation of Platinum Drugs: Targeted Pt(II) Agents, Nanoparticle Delivery, and Pt(IV) Prodrugs," *Chem. Rev.*, vol. 116, no. 5, pp. 3436–3486, Mar. 2016, doi: 10.1021/acs.chemrev.5b00597.

[41] R. Oun, Y. E. Moussa, and N. J. Wheate, "The side effects of platinum-based chemotherapy drugs: a review for chemists," *Dalton Trans.*, vol. 47, no. 19, pp. 6645–6653, 2018, doi: 10.1039/C8DT00838H.

[42] R. C. Todd and S. J. Lippard, "Inhibition of transcription by platinum antitumor compounds," *Metallomics*, vol. 1, no. 4, p. 280, 2009, doi: 10.1039/b907567d.

[43] M. Cemazar, R. Milacic, D. Miklavcic, V. Dolzan, and G. Sersa, "Intratumoral cisplatin administration in electrochemotherapy: antitumor effectiveness, sequence dependence and platinum content," p. 6.

[44] S. Dasari and P. Bernard Tchounwou, "Cisplatin in cancer therapy: Molecular mechanisms of action," *European Journal of Pharmacology*, vol. 740, pp. 364–378, Oct. 2014, doi: 10.1016/j.ejphar.2014.07.025.

[45] A. Martincic, R. Milacic, M. Cemazar, G. Sersa, and J. Scancar, "The use of CIM-DEAE monolithic chromatography coupled to ICP-MS to study the distribution of cisplatin in human serum," *Anal. Methods*, vol. 4, no. 3, p. 780, 2012, doi: 10.1039/c2ay05603h.

[46] Y.-H. Chu *et al.*, "Systemic Delivery and Biodistribution of Cisplatin *in Vivo*," *Mol. Pharmaceutics*, vol. 13, no. 8, pp. 2677–2682, Aug. 2016, doi: 10.1021/acs.molpharmaceut.6b00240.

[47] K. A. Doucette, K. N. Hassell, and D. C. Crans, "Selective speciation improves efficacy and lowers toxicity of platinum anticancer and vanadium antidiabetic drugs," *Journal of Inorganic Biochemistry*, vol. 165, pp. 56–70, Dec. 2016, doi: 10.1016/j.jinorgbio.2016.09.013.

[48] X. Le and E. Y. Hanna, "Optimal regimen of cisplatin in squamous cell carcinoma of head and neck yet to be determined," *Ann. Transl. Med*, vol. 6, no. 11, pp. 229–229, Jun. 2018, doi: 10.21037/atm.2018.05.10.

[49] M. J. Yaffe, "Emergence of 'Big Data' and Its Potential and Current Limitations in Medical Imaging," *Seminars in Nuclear Medicine*, vol. 49, no. 2, pp. 94–104, Mar. 2019, doi: 10.1053/j.semnuclmed.2018.11.010.

[50] D. D. Pobirci, F. Bogdan, O. Pobirci, C. A. Petcu, and E. Ro, "Study of malignant fibrous histiocytoma: clinical, statistic and histopatological interrelation," p. 4.

[51] A. Fernandez and M. Vendrell, "Fluorophore–Drug Conjugates To Unravel the Mechanisms of Action of Therapeutic Assets," *Biochemistry*, vol. 57, no. 2, pp. 175–176, Jan. 2018, doi: 10.1021/acs.biochem.7b00889.

[52] P. M. Uribe *et al.*, "Dimethyl Sulfoxide (DMSO) Exacerbates Cisplatin-induced Sensory Hair Cell Death in Zebrafish (Danio rerio)," *PLoS ONE*, vol. 8, no. 2, p. e55359, Feb. 2013, doi: 10.1371/journal.pone.0055359.

[53] A. E. Egger *et al.*, "Extravasation of Pt-based chemotherapeutics – bioimaging of their distribution in resectates using laser ablation-inductively coupled plasma-mass spectrometry (LA-ICP-MS)," *Metallomics*, vol. 7, no. 3, pp. 508–515, 2015, doi: 10.1039/C4MT00308J.

[54] A. Arakawa *et al.*, "Quantitative Imaging of Silver Nanoparticles and Essential Elements in Thin Sections of Fibroblast Multicellular Spheroids by High Resolution Laser Ablation Inductively Coupled Plasma Time-of-Flight Mass Spectrometry,"

Anal. Chem., vol. 91, no. 15, pp. 10197–10203, Aug. 2019, doi: 10.1021/acs.analchem.9b02239.

[55] M. Zhou *et al.*, "Radiomics in Brain Tumor: Image Assessment, Quantitative Feature Descriptors, and Machine-Learning Approaches," *AJNR Am J Neuroradiol*, vol. 39, no. 2, pp. 208–216, Feb. 2018, doi: 10.3174/ajnr.A5391.

[56] H. U. Holtkamp and C. G. Hartinger, "Advanced metallomics methods in anticancer metallodrug mode of action studies," *TrAC Trends in Analytical Chemistry*, vol. 104, pp. 110–117, Jul. 2018, doi: 10.1016/j.trac.2017.09.023.

[57] R. F. S. Lee, S. Theiner, A. Meibom, G. Koellensperger, B. K. Keppler, and P. J. Dyson, "Application of imaging mass spectrometry approaches to facilitate metal-based anticancer drug research," *Metallomics*, vol. 9, no. 4, pp. 365–381, 2017, doi: 10.1039/C6MT00231E.

[58] D. Pozebon, G. L. Scheffler, and V. L. Dressler, "Recent applications of laser ablation inductively coupled plasma mass spectrometry (LA-ICP-MS) for biological sample analysis: a follow-up review," *J. Anal. At. Spectrom.*, vol. 32, no. 5, pp. 890–919, 2017, doi: 10.1039/C7JA00026J.

[59] S. Theiner *et al.*, "Tumor microenvironment in focus: LA-ICP-MS bioimaging of a preclinical tumor model upon treatment with platinum(IV)-based anticancer agents," *Metallomics*, vol. 7, no. 8, pp. 1256–1264, 2015, doi: 10.1039/C5MT00028A.

[60] S. R. Ellis, A. L. Bruinen, and R. M. A. Heeren, "A critical evaluation of the current state-of-the-art in quantitative imaging mass spectrometry," *Anal Bioanal Chem*, vol. 406, no. 5, pp. 1275–1289, Feb. 2014, doi: 10.1007/s00216-013-7478-9.

[61] P. Sylvester, *Laser Ablation ICP-MC in the Earth Sciences Current Practices and Outstanding Issues*, vol. 40. 2008.

[62] D. P. Bishop *et al.*, "Elemental bio-imaging using laser ablation-triple quadrupole-ICP-MS," *J. Anal. At. Spectrom.*, vol. 31, no. 1, pp. 197–202, 2016, doi: 10.1039/C5JA00293A.

[63] D. Pozebon, G. L. Scheffler, V. L. Dressler, and M. A. G. Nunes, "Review of the applications of laser ablation inductively coupled plasma mass spectrometry (LA-ICP-MS) to the analysis of biological samples," *J. Anal. At. Spectrom.*, vol. 29, no. 12, pp. 2204–2228, 2014, doi: 10.1039/C4JA00250D.

[64] T. Van Acker *et al.*, "High-resolution imaging and single-cell analysis via laser ablation-inductively coupled plasma-mass spectrometry for the determination of membranous receptor expression levels in breast cancer cell lines using receptor-specific hybrid tracers," *Analytica Chimica Acta*, vol. 1074, pp. 43–53, Oct. 2019, doi: 10.1016/j.aca.2019.04.064.

[65] J. S. Becker *et al.*, "Bioimaging of metals by laser ablation inductively coupled plasma mass spectrometry (LA-ICP-MS): BIOIMAGING OF METALS BY LA-ICP-MS," *Mass Spectrom. Rev.*, vol. 29, no. 1, pp. 156–175, Jan. 2010, doi: 10.1002/mas.20239.

[66] I. Konz, B. Fernández, M. L. Fernández, R. Pereiro, and A. Sanz-Medel, "Laser ablation ICP-MS for quantitative biomedical applications," *Anal Bioanal Chem*, vol. 403, no. 8, pp. 2113–2125, Jun. 2012, doi: 10.1007/s00216-012-6023-6.

[67] A. Sajnóg, A. Hanć, and D. Barałkiewicz, "Metrological approach to quantitative analysis of clinical samples by LA-ICP-MS: A critical review of recent studies," *Talanta*, vol. 182, pp. 92–110, May 2018, doi: 10.1016/j.talanta.2018.01.050.

[68] A. Sajnóg, A. Hanć, and D. Barałkiewicz, "Metrological approach to quantitative analysis of clinical samples by LA-ICP-MS: A critical review of recent studies," *Talanta*, vol. 182, pp. 92–110, May 2018, doi: 10.1016/j.talanta.2018.01.050.

[69] S. J. M. Van Malderen, A. J. Managh, B. L. Sharp, and F. Vanhaecke, "Recent developments in the design of rapid response cells for laser ablation-inductively coupled plasma-mass spectrometry and their impact on bioimaging applications," *J. Anal. At. Spectrom.*, vol. 31, no. 2, pp. 423–439, 2016, doi: 10.1039/C5JA00430F.

[70] N. Miliszkiewicz, S. Walas, and A. Tobiasz, "Current approaches to calibration of LA-ICP-MS analysis," *J. Anal. At. Spectrom.*, vol. 30, no. 2, pp. 327–338, 2015, doi: 10.1039/C4JA00325J.

[71] H. Sela, Z. Karpas, H. Cohen, Y. Zakon, and Y. Zeiri, "Preparation of stable standards of biological tissues for laser ablation analysis," *International Journal of Mass Spectrometry*, vol. 307, no. 1–3, pp. 142–148, Oct. 2011, doi: 10.1016/j.ijms.2011.01.022.

[72] J. T. van Elteren, V. S. Šelih, M. Šala, S. J. M. Van Malderen, and F. Vanhaecke, "Imaging Artifacts in Continuous Scanning 2D LA-ICPMS Imaging Due to Nonsynchronization Issues," *Anal. Chem.*, vol. 90, no. 4, pp. 2896–2901, Feb. 2018, doi: 10.1021/acs.analchem.7b05134.

[73] J. T. van Elteren, D. Metarapi, M. Šala, V. S. Šelih, and C. C. Stremtan, "Fine-tuning of LA-ICP-QMS conditions for elemental mapping," *J. Anal. At. Spectrom.*, vol. 35, no. 11, pp. 2494–2497, 2020, doi: 10.1039/D0JA00322K.

[74] T. Van Acker *et al.*, "Analytical figures of merit of a low-dispersion aerosol transport system for high-throughput LA-ICP-MS analysis," *J. Anal. At. Spectrom.*, vol. 36, no. 6, pp. 1201–1209, 2021, doi: 10.1039/D1JA00110H.

[75] J. T. van Elteren, V. S. Šelih, and M. Šala, "Insights into the selection of 2D LA-ICP-MS (multi)elemental mapping conditions," *J. Anal. At. Spectrom.*, vol. 34, no. 9, pp. 1919–1931, 2019, doi: 10.1039/C9JA00166B.

[76] S. Theiner *et al.*, "Laser Ablation-Inductively Coupled Plasma Time-of-Flight Mass Spectrometry Imaging of Trace Elements at the Single-Cell Level for Clinical Practice," *Anal. Chem.*, vol. 91, no. 13, pp. 8207–8212, Jul. 2019, doi: 10.1021/acs.analchem.9b00698.

[77] M. S. A. Horstwood, "Data reduction strategies, uncertainty assessment and resolution," p. 43.

[78] L. J. Castellanos-García, S. Gokhan Elci, and R. W. Vachet, "Reconstruction, analysis, and segmentation of LA-ICP-MS imaging data using Python for the identification of sub-organ regions in tissues," *Analyst*, vol. 145, no. 10, pp. 3705–3712, 2020, doi: 10.1039/C9AN02472G.

[79] R. Weiskirchen, S. Weiskirchen, P. Kim, and R. Winkler, "Software solutions for evaluation and visualization of laser ablation inductively coupled plasma mass spectrometry imaging (LA-ICP-MSI) data: a short overview," *J Cheminform*, vol. 11, no. 1, p. 16, Dec. 2019, doi: 10.1186/s13321-019-0338-7.

[80] H. López-Fernández *et al.*, "LA-iMageS: a software for elemental distribution bioimaging using LA–ICP–MS data," *J Cheminform*, vol. 8, no. 1, p. 65, Dec. 2016, doi: 10.1186/s13321-016-0178-7.

[81] M. F. Al-Hakkani, "Guideline of inductively coupled plasma mass spectrometry 'ICP–MS': fundamentals, practices, determination of the limits, quality control, and method validation parameters," *SN Appl. Sci.*, vol. 1, no. 7, p. 791, Jul. 2019, doi: 10.1007/s42452-019-0825-5.

[82] S. Wilschefski and M. Baxter, "Inductively Coupled Plasma Mass Spectrometry: Introduction to Analytical Aspects," *CBR*, vol. 40, no. 3, pp. 115–133, Aug. 2019, doi: 10.33176/AACB-19-00024.

[83] D. Pröfrock and A. Prange, "Inductively Coupled Plasma–Mass Spectrometry (ICP-MS) for Quantitative Analysis in Environmental and Life Sciences: A Review of Challenges, Solutions, and Trends," *Appl Spectrosc*, vol. 66, no. 8, pp. 843–868, Aug. 2012, doi: 10.1366/12-06681.

[84] S. Sindern, "Analysis of Rare Earth Elements in Rock and Mineral Samples by ICP-MS and LA-ICP-MS," *Physical Sciences Reviews*, vol. 2, no. 2, Feb. 2017, doi: 10.1515/psr-2016-0066.

[85] M. D. Montaño, J. W. Olesik, A. G. Barber, K. Challis, and J. F. Ranville, "Single Particle ICP-MS: Advances toward routine analysis of nanomaterials," *Anal Bioanal Chem*, vol. 408, no. 19, pp. 5053–5074, Jul. 2016, doi: 10.1007/s00216-016-9676-8.

[86] B. Gulson, G. Kamenov, W. Manton, and M. Rabinowitz, "Concerns about Quadrupole ICP-MS Lead Isotopic Data and Interpretations in the Environment and Health Fields," *IJERPH*, vol. 15, no. 4, p. 723, Apr. 2018, doi: 10.3390/ijerph15040723.

[87] S. Miyashita, A. S. Groombridge, S. Fujii, A. Takatsu, K. Chiba, and K. Inagaki, "Time-resolved ICP-MS Measurement: a New Method for Elemental and Multiparametric Analysis of Single Cells," *Anal. Sci.*, vol. 30, no. 2, pp. 219–224, 2014, doi: 10.2116/analsci.30.219.

[88] M. Burger *et al.*, "High-Speed, High-Resolution, Multielemental LA-ICP-TOFMS Imaging: Part II. Critical Evaluation of Quantitative Three-Dimensional Imaging of Major, Minor, and Trace Elements in Geological Samples," *Anal. Chem.*, vol. 87, no. 16, pp. 8259–8267, Aug. 2015, doi: 10.1021/acs.analchem.5b01977.

[89] D. Rubatto *et al.*, "Identification of growth mechanisms in metamorphic garnet by high-resolution trace element mapping with LA-ICP-TOFMS," *Contrib Mineral Petrol*, vol. 175, no. 7, p. 61, Jul. 2020, doi: 10.1007/s00410-020-01700-5.

[90] N. Jakubowski, L. Moens, and F. Vanhaecke, "Sector field mass spectrometers in ICP-MS," *Spectrochimica Acta Part B: Atomic Spectroscopy*, vol. 53, no. 13, pp. 1739–1763, Nov. 1998, doi: 10.1016/S0584-8547(98)00222-5.

[91] F. Vanhaecke, L. Balcaen, and D. Malinovsky, "Use of single-collector and multi-collector ICP-mass spectrometry for isotopic analysis," *J. Anal. At. Spectrom.*, vol. 24, no. 7, p. 863, 2009, doi: 10.1039/b903887f.

[92] T. Pettke *et al.*, "Recent developments in element concentration and isotope ratio analysis of individual fluid inclusions by laser ablation single and multiple collector

ICP-MS," *Ore Geology Reviews*, vol. 44, pp. 10–38, Feb. 2012, doi: 10.1016/j.oregeorev.2011.11.001.

[93] W. Zhang *et al.*, "Direct lead isotope analysis in Hg-rich sulfides by LA-MC-ICP-MS with a gas exchange device and matrix-matched calibration," *Analytica Chimica Acta*, vol. 948, pp. 9–18, Dec. 2016, doi: 10.1016/j.aca.2016.10.040.

[94] W. Zhang and Z. Hu, "A critical review of isotopic fractionation and interference correction methods for isotope ratio measurements by laser ablation multi-collector inductively coupled plasma mass spectrometry," *Spectrochimica Acta Part B: Atomic Spectroscopy*, vol. 171, p. 105929, Sep. 2020, doi: 10.1016/j.sab.2020.105929.

[95] L. Gorojovsky and O. Alard, "Optimisation of laser and mass spectrometer parameters for the *in situ* analysis of Rb/Sr ratios by LA-ICP-MS/MS," *J. Anal. At. Spectrom.*, vol. 35, no. 10, pp. 2322–2336, 2020, doi: 10.1039/D0JA00308E.

[96] G. L. Donati, R. S. Amais, and J. A. Nóbrega, "Strategies to improve accuracy and sensitivity in phosphorus determinations by inductively coupled plasma quadrupole mass spectrometry," *J. Braz. Chem. Soc.*, vol. 23, no. 4, pp. 786–791, Apr. 2012, doi: 10.1590/S0103-50532012000400026.

[97] A. Hineman and C. Stephan, "Effect of dwell time on single particle inductively coupled plasma mass spectrometry data acquisition quality," *J. Anal. At. Spectrom.*, vol. 29, no. 7, pp. 1252–1257, 2014, doi: 10.1039/C4JA00097H.

[98] H. El Hadri, E. J. Petersen, and M. R. Winchester, "Impact of and correction for instrument sensitivity drift on nanoparticle size measurements by single-particle ICP-MS," *Anal Bioanal Chem*, vol. 408, no. 19, pp. 5099–5108, Jul. 2016, doi: 10.1007/s00216-016-9397-z.

[99] Y. Liu, Z. Hu, M. Li, and S. Gao, "Applications of LA-ICP-MS in the elemental analyses of geological samples," *Chin. Sci. Bull.*, vol. 58, no. 32, pp. 3863–3878, Nov. 2013, doi: 10.1007/s11434-013-5901-4.

[100] M. Šala, V. S. Šelih, C. C. Stremtan, T. Tămaş, and J. T. van Elteren, "Implications of laser shot dosage on image quality in LA-ICP-QMS imaging," *J. Anal. At. Spectrom.*, vol. 36, no. 1, pp. 75–79, 2021, doi: 10.1039/D0JA00381F.

[101] B. Fernández, F. Claverie, C. Pécheyran, O. F. X. Donard, and F. Claverie, "Direct analysis of solid samples by fs-LA-ICP-MS," *TrAC Trends in Analytical Chemistry*, vol. 26, no. 10, pp. 951–966, Nov. 2007, doi: 10.1016/j.trac.2007.08.008.

[102] I. Horn, M. Guillong, and D. GuÈnther, "Wavelength dependant ablation rates for metals and silicate glasses using homogenized laser beam pro®les Ð implications for LA-ICP-MS," *Applied Surface Science*, p. 12, 2001.

[103] S. J. M. Van Malderen, T. Van Acker, and F. Vanhaecke, "Sub-micrometer Nanosecond LA-ICP-MS Imaging at Pixel Acquisition Rates above 250 Hz via a Low-Dispersion Setup," *Anal. Chem.*, vol. 92, no. 8, pp. 5756–5764, Apr. 2020, doi: 10.1021/acs.analchem.9b05056.

[104] M. E. Shaheen, J. E. Gagnon, and B. J. Fryer, "Femtosecond (fs) lasers coupled with modern ICP-MS instruments provide new and improved potential for in situ elemental and isotopic analyses in the geosciences," *Chemical Geology*, vol. 330–331, pp. 260–273, Nov. 2012, doi: 10.1016/j.chemgeo.2012.09.016.

[105] J. T. van Elteren, M. Šala, and V. S. Šelih, "Perceptual Image Quality Metrics Concept in Continuous Scanning 2D Laser Ablation-Inductively Coupled Plasma Mass Spectrometry Bioimaging," *Anal. Chem.*, vol. 90, no. 9, pp. 5916–5922, May 2018, doi: 10.1021/acs.analchem.8b00751.

[106] S. J. M. Van Malderen, J. T. van Elteren, V. S. Šelih, and F. Vanhaecke, "Considerations on data acquisition in laser ablation-inductively coupled plasma-mass spectrometry with low-dispersion interfaces," *Spectrochimica Acta Part B: Atomic Spectroscopy*, vol. 140, pp. 29–34, Feb. 2018, doi: 10.1016/j.sab.2017.11.007.

[107] B. Hattendorf, U. Hartfelder, and D. Günther, "Skip the beat: minimizing aliasing error in LA-ICP-MS measurements," *Anal Bioanal Chem*, vol. 411, no. 3, pp. 591–602, Jan. 2019, doi: 10.1007/s00216-018-1314-1.

[108] C. J. Greenhalgh *et al.*, "Exploration of Matrix Effects in Laser Ablation Inductively Coupled Plasma Mass Spectrometry Imaging of Cisplatin-Treated Tumors," *Anal. Chem.*, vol. 92, no. 14, pp. 9847–9855, Jul. 2020, doi: 10.1021/acs.analchem.0c01347.

[109] M. Gaboardi and M. Humayun, "Elemental fractionation during LA-ICP-MS analysis of silicate glasses: implications for matrix-independent standardization," *J. Anal. At. Spectrom.*, vol. 24, no. 9, p. 1188, 2009, doi: 10.1039/b900876d.

[110] C. M. Allen and I. H. Campbell, "Identification and elimination of a matrix-induced systematic error in LA–ICP–MS 206Pb/238U dating of zircon," *Chemical Geology*, vol. 332–333, pp. 157–165, Nov. 2012, doi: 10.1016/j.chemgeo.2012.09.038.

[111] D. Hare, C. Austin, and P. Doble, "Quantification strategies for elemental imaging of biological samples using laser ablation-inductively coupled plasma-mass spectrometry," *Analyst*, vol. 137, no. 7, p. 1527, 2012, doi: 10.1039/c2an15792f.

[112] J. Lin, Y. Liu, Y. Yang, and Z. Hu, "Calibration and correction of LA-ICP-MS and LA-MC-ICP-MS analyses for element contents and isotopic ratios," *Solid Earth Sciences*, vol. 1, no. 1, pp. 5–27, Jun. 2016, doi: 10.1016/j.sesci.2016.04.002.

[113] M. Šala, V. S. Šelih, and J. T. van Elteren, "Gelatin gels as multi-element calibration standards in LA-ICP-MS bioimaging: fabrication of homogeneous standards and microhomogeneity testing," *Analyst*, vol. 142, no. 18, pp. 3356–3359, 2017, doi: 10.1039/C7AN01361B.

[114] O. B. Bauer, C. Köppen, M. Sperling, H.-J. Schurek, G. Ciarimboli, and U. Karst, "Quantitative Bioimaging of Platinum via Online Isotope Dilution-Laser Ablation-Inductively Coupled Plasma Mass Spectrometry," *Anal. Chem.*, vol. 90, no. 11, pp. 7033–7039, Jun. 2018, doi: 10.1021/acs.analchem.8b01429.

[115] P. Rodríguez-González, J. M. Marchante-Gayón, J. I. García Alonso, and A. Sanz-Medel, "Isotope dilution analysis for elemental speciation: a tutorial review," *Spectrochimica Acta Part B: Atomic Spectroscopy*, vol. 60, no. 2, pp. 151–207, Feb. 2005, doi: 10.1016/j.sab.2005.01.005.

[116] M. T. Westerhausen *et al.*, "Low background mould-prepared gelatine standards for reproducible quantification in elemental bio-imaging," *Analyst*, vol. 144, no. 23, pp. 6881–6888, 2019, doi: 10.1039/C9AN01580A.

[117] M. Vašinová Galiová *et al.*, "Elemental mapping in fossil tooth root section of Ursus arctos by laser ablation inductively coupled plasma mass spectrometry (LA-ICP-MS)," *Talanta*, vol. 105, pp. 235–243, Feb. 2013, doi: 10.1016/j.talanta.2012.12.037.

[118] M. Costas-Rodríguez *et al.*, "Laser ablation-inductively coupled plasma-mass spectrometry for quantitative mapping of the copper distribution in liver tissue sections from mice with liver disease induced by common bile duct ligation," *J. Anal. At. Spectrom.*, vol. 32, no. 9, pp. 1805–1812, 2017, doi: 10.1039/C7JA00134G.

[119] H.-J. Stärk and R. Wennrich, "A new approach for calibration of laser ablation inductively coupled plasma mass spectrometry using thin layers of spiked agarose gels as references," *Anal Bioanal Chem*, vol. 399, no. 6, pp. 2211–2217, Feb. 2011, doi: 10.1007/s00216-010-4413-1.

[120] M. Bonta, B. Hegedus, and A. Limbeck, "Application of dried-droplets deposited on pre-cut filter paper disks for quantitative LA-ICP-MS imaging of biologically relevant minor and trace elements in tissue samples," *Analytica Chimica Acta*, vol. 908, pp. 54–62, Feb. 2016, doi: 10.1016/j.aca.2015.12.048.

[121] A. J. Herrmann *et al.*, "A simple metal staining procedure for identification and visualization of single cells by LA-ICP-MS," *Analyst*, vol. 142, no. 10, pp. 1703–1710, 2017, doi: 10.1039/C6AN02638A.

[122] I. Moraleja *et al.*, "An approach for quantification of platinum distribution in tissues by LA-ICP-MS imaging using isotope dilution analysis," *Talanta*, vol. 178, pp. 166–171, Feb. 2018, doi: 10.1016/j.talanta.2017.09.031.

[123] K. Halbach, S. Wagner, S. Scholz, T. Luckenbach, and T. Reemtsma, "Elemental imaging (LA-ICP-MS) of zebrafish embryos to study the toxicokinetics of the acetylcholinesterase inhibitor naled," *Anal Bioanal Chem*, vol. 411, no. 3, pp. 617–627, Jan. 2019, doi: 10.1007/s00216-018-1471-2.

[124] D. J. Hare *et al.*, "Imaging Metals in Brain Tissue by Laser Ablation - Inductively Coupled Plasma - Mass Spectrometry (LA-ICP-MS)," *JoVE*, no. 119, p. 55042, Jan. 2017, doi: 10.3791/55042.

[125] S. Theiner, E. Schreiber-Brynzak, M. A. Jakupec, M. Galanski, G. Koellensperger, and B. K. Keppler, "LA-ICP-MS imaging in multicellular tumor spheroids – a novel tool in the preclinical development of metal-based anticancer drugs," *Metallomics*, vol. 8, no. 4, pp. 398–402, 2016, doi: 10.1039/C5MT00276A.

[126] M. Bonta, S. Török, B. Hegedus, B. Döme, and A. Limbeck, "A comparison of sample preparation strategies for biological tissues and subsequent trace element analysis using LA-ICP-MS," *Anal Bioanal Chem*, vol. 409, no. 7, pp. 1805–1814, Mar. 2017, doi: 10.1007/s00216-016-0124-6.

[127] A.-C. Niehoff *et al.*, "Quantitative bioimaging of platinum group elements in tumor spheroids," *Analytica Chimica Acta*, vol. 938, pp. 106–113, Sep. 2016, doi: 10.1016/j.aca.2016.07.021.

[128] E. Schreiber-Brynzak *et al.*, "Behavior of platinum(IV) complexes in models of tumor hypoxia: cytotoxicity, compound distribution and accumulation," *Metallomics*, vol. 8, no. 4, pp. 422–433, 2016, doi: 10.1039/C5MT00312A.

[129] S. Theiner *et al.*, "Fast High-Resolution Laser Ablation-Inductively Coupled Plasma Mass Spectrometry Imaging of the Distribution of Platinum-Based Anticancer Compounds in Multicellular Tumor Spheroids," *Anal. Chem.*, vol. 89, no. 23, pp. 12641–12645, Dec. 2017, doi: 10.1021/acs.analchem.7b02681.

[130] M. Brloznik *et al.*, "Contrast-enhanced ultrasound for evaluation of tumor perfusion and outcome following treatment in a murine melanoma model," *Bioelectrochemistry*, vol. 142, p. 107932, Dec. 2021, doi: 10.1016/j.bioelechem.2021.107932.

[131] S. Marković, L. Levstek, D. Žigon, J. Ščančar, and R. Milačič, "Speciation and Bio-Imaging of Chromium in Taraxacum officinale Using HPLC Post-column ID-ICP-MS, High Resolution MS and Laser Ablation ICP-MS Techniques," *Front. Chem.*, vol. 10, p. 863387, May 2022, doi: 10.3389/fchem.2022.863387.

[132] V. M. Gonzalez, M. A. Fuertes, C. Alonso, and J. M. Perez, "Is Cisplatin-Induced Cell Death Always Produced by Apoptosis?," *Mol Pharmacol*, vol. 59, no. 4, pp. 657–663, Apr. 2001, doi: 10.1124/mol.59.4.657.

[133] A. Kötschau, G. Büchel, J. W. Einax, C. Fischer, W. von Tümpling, and D. Merten, "Mapping of macro and micro elements in the leaves of sunflower (Helianthus annuus) by Laser Ablation–ICP–MS," *Microchemical Journal*, vol. 110, pp. 783–789, Sep. 2013, doi: 10.1016/j.microc.2012.12.011.

[134] A. Pedrosa Diniz, A. Rodrigues Kozovits, C. de Carvalho Lana, A. Trópia de Abreu, and M. Garcia Praça Leite, "Quantitative analysis of plant leaf elements using the LA-ICP-MS technique," *International Journal of Mass Spectrometry*, vol. 435, pp. 251–258, Jan. 2019, doi: 10.1016/j.ijms.2018.10.037.

[135] M. C. Shelden, S. E. Gilbert, and S. D. Tyerman, "A laser ablation technique maps differences in elemental composition in roots of two barley cultivars subjected to salinity stress," *Plant J*, vol. 101, no. 6, pp. 1462–1473, Mar. 2020, doi: 10.1111/tpj.14599.

[136] W. Huang *et al.*, "Localization and Speciation of Chromium in Coptis chinensis Franch. using Synchrotron Radiation X-ray Technology and Laser Ablation ICP-MS," *Sci Rep*, vol. 8, no. 1, p. 8603, Dec. 2018, doi: 10.1038/s41598-018-26774-x.

Bibliography

Publications Related to the Thesis

Journal Articles

S. Marković, L. Levstek, D. Žigon, J. Ščančar, and R. Milačič, "Speciation and Bio-Imaging of Chromium in Taraxacum officinale Using HPLC Post-column ID-ICP-MS, High Resolution MS and Laser Ablation ICP-MS Techniques," *Front. Chem.*, vol. 10, p. 863387, May 2022, doi: 10.3389/fchem.2022.863387.

S. Marković, K. Uršič, M. Čemažar, G. Serša, B. Starešinič. R. Milačič and J. Ščančar, "High spatial resolution imaging of cisplatin and Texas Red cisplatin in tumour spheroids using laser ablation isotope dilution inductively coupled plasma mass spectrometry and confocal fluorescence microscopy," Analytica Chimica Acta, vol. 1162, p. 338424, Jun. 2021, doi: 10.1016/j.aca.2021.338424.

Other Publications

Journal Articles

A. Vižintin, S. Marković, J. Ščančar, J. Kladnik, I. Turel and D. Miklavičič, "Nanosecond electric pulses are equally effective in electrochemotherapy with cisplatin as microsecond pulses," Radiology and Oncology, accepted, 2022

S. Marković, M. Gabrič, M. Islamčević Razboršek, R. Milačič, and J. Ščančar, "The use of enriched stable isotopic tracers of 50Cr(VI) and 53Cr(III) in a study of Cr speciation in wine and beer," Journal of Food Composition and Analysis, vol. 108, p. 104422, May 2022, doi: 10.1016/j.jfca.2022.104422.

S. Nübler et al., "Interlaboratory Comparison Investigations (ICIs) for human biomonitoring of chromium as part of the quality assurance programme under HBM4EU," Journal of Trace Elements in Medicine and Biology, vol. 70, p. 126912, Mar. 2022, doi: 10.1016/j.jtemb.2021.126912.

A. Vižintin, S. Marković, J. Ščančar, and D. Miklavčič, "Electroporation with nanosecond pulses and bleomycin or cisplatin results in efficient cell kill and low metal release from electrodes," Bioelectrochemistry, vol. 140, p. 107798, Aug. 2021, doi: 10.1016/j.bioelechem.2021.107798.

K. Marković, R. Milačič, J. Vidmar, S. Marković, K. Uršič, M. Žakelj, M. Čemažar, G. Serša, M. Unk, and J. Ščančar, "Monolithic chromatography on conjoint liquid chromatography columns for speciation of platinum-based chemotherapeutics in serum of cancer patients," Journal of Trace Elements in Medicine and Biology, vol. 57, pp. 28–39, Jan. 2020, doi: 10.1016/j.jtemb.2019.09.011.

K. Marković, R. Milačič, S. Marković, J. Kladnik, I. Turel, and J. Ščančar, "Binding Kinetics of Ruthenium Pyrithione Chemotherapeutic Candidates to Human Serum

Proteins Studied by HPLC-ICP-MS," Molecules, vol. 25, no. 7, p. 1512, Mar. 2020, doi: 10.3390/molecules25071512.

Biography

Stefan Marković, born 19-06-1993 in Čačak, Serbia, graduated with honours in 2012. In the period 2012–2017 he studied at the University of Belgrade, Faculty of Chemistry, where he researched the reuse of waste high-density polyethylene (HDPE) and low-quality lignite coal, by pyrolysis in a nitrogen atmosphere producing synthetic crude oil and analysing products with GC-MS. In September 2017 he graduated and obtained a master's degree in environmental chemistry with a special honour for his contribution to the development of the Faculty of Chemistry in Belgrade. In October 2017 he enrolled in doctoral studies at the Jožef Stefan International Postgraduate School, doctoral study programme Ecotechnologies. His research is dedicated to developing approaches for quantitative elemental imaging using laser ablation inductively coupled plasma mass spectrometry.